Naval Research Laboratory

Washington, DC 20375-5320

Stochastic Cross-Sections Based on the Small Slope Approximation: Theory

Daniel Wurmser

Acoustic Systems Branch
Acoustics Division

January 18, 2005

REPORT DOCUMENTATION PAGE

1. REPORT DATE *(DD-MM-YYYY)* 18-01-2005	2. REPORT TYPE Memorandum	3. DATES COVERED *(From - To)* January 2003-December 2004

4. TITLE AND SUBTITLE Stochastic Cross-Sections Based on the Small Slope Approximation: Theory	5a. CONTRACT NUMBER
	5b. GRANT NUMBER
	5c. PROGRAM ELEMENT NUMBER 62747N

6. AUTHOR(S) Daniel Wurmser	5d. PROJECT NUMBER
	5e. TASK NUMBER UW-747-014
	5f. WORK UNIT NUMBER 71-6832

7. PERFORMING ORGANIZATION NAME(S) AND ADDRESS(ES) Naval Research Laboratory, Code 7140 4555 Overlook Avenue, SW Washington, DC 20375-5320	8. PERFORMING ORGANIZATION REPORT NUMBER NRL/MR/7140--05-8816

9. SPONSORING / MONITORING AGENCY NAME(S) AND ADDRESS(ES) Office of Naval Research 800 North Quincy Street Arlington, VA 22217-5660	10. SPONSOR / MONITOR'S ACRONYM(S)
	11. SPONSOR / MONITOR'S REPORT NUMBER(S)

12. DISTRIBUTION / AVAILABILITY STATEMENT

Approved for public release; distribution is unlimited.

13. SUPPLEMENTARY NOTES

14. ABSTRACT

The small slope approximation is widely used to model the incoherent scattering cross-section per unit area from stochastic rough interfaces. It consists of an integral multiplied by a prefactor. The prefactor involves a closed-form algebraic expression, but evaluation of the integral is nontrivial. This paper develops tractable methods for evaluating the integral. The rough-surface scenarios considered generally assume spectra that have tails that decrease according to a single specified power law. This assumption is typically valid for the air-sea interface and ocean bottom at frequencies below 10 and 40 kHz respectively. The scenarios involve various tradeoffs, but the most significant tradeoff involves tractability vs broad applicability. In the most tractable scenario, it is assumed that only the isotropic tail of the spectrum is relevant. Alternately, information about the spectral peak and the power-law tail can be used to generate an isotropic "difference spectrum" formed by taking the difference between two power laws. The difference spectrum peak can be sharpened either by grafting it to a decaying exponential at low-wavenumber, or by replacing it entirely with a Pierson-Moskowitz (isotropic) spectrum modified by substituting its exponential factor $\exp(-a/k^2)$ with $\exp(-a/k)$. The latter spectrum is tractable, and while incorporating very sharp spectral peaks, it is rather inflexible. A typical azimuthal dependence is also considered.

15. SUBJECT TERMS

Acoustics; Rough surfaces; Scattering theory; Small slope approximation

16. SECURITY CLASSIFICATION OF:			17. LIMITATION OF ABSTRACT	18. NUMBER OF PAGES	19a. NAME OF RESPONSIBLE PERSON Daniel Wurmser
a. REPORT Unclassified	b. ABSTRACT Unclassified	c. THIS PAGE Unclassified	UL	76	19b. TELEPHONE NUMBER *(include area code)* (202) 404-4817

TABLE OF CONTENTS

STOCHASTIC CROSS-SECTIONS BASED ON THE SMALL SLOPE APPROXIMATION: THEORY

1 Introduction

1.1 Background and motivation

The reverberation of underwater sound is frequently modeled using ray theory. Particularly in shallow water, such a scenario involves bounces from stochastic rough surfaces such as the air-sea interface and the ocean bottom. The stochastic incoherent scattering cross-section as a function of the incoming grazing angle and the scattered angle is used to specify the intensity of the field that is incoherently scattered by the surface roughness.

For decades, perturbation theory based on small surface height approximation [1] has been used to calculate this stochastic incoherent cross-section. This result depends on surface roughness on the order of the Bragg scale. The Bragg scale corresponds to the spacing of a diffraction gating that produces primary maxima in the direction specified. Such scattering is known as Bragg scattering. In general, the effective diffraction gratings are tilted by larger-scale features, but perturbation theory ignores this. However, at high grazing angles, this effect can be significant after only a single scattering event [2]. Consequently, there is often a need to improve the accuracy of the cross-section by incorporating the effects associated with the large-scale tilts that modulate Bragg scattering. The challenge is therefore to develop formulations of the scattering problem that both improve on perturbation theory by incorporating large-scale tilts and also lead to tractable calculations.

This paper imposes the tractability requirement set in reference [3]: no more than a 2-dimensional integration for 2-dimensional surfaces. In most cases considered below, this requirement is exceeded, because spherically symmetric geometry is assumed and then used to reduce the two dimensional integral to a one-dimensional integral. Furthermore, spectra are chosen so that the associated autocorrelation functions, which appear in the intergrand of this primary (one-dimensional) integral, have closed-form solutions or at worst involve one-dimensional integrals of finite domain. As in reference [3], we will emphasize one particular approximation that leads to expressions for the scattering cross-section that are both consistent with our tractability requirement and incorporate large-scale tilt. This approximation is the lowest-order small slope approximation. It was developed by Voronovich in the early 1980s [4, 5]. Since then, it has become a widely used and well-developed technique for calculating stochastic cross-sections for scattering from quasi-planar rough interfaces of the sort that occur, for example, on the ocean's air-sea interface [6, 7, 8, 9, 10, 11, 12] or ocean bottom [13, 14, 15, 16]. (See Section I of reference [6] for a discussion of how the small slope approximation incorporates large-scale tilt.)

_____

The small slope approximation for the cross-section consists of the sum of a term corresponding to specular reflection and an incoherent scattering cross-section. The former is proportional to a δ-function, and the coefficient of this δ-function corresponds to the fraction of the incoming field's intensity that is specularly (i.e., coherently) reflected from the interface. This coefficient accounts for the energy that is transferred from the coherent to the incoherent field, and it must be a fraction between zero and one. This coefficient is relatively easy to evaluate.

The incoherent scattering cross-section is a function of the incident angle and the angular direction of the observer. It is proportional to the intensity of the field incoherently scattered into this direction, and it takes the form of a product between a prefactor and an integral. All information about the nature of the media involved and consequently the boundary conditions resides in the prefactor, which is a straightforward algebraic expression and is consequently easy to evaluate. The integral is the same for all media and boundary conditions, but it contains information about the surface roughness. Specifically, for a quasi-planar rough surface defined by a surface height function $h(\underline{x})$, it is a two-dimensional integral over the horizontal plane $\underline{x}$ with the autocorrelation function $\langle h(\underline{x})h(0)\rangle$ appearing in the integrand. (As discussed in reference [6], translational invariance and Gaussian statistics are implicit in this result.)

If the autocorrelation function is known in closed form, then we have met our tractability condition. Unfortunately, it is rarely convenient to directly characterize a random rough surface by explicitly specifying the autocorrelation function. The surface roughness is more typically characterized using the Fourier transform of the autocorrelation function. This quantity is called the surface roughness spectrum $S(\underline{l})$. If the spectrum can be transformed back to give a closed form of the autocorrelation function, then our tractable condition is automatically satisfied. A central focus of this paper will be to develop and examine spectra that are both physically realistic and either meet or at least nearly meet this condition.

1.2 The tradeoffs involved

As noted above, throughout most of this paper (Sections 3 through 6), a considerable simplification is obtained by invoking spherical symmetry to reduce the two-dimensional integral over $\underline{x}$ to a one dimensional integral over the magnitude $|\underline{x}|$. This integral contains a very slowly decreasing oscillating integrand, and it is still fairly difficult to evaluate. Spectra must be formulated in such a way that the integrand is easy to evaluate. The various spectra discussed below involve various tradeoffs, but two are most significant. The first tradeoff involves the ease of obtaining the autocorrelation function (i.e., tractability) versus the ability of the spectrum to incorporate as many known attributes of actual the physical rough surface spectrum as possible. Models whose characterization of the surface is comparatively less faithful may still give accurate cross-

sections under many important scenarios, but they are unlikely to be as broadly applicable as those that incorporate a more accurate and/or detailed description of the interface. Thus, the most significant tradeoff between spectra involves tractability versus applicability to a broad variety of physical scenarios. The second tradeoff will involve spectra that offer comparable tractability, but employ different simplifying assumptions. In this case, the goal will be to match a given application with the optimal model. Even in this context, a premium will be placed on models that have the broadest applicability.

An example of the first tradeoff was explored in reference [6]. A pair of spectra were considered and the techniques for solving the associated integrals in the cross-section were developed. This reference constructed two spectra that satisfied certain characteristics assumed to hold for the surface-roughness spectrum of the air-sea interface. In the most tractable scenario, it was assumed that only the (transversely) isotropic tail of the spectrum was relevant. The integration was solved and the associated cross-section involved no numerical integrations. In a second scenario, information about the spectral peak as well as the tail of the spectrum was used to generate an isotropic "difference spectrum" formed by taking the difference between two power laws. In this case, the integrand in the cross-section's one-dimensional integral from zero to infinity appeared in closed form and the intergral was solved using specialized methods. This paper applies the pure power-law and difference spectra to parameter sets other than those considered in reference [6], and it furthermore introduces classes of spectra not considered in reference [6] (see Fig. 1).

While the difference spectrum can accommodate an arbitrary peak location and power-law tail behavior, there are limits to the sharpness of the peak. The difference spectrum peak is therefore sharpened either by replacing it at low wavenumbers with a decaying exponential function, or by replacing it entirely with a Pierson-Moskowitz spectrum modified so that the exponential e^{-a/l^2} is replaced with $e^{-a/l}$.

In the former case, the low-wavenumber exponential function generates an autocorrelation function with a relatively easy-to-evaluate one-dimensional numerical integral (that is in turn nested in the integrand of the infinite integral that appears in the cross-section). Thus, for the cutoff difference spectra, we have, relative to the difference spectrum, a modest decrease in tractability and a modest increase in the completeness of the physical description.

This modification to Pierson-Moskowitz spectrum is made so that the autocorrelation function has a closed-form solution. This spectrum therefore turns out to be as tractable as the difference spectrum and it also incorporates sharper spectral peaks than any of the other spectra considered (see Fig. 1), but it *only meets these tractability conditions for integer power laws*. Furthermore, the height of the spectral peak and its location are correlated, and so the modified Pierson-Moskowitz spectrum is the least flexible of all the spectra considered. The primary tradeoff between tractability and broadness of applicability cannot be used to distinguish between the difference spectrum and the modified Pierson-Moskowitz spectrum. These spectra accurately incorporate different aspects of reality. The difference spectrum accurately models the behavior of a wide

variety of spectral tails, while it makes approximations concerning the nature of the peak. The <u>modified</u> Pierson-Moskowitz spectrum will accurately reflect the shape of the peak, while it will be forced to make approximations about the tail (say be restricted to integer power laws). A central theme of this paper will be to evaluate this tradeoff, and a key conclusion will be that the difference spectrum that accurately reproduces a variety of tail behaviors provides a more useful compromise than the <u>modified</u> Pierson-Moskowitz spectrum that emphasizes peak shape at the expense of describing only integer power-law tails.
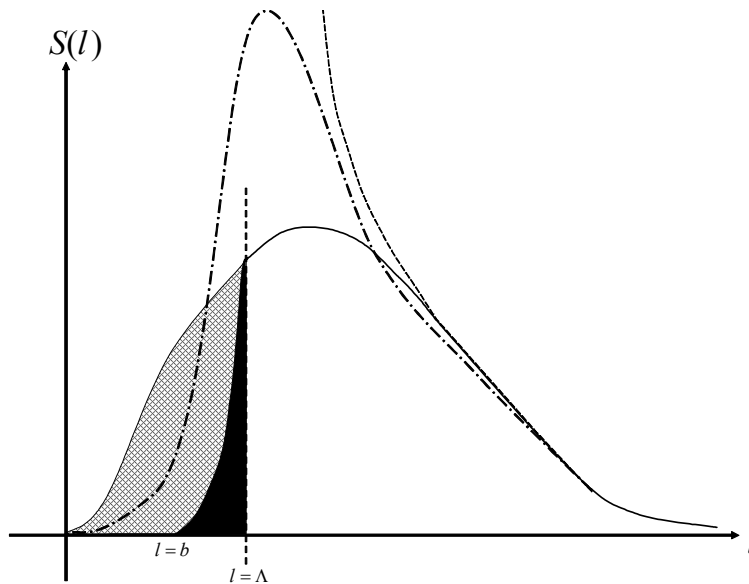
Fig. 1 - The various types of isotropic spectra considered in this paper. Note that this graph uses linear scales for both axes. The pure power law spectrum is given by the dashed line. The difference spectrum is given by the solid line. The difference spectrum is made narrower in one of two ways; by introducing either a step cutoff at wavenumber Λ, or an exponential cutoff. The autocorrelation function corresponding to the step cutoff is proportional to the autocorrelation function corresponding to the difference function minus the contribution from the cross-hatched and black areas. The autocorrelation function corresponding to the exponential cutoff spectrum differs from that for the step cutoff in that the area in black (i.e., under the exponential) contributes to the Fourier transform of the spectrum. In this illustration $c < 0$, and the exponential cutoff spectrum is concave from the left. In order to produce a peak that is both narrower *and taller* (relative to the power-law tail) than the difference spectrum, a <u>modified</u> Pierson-Moskowitz spectrum is considered (dash-dot line). This spectrum only meets our tractability conditions for integer power laws.

In the final scenario considered here, the difference spectrum is generalized to include an azimuthal dependence, and the associated scattering cross-section is shown to be reducible to a sum of tractable one-dimensional integrals.

The newly expanded technique has recently been used to develop improved algorithms for scattering from the air-sea interface [17, 18], and to study the scattering behavior of the ocean bottom [2, 19, 20]. An overview of some of the material discussed below is published in reference [21].

1.3 Roadmap of the paper

For completeness, the perturbation theory result for the stochastic cross-section per unit area is outlined in Section 2. It is presented in a way that puts this approximation into the context of the formalism throughout the rest of the paper. Perturbation theory is shown to be an approximation to the small slope approximation that can easily be derived from it. Perturbation theory is much easier to evaluate than the small slope approximation, and its accuracy often suffices away from specular.

The small slope approximation is then examined in the context of several spectra. It is assumed that a typical spectrum goes to zero for very large scales (i.e., as the wavenumber approaches zero), rises to some peak and then falls off as a power law. For wavenumbers corresponding to frequencies below below 10 kHz, the ocean surface spectrum is dominated by gravity waves (to about 10 times the peak frequency) and then enters a mixed gravity-capillary wave region that extends down to cm scales. For a part of the mixed region that extends up to wavenumbers of at least 40 m^{-1} (corresponding roughly to the Bragg scale for 10 kHz), the power-law tail inherited from gravity wave still holds, and the model above applies [22, 23, 24]. (At higher wavenumbers, capillary waves first cause the spectrum to drop off more slowly as a function of the wavenumber and then to fall off sharply–e.g., see references [22, 24].) The ocean bottom roughness at scales relevant to acoustic fields below 40 kHz results from sedimentation and erosion, and this type of rough surface again fits our model. (At smaller scales (i.e., larger wavenumbers and frequencies), the ocean bottom is characterized by the presence of small objects such as sea shells and pebbles, and such objects generate power-law spectra that drop off more rapidly as a function of wavenumber. This leads to a kink in the spectrum at around 40 kHz [25].) Thus, our assumption that the spectrum hits a peak and then falls off as a single power law is appropriate for the air-sea interface at acoustic frequencies roughly below 10 kHz and for the ocean bottom at acoustic frequencies roughly below 40 kHz.

On the air-sea interface, both the tail and the peak can generally be expressed in terms of measurable physical quantities such as the wind speed. For various types of ocean bottom, there are criteria for determining the power of the drop-off of the tail. For example, for exposed rock the wavenumber typically drops off with a power in the range 2.6-2.8 [2, 15], gravel with a power 3.0 [15], and undulating sand drops off with a power in the range 3.0-3.25 [3, 15]. However, no general criteria have found wide acceptance for determining the peak of the ocean-bottom spectrum. It is therefore useful to begin with an examination of an approach for calculating the stochastic scattering cross-section when only the behavior of the tail of the spectrum is known. Section 3 outlines such an approach. As outlined in references [2, 20], these results have been used to deduce bottom parameters such as the sound speed, density and roughness spectrum by inverting backscattering results for the ocean bottom. These parameters can in turn be substituted into the theory to predict a wide variety of monostatic and even bistatic scattering results.

Section 4 presents the cross-section for a simple peaked spectrum formed by taking the difference between two power-law spectra (denoted below as the difference spectrum).

This form is useful in establishing general attributes of the cross-section related to a spectral peak, and it may accurately describe the spectra found along some ocean bottoms, but for other applications the peak generated in this way may not be sharp enough. This peak is not as sharp as some found at the air-sea interface, and one of the goals of this paper will be to compare this spectrum with spectra that have sharper peaks, and to examine the implications for the modeling of scattering from the air-sea interface. In fact, Section 6 will demonstrate that the flexible and mathematically tractable difference spectrum provides an adequate description of the air-sea interface despite its comparatively gentle peak.

Section 5 introduces two spectra with sharper peaks. These two peaked spectra are more realistic, for example, in considering the air-sea interface. In the first case, a cutoff is introduced, and the spectrum of Section 4 is set equal to zero below this cutoff. In the second case, a spectrum very similar to the Pierson-Moskowitz spectrum is considered. The Pierson-Moskowitz spectrum is modified so that the integral giving the autocorrelation function has a closed form solution.

Section 6 considers the pure power law spectrum, the difference spectrum and the modified Pierson-Moskowitz spectrum. After comparing the spectra directly and with the true Pierson-Moskowitz spectrum, this section illustrates their implications with a few air-sea interface examples. The stochastic scattering cross-section generated by the pure power law spectrum, the difference spectrum and the modified Pierson-Moskowitz spectrum are compared and contrasted.

Section 0 examines the stochastic scattering cross-section corresponding to an angle-dependent surface spectrum. A specific angular dependence is considered, that proposed by Elfouhaily *et al.* [22] for the air-sea interface. This angular dependence is based on the lowest term of a Fourier series expansion subject to general constraints that must be imposed on a steady-state rough surface spectrum. It is therefore quite general, and should apply to a variety of angle-dependent spectra. The angle-dependent spectrum is the product of an isotropic component and the angle-dependent term. At first, the isotropic component is kept general, and the corresponding scattering cross-section per unit area corresponding is derived. Then a spectrum that combines the angular dependence of Elfouhaily *et al.* with the isotropic difference spectrum of Section 4 is considered. Setting the Fourier coefficient to be a constant, and imposing another lowest order expansion, the result once again reduces to a sum of tractable one-dimensional integrations.

Section 8 summarizes the key findings of this effort and Section 9 provides some concluding thoughts.

1.4 The formalism

This section outlines the formalism used throughout this paper. Subsection 1.4.1 discusses the meaning of a cross-section per unit area in the context of a quasi-planar

rough interface. Subsection 1.4.2 derives the basic equations needed to evaluate the stochastic cross-section per unit area. Subsection 1.4.3 discusses the parameterization of scattering geometry–i.e., incoming wave vector and observer coordinates (or equivalently, outgoing wave vector).

1.4.1 The meaning of the scattering amplitude and cross-section for a quasi-planar surface

Consider a quasi-planar 2-dimensional rough surface defined by $z = h(\underline{x})$, where $\underline{x} = (x, y)$ is a coordinate in a 2-dimensional plane. By convention, vectors in the $\underline{x}$-plane will be underlined in this paper. An incoming plane wave of the form $e^{i\vec{k}\cdot\vec{r}}$ ($\vec{r} = (\underline{x}, z)$ with $z > 0$ is some arbitrary coordinate in 3-dimensional half space) scatters from this surface. The total field in the half space defined by $z > h(\underline{x})$ is given by the sum of the scattered wave $\Psi_{\vec{k}}(\vec{r})$ and the incoming plane wave $e^{i\vec{k}\cdot\vec{r}}$.

Following reference [6], the 2-dimensional Fourier transform of the scattered wave is given by

$$\Phi_{\vec{k}}(\underline{q}, z) \equiv \int \Psi_{\vec{k}}(\underline{x}, z) e^{-i\underline{q}\cdot\underline{x}} \frac{d^2 x}{(2\pi)^2}$$

and

$$\Psi_{\vec{k}}(\vec{r}) = \int \Phi_{\vec{k}}(\underline{q}, z) e^{i\underline{q}\cdot\underline{x}} d^2 q .$$

According to the Rayleigh hypothesis, the scattered field can be modeled by a superposition of outgoing plane waves, and so $\Phi_{\vec{k}}(\underline{q}, z)$ must be of the basic form $\Phi_{\vec{k}}(\underline{q}, z) = \varphi_{\vec{k}}(\underline{q}, q_z) e^{iq_z z}$ where

$$q_z \equiv \begin{cases} +\sqrt{k^2 - \underline{q}\cdot\underline{q}}, & k^2 > \underline{q}\cdot\underline{q} \\ +i\sqrt{\underline{q}\cdot\underline{q} - k^2}, & k^2 < \underline{q}\cdot\underline{q} \end{cases}$$

and

$$\Psi_{\vec{k}}(\vec{r}) = \int \varphi_{\vec{k}}(\underline{q}, q_z) e^{i\underline{q}\cdot\underline{x}} e^{iq_z z} d^2 q = \int \varphi_{\vec{k}}(\vec{q}) e^{i\vec{q}\cdot\vec{r}} d^2 q . \qquad (1.1)$$

Formally taking the stationary phase as $r \to \infty$ ($r \equiv |\vec{r}|$), we find that the scattered field takes the familiar form

$$\Psi_{\vec{k}}(\vec{r}) = (2\pi i q_z) \varphi_{\vec{k}}(\vec{q}) \frac{e^{ik_0 r}}{r}, \qquad (1.2)$$

where now $\vec{q} = k_0 \hat{r}$ and k_0 is the wavenumber in the half space. From Eq. (1.2), we can read off the two forms of the scattering amplitude $f_{\vec{k}}(\hat{r})$ and $T(\vec{q}, \vec{k})$,

$$f_{\vec{k}}(\hat{r}) = \frac{T(\vec{q}, \vec{k})}{4\pi} = (2\pi i q_z) \varphi_{\vec{k}}(\vec{q}) .$$

Formally, the scattering cross-section is given by

$$\sigma = \left| f_{\vec{k}}(\hat{r}) \right|^2 = \frac{\left| T(\vec{q}, \vec{k}) \right|^2}{16\pi^2} .$$ (1.3)

As noted in reference [6], this quantity is ill-defined for an infinite deterministic surface, but if we consider a translationally-invariant ensemble (i.e., the autocorrelation function only depends on the distance between two points on the surface), the stochastic cross-section divided by the area $\langle \sigma \rangle / a$ is an observable physical quantity. This quantity will be discussed next in the subsection 1.4.2.

1.4.2 The basic form of the lowest-order small slope approximation for the scattering amplitude and cross-section

The lowest-order small slope scattering amplitude corresponding to an observer located in the direction $\vec{q} / |\vec{q}|$ is in general of the form

$$T(\vec{q}, \vec{k}) = \beta \frac{i}{Q_z} \int d^2x \, e^{i\underline{Q} \cdot \underline{x}} e^{iQ_z h} .$$ (1.4)

where $\vec{Q} \equiv \vec{k} - \vec{q}$.

The prefactor β is an algebraic expression, and it is not difficult to evaluate. All information about the boundary conditions resides in this prefactor, but it contains no information about the interface $h(\underline{x})$. The precise form of the prefactor β for an acoustic field incident on Dirichlet, Neumann and 2-fluid boundary conditions, and for an electromagnetic field incident on a perfect conductor can be read off from the results given in Appendix C.1 of reference [6]. The prefactor for an acoustic field incident on a fluid-elastic solid interface can be deduced from Eq. (3.23) in reference [14], and the details are provided in Appendix A .[a]

The integral in Eq. (1.4),

$$\frac{i}{Q_z} \int d^2x \, e^{i\underline{Q} \cdot \underline{x}} e^{iQ_z h}$$

is the same for all boundary conditions. It contains all the information in $T(\vec{q}, \vec{k})$ about the surface $h(\underline{x})$, and it also depends on the scattering geometry, but it is not influenced by the nature of the boundary conditions or the media involved.

---

[a] Using the techniques developed in references [6] and [14], the prefactor β and consequently the scattering amplitude $T(\vec{q}, \vec{k})$ always manifestly obey reciprocity (i.e., $T(\vec{q}, \vec{k}) = T(-\vec{k}, -\vec{q})$ or equivalently $T(\theta_{in}, \theta_{out}, \varphi_{out}) = T(\theta_{out}, \theta_{in}, \varphi_{out})$). Some other versions of the small slope at fluid-fluid and fluid-elastic interfaces (e.g., that used in reference [13]) do not *manifestly* obey reciprocity since they are ultimately derived using an approach that invokes a non-reciprocal version of perturbation theory.

The next step is to obtain the stochastic scattering cross-section per unit area for a translationally invariant interface. The latter condition implies that the autocorrelation function between two values of the surface height depends only on the vector from one to the other:

$$\langle h(\underline{x})h(\underline{x}')\rangle = A(\underline{x}-\underline{x}').$$

Taking the magnitude squared and ensemble averaging Eq. (1.3) and using Eq. (1.4) to substitute for $T(\vec{q},\vec{k})$, we have

$$\langle \sigma \rangle = \frac{\left\langle \left| T(\vec{q},\vec{k}) \right|^2 \right\rangle}{16\pi^2} = \frac{|\beta|^2}{16\pi^2 Q_z^2}\int d^2\underline{x}\, d^2\underline{x}' \left\langle e^{iQ_z(h(\underline{x})-h(\underline{x}'))}\right\rangle e^{i\underline{Q}\cdot(\underline{x}-\underline{x}')}.$$

Next, use Eq. (36) of reference [6] (good for a translationally invariant Gaussian surface):

$$\left\langle e^{iQ_z(h(\underline{x})-h(\underline{x}'))}\right\rangle = \exp\left(-\frac{Q_z^2}{2}\rho(\underline{x}-\underline{x}')\right), \tag{1.5}$$

where

$$\rho(\underline{x}-\underline{x}') \equiv 2\left[A(0)-A(\underline{x}-\underline{x}')\right]. \tag{1.6}$$

We now have

$$\langle \sigma \rangle = \frac{|\beta|^2}{16\pi^2 Q_z^2}\int d^2\underline{x}\, d^2\underline{x}'\, e^{-\frac{Q_z^2}{2}\rho(\underline{x}-\underline{x}')}e^{i\underline{Q}\cdot(\underline{x}-\underline{x}')}.$$

(Note that for the moment, no assumption of isotropy is made yet. This will come below just above Eq. (1.10).)

Perform the change of variables

$$\underline{v} = \underline{x}-\underline{x}' \quad ; \quad \underline{w} = \frac{1}{2}(\underline{x}+\underline{x}') \quad \Rightarrow \quad \int d^2\underline{x}\, d^2\underline{x}' = \int d^2\underline{v}\, d^2\underline{w},$$

and note that the integral $\int d^2\underline{w}$ gives the area a of the ensonified region, and we have

$$\frac{\langle \sigma \rangle}{a} = \frac{|\beta|^2}{16\pi^2 Q_z^2}\int d^2\underline{v}\, e^{-\frac{Q_z^2}{2}\rho(\underline{v})}e^{i\underline{Q}\cdot\underline{v}}. \tag{1.7}$$

Generally speaking, the integrand fails to approach zero at infinity and it is necessary to extract a specular δ-function from the integral to obtain the following alternate form of Eq. (1.7):

$$\frac{\langle \sigma \rangle}{a} = \frac{|\beta|^2}{16\pi^2 Q_z^2}\left[(2\pi)^2 e^{-\frac{Q_z^2}{2}\rho(\infty)}\delta(\underline{Q})+\int d^2\underline{v}\left(e^{-\frac{Q_z^2}{2}\rho(\underline{v})}-e^{-\frac{Q_z^2}{2}\rho(\infty)}\right)e^{i\underline{Q}\cdot\underline{v}}\right]. \tag{1.8}$$

Even so, the integral

$$I = \int d^2\underline{v}\left(e^{-\frac{Q_z^2}{2}\rho(\underline{v})}-e^{-\frac{Q_z^2}{2}\rho(\infty)}\right)e^{i\underline{Q}\cdot\underline{v}} \tag{1.9}$$

9

is difficult to evaluate, and this manuscript primarily addresses this issue for various classes of $\rho(\underline{v})$.

In all the cases considered below except Section 07, the function $\rho(\underline{v})$ is spherically symmetric, and Eq. (1.8) reduces to

$$\frac{\langle\sigma\rangle}{a} = \frac{|\beta|^2}{16\pi^2 Q_z^2}\left[(2\pi)^2 e^{-\frac{Q_z^2}{2}\rho(\infty)}\delta(\underline{Q}) + 2\pi\int dv\, v\left(e^{-\frac{Q_z^2}{2}\rho(v)} - e^{-\frac{Q_z^2}{2}\rho(\infty)}\right)J_0(Qv)\right]. \quad (1.10)$$

This integral can be evaluated numerically provided that $\rho(v)$ and $\rho(\infty)$ are known.

1.4.3 Conventions used to characterize $\vec{k}$ and $\vec{q}$ in terms of angles

Fig. 2 outlines the conventions used in this paper to characterize $\vec{k}$ and $\vec{q}$.
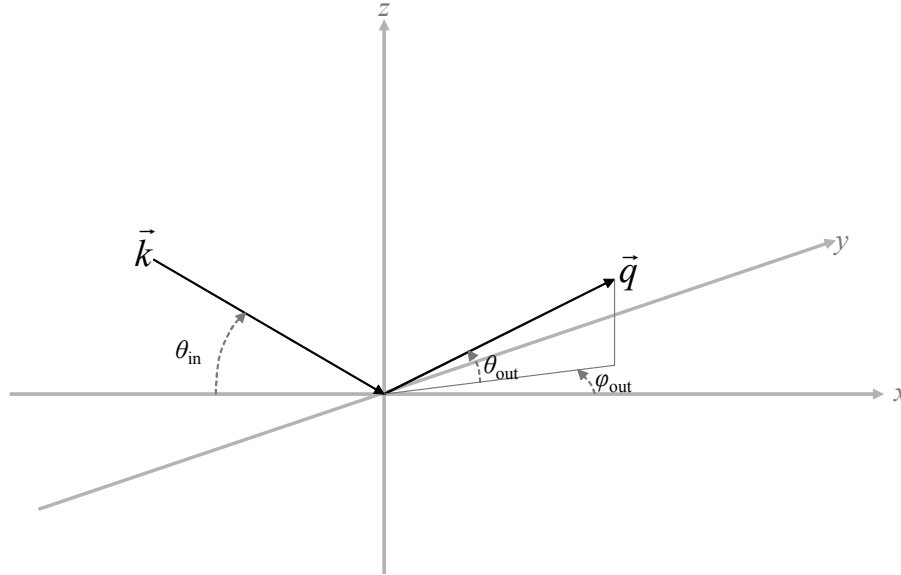
Fig. 2 - An incoming plane wave is characterized by a wave vector $\vec{k}$ that lies in the x-z plane at an angle θ_{in} relative to the x-axis. An observer is at solid angle $\vec{q}/|\vec{q}| = \vec{q}/k_0$ and labeled by the vertical and azimuthal angles θ_{out} and φ_{out} respectively. This notation follows reference [15]. Note that $\varphi_{out} = 180\deg$ corresponds to backscattering.

These conventions lead to the formulas

$$\begin{aligned}\vec{k} &= k_0\left(\cos\theta_{in}\hat{x} - \sin\theta_{in}\hat{z}\right)\\\vec{q} &= k_0\left(\cos\theta_{out}\left(\cos\varphi_{out}\hat{x} + \sin\varphi_{out}\hat{y}\right) + \sin\theta_{out}\hat{z}\right)\end{aligned}. \quad (1.11)$$

Recall that k_0 is the wavenumber in the half space.

These definitions give us the magnitudes of the horizontal and vertical components of $\vec{Q} = \vec{k} - \vec{q}$:

$$Q_z = \hat{z} \cdot (\vec{k} - \vec{q}) \Rightarrow Q_z = -k_0 (\sin\theta_{in} + \sin\theta_{out})$$

$$\underline{Q} = (1 - \hat{z}\hat{z}) \cdot (\vec{k} - \vec{q}) \Rightarrow |\underline{Q}| = k_0 \sqrt{\cos^2\theta_{in} + \cos^2\theta_{out} - 2\cos\theta_{in}\cos\theta_{out}\cos\varphi_{out}} \quad . \quad (1.12)$$

1.4.4 Validity criteria for the small slope approximation

As its name suggests, the small slope approximation is valid when the slope of the surface given by the function $h(\underline{x})$ is in some sense small. In this section, we state this condition in more precise form.

The small slope condition is that root mean square of the slope $\langle \nabla h^2_{rms} \rangle$ be less than one. Let us estimate this quantity.

Often, the tail dominates the calculation of the slope. Therefore, begin by considering a typical power-law tail for a spectrum:

$$S(\underline{l}) = \frac{w_2}{(h_0 |\underline{l}|)^{\gamma_2}} , \qquad (1.13)$$

where w_2 is some known scalar with units meters to the 4th power (m^4), the scaling parameter h_0 is 1 meter[b], and the power-law parameter γ_2 is a number above 2 (in principle, there is no upper limit on γ_2). The notation of Eq. (1.13) follows reference [15]. Recall that the integral I appears in expression (1.10) for the stochastic cross-section. For such a tail (valid roughly between some peak wavenumber l_p and the characteristic scale for Bragg scattering $|\underline{Q}|$ –higher wavenumbers are transparent to the field), we have

---

[b] The parameter h_0 is optional. If it is present, then w_2 has units [length]^4, but if it is absent it has units of length to a fractional power: $4 - \gamma_2$. Since it can lead to confusion in the conversion of units, its use by the underwater acoustics community has recently declined.

$$\left\langle \nabla h_{\text{rms}}^2 \right\rangle_{\text{tail}} = \frac{2\pi w_2}{h_0^{\gamma_2}} \int_{l_p}^{|\underline{Q}|} \frac{l\, dl \cdot l^2}{l^{\gamma_2}}$$

$$= \frac{2\pi w_2}{h_0^{\gamma_2}} \begin{cases} \left[\dfrac{|\underline{Q}|^{4-\gamma_2}}{4-\gamma_2} - \dfrac{l_p^{4-\gamma_2}}{4-\gamma_2} \right] & \gamma_2 \neq 4 \\[2em] \ln\left(\dfrac{|\underline{Q}|}{l_p} \right) & \gamma_2 = 4 \end{cases} \tag{1.14}$$

The Bragg scale will in most cases dominate the average slope, but for completeness, we keep the contribution from the spectral peak and now proceed to estimate the contribution from lower wavenumbers between zero and l_p. To do so, approximate the bottom part of the spectrum by the basic form

$$S(\underline{l}) = Al^\beta \quad 0 < l < l_p,$$

where $A, \beta > 0$. Enforcing continuity at l_p, we have

$$Al_p^\beta = \frac{w_2}{h_0^{\gamma_2}} \frac{1}{l_p^{\gamma_2}} \Rightarrow A = \frac{w_2}{h_0^{\gamma_2}} \frac{1}{l_p^{\gamma_2+\beta}}$$

and

$$S(\underline{l}) = S_{\text{tail}}(\underline{l}) \left(\frac{l}{l_p} \right)^\beta = \frac{w_2}{h_0^{\gamma_2}} \frac{1}{l_p^{\gamma_2}} \left(\frac{l}{l_p} \right)^\beta \quad 0 < l < l_p. \tag{1.15}$$

Thus,

$$\left\langle \nabla h_{\text{rms}}^2 \right\rangle_{\text{low } l} = \frac{2\pi w_2}{h_0^{\gamma_2} l_p^{\gamma_2+\beta}} \int_0^{l_p} l\, dl \cdot l^2 l^\beta = \frac{2\pi w_2}{h_0^{\gamma_2} l_p^{\gamma_2+\beta}} \left[\frac{l_p^{\beta+4}}{\beta+4} \right]$$

$$= \frac{2\pi w_2}{h_0^{\gamma_2}} \left[\frac{l_p^{4-\gamma_2}}{\beta+4} \right]. \tag{1.16}$$

Adding the two contributions gives us

$$\left\langle \nabla h_{\text{rms}}^2 \right\rangle = \frac{2\pi w_2}{h_0^{\gamma_2}} \left[\frac{|\underline{Q}|^{4-\gamma_2}}{4-\gamma_2} - l_p^{4-\gamma_2} \left(\frac{1}{4-\gamma_2} - \frac{1}{\beta+4} \right) \right] \quad \forall\, \gamma_2 \neq 4. \tag{1.17}$$

Typically, $\beta = 1$. For $\gamma_2 = 4$, we have

$$\left\langle \nabla h_{\text{rms}}^2 \right\rangle = \frac{2\pi w_2}{h_0^4} \left[\ln\left(\frac{|\underline{Q}|}{l_p} \right) + \frac{1}{\beta+4} \right]. \tag{1.18}$$

Thus, the small slope approximation is valid roughly as long as $\left\langle \nabla h_{\text{rms}}^2 \right\rangle$ as defined by equation (1.17)/(1.18) is less than one. This is a crude criterion, both because the calculation of the rms slope is approximate and more importantly since the small slope

actually depends on a generalized slope[c], but it provides a good first indication for the region of validity of the small slope approximation. If this quantity is close to but less than one[d], then the higher order small-slope approximation should be considered [8, 9, 26]. As noted by Ivakin [25], for typical ocean bottoms, slopes are generally "small" on size scales roughly down to the typical Bragg scale for acoustic fields below 40 kHz. Above this frequency, other methods must be used.

For the pure power law, use results (1.17) with the term including l_p dropped along with (1.18).

For completeness, note that the rms surface height calculated using the same procedure is

$$\left\langle h_{rms}^2 \right\rangle = \frac{2\pi w_2}{h_0^{\gamma_2}} \left[l_p^{2-\gamma_2} \left(\frac{1}{\gamma_2 - 2} + \frac{1}{\beta + 2} \right) - \frac{\left| \underline{Q} \right|^{2-\gamma_2}}{\gamma_2 - 2} \right]. \tag{1.19}$$

This result should be used very cautiously because it is much more sensitive to the behavior of the spectrum at and below the peak wavenumber. The approximations used in this region are quite crude. However, other models for the spectral peak give qualitatively similar results. For a cutoff version of spectrum (1.13) used in reference [2]

$$S\left(\underline{l} \right) = \frac{w_2}{\left(1 + \left(h_0 \left| \underline{l} \right| \right)^2 \right)^{\gamma_2/2}},$$

the rms surface height is given by

$$h_{rms}^2 = \frac{2\pi w_2}{h_0^2 \left(\gamma_2 - 2 \right)}. \tag{1.20}$$

For the difference spectrum given by Eq. (4.1)/(4.2), this result becomes

$$h_{rms}^2 = \frac{2\pi w_2 \left(1 - a_2^2 \right)}{\left[b_2^2 h_0^2 \left(\gamma_2 - 2 \right) \right]} \tag{1.21}$$

with a_2 a free parameter smaller than one and b_2 given by Eq. (4.11) in terms of the peak wavenumber l_p, γ_2 and a_2. Note that all these versions of the result indicate that h_{rms}, w_2 and γ_2 are not independent. Also note that Eqs. (1.20) and (1.21) are valid for $\gamma_2 > 2$, and do not depend on the Bragg scale. In fact, Eq. (1.19) only weakly depends on the Bragg scale for $\gamma_2 > 2$. The dependence on the Bragg scale for the slope was driven by

---

[c] The true expansion parameter for the small slope approximation is in fact a modified slope [6, 8, 9]. This quantity roughly corresponds to the average surface height variation over a correlation length divided by the correlation length. This is a difficult quantity to calculate. Furthermore, the expansion strictly speaking becomes convergent rather than asymptotic only when the scattering theory is properly renormalized (e.g., R. Dashen and G. J. Orris, "Rough surfaces and the renormalization group," J. Math. Phys., **31** 2352-2360 (1990)). An impeccably accurate calculation of the effective slope would have to take this into account as well.

[d] Subject to the caveats in footnote c, when the expansion parameter is greater than one, then the series diverges.

the extra factor l^2 in the integrand of Eq. (1.16). The dependence on the Bragg scale in Eq. (1.17) is only strong for $\gamma_2 < 4$.

2 1$^{\text{st}}$-order perturbation theory

To obtain 1$^{\text{st}}$-order perturbation theory, take the expression for $\langle\sigma\rangle/a$ given by Eq. (1.8), expand the integrand of I in powers of the autocorrelation function $A(\underline{u})$ and drop all specular δ-functions that appear. Using the convention in the definition of the surface roughness spectrum given by Eq. (42) of reference [6], namely,

$$S(\underline{l}) \equiv \int \frac{d^2\underline{x}}{(2\pi)^2} \, A(\underline{x}) e^{i\underline{l}\cdot\underline{x}}, \qquad (2.1)$$

we are left with

$$\left\langle |I|^2 \right\rangle = \int d^2\underline{v} \, A(\underline{v}) e^{i\underline{Q}\cdot\underline{v}} = (2\pi)^2 S(\underline{Q}).$$

This gives us the first-order perturbation result for the scattering cross-section per unit area

$$\frac{\langle\sigma\rangle}{a} = \frac{|\beta|^2}{4} S(\underline{Q}). \qquad (2.2)$$

Note that the prefactor $|\beta|^2$ is similar to, but not identical to that in Eq. (17) of reference [15]. The prefactor $|\beta|^2$ manifestly exhibits symmetry between $\vec{k}$ and $-\vec{q}$.

The spectra considered in Sections 3 to 6 are direction-independent: $S(\underline{Q}) = S(|\underline{Q}|)$. In such cases, we can use Eqs. (1.11) to evaluate $|\underline{Q}|$:

$$|\underline{Q}| = |\underline{k} - \underline{q}| = k_0 \sqrt{\cos^2\theta_{\text{in}} + \cos^2\theta_{\text{out}} - 2\cos\theta_{\text{in}}\cos\theta_{\text{out}}\cos\varphi_{\text{out}}}.$$

3 Cross-section corresponding to a power-law spectrum with an indeterminate peak

This section evaluates the integral I defined in Eq. (1.9) for a power-law spectrum given by equation (1.13).

In reference [6], a spectrum of this form was used to characterize the air-sea interface. In this case (interjecting a factor $h_0^{\gamma_2}$ to bring the notation in line with that used elsewhere in this paper)

$$w_2 = \frac{\alpha_{\text{TOBA}}}{100\pi} h_0^{\gamma_2} \sqrt{\frac{u^2}{g}},$$

where α_{TOBA} is the coefficient of the Toba spectrum, u is the wind speed and g represents the constant of gravitational acceleration. In reference [6] where $\gamma_2 = 3.5$, the parameter α_{TOBA} was dimensionless, but more generally α_{TOBA} carries units of length to the power $3.5 - \gamma_2$ (if $h_0 = 1\,\text{m}$, then it can be absorbed into α_{TOBA} to give it a power 3.5).

Since no assumptions are made about the spectral peak, the results in this section are particularly useful in problems such as scattering from the ocean bottom, where the nature of the spectral peak is site specific and rarely well-known. References [2, 17, 19] provide further information concerning the background and application of the expression for the stochastic cross-section derived here in Section 3.

To evaluate expression (1.9) for I, we will need to evaluate the autocorrelation function $A(\underline{v})$, which also happens to be the Fourier transform of spectrum (1.13). However, a pure power-law spectrum such as given in (1.13) has an infrared divergence (i.e., as $|\underline{k}| \to 0$, the integrand has a non-integrable singularity), and so we will have to temporarily introduce some sort of spectral cutoff. Once we have obtained an expression for the autocorrelation function $A(\underline{v}) = A(|\underline{v}|)$, we can expand it in $|\underline{v}|$ and keep only the first term. This results in a power law expression for $A(|\underline{v}|)$. It turns out that this power-law expression for the autocorrelation function corresponds to the only part of the spectrum that we knew in the first place, the power law tail given in Eq. (1.13). Furthermore, for a power-law autocorrelation function, $\rho(\infty) \to \infty$ (recall that Eq. (1.6) gives us $\rho(\infty) = 2[A(\infty) - A(0)]$), and the second term in the integrand of I goes to zero (i.e., the form of the integral given in Eq. (1.7) is valid).

The integral that is left is still nontrivial. Its integrand is characterized by rapid oscillations bounded by a slowly decreasing envelope. Two series expansions with overlapping domains of validity will be used to characterize the integral.

3.1 Obtaining $A(\underline{v})$

Consider the integral that results when we take a Fourier transformation to obtain the autocorrelation function $A(\underline{v})$ from the now cutoff power law

$$S^{\text{cutoff}}(\underline{l}) = \frac{w_2}{\left(1 + \left(h_0 |\underline{l}|\right)^2\right)^{\frac{\gamma_2}{2}}}. \tag{3.1}$$

We have

$$A(\underline{v}) = \int d^2 \underline{l}\, S(\underline{l}) e^{i\underline{L}\cdot\underline{v}} = 2\pi \int_0^\infty dl\, l S(l) J_0(lv), \tag{3.2}$$

15

where $v = |\underline{v}|$ and $l = (\underline{l})$. Substituting $S^{\text{cutoff}}(\underline{l})$ for $S(\underline{l})$ in (3.2), we have

$$A(\underline{v}) = 2\pi w_2 \int_0^\infty \frac{J_0(lv) l\, dl}{\left(1 + (h_0 l)^2\right)^{\frac{\gamma_2}{2}}} \, . \tag{3.3}$$

Now, evaluate (3.3) using Eq. (20) from Section 8.5 of reference [27]:

$$\int_0^\infty f(x) J_0(xy) \sqrt{xy}\, dx = \frac{a^{v-\mu} y^{\mu+\frac{1}{2}} K_{v-\mu}(ay)}{2^\mu \Gamma(\mu+1)}, \tag{3.4}$$

with

$$f(x) \equiv x^{v+\frac{1}{2}} \left(x^2 + a^2\right)^{-\mu-1}.$$

In this equation, set $v = 0$, $\mu = \gamma_2/2 - 1$, and make the substitutions $x \to l$, $y \to v$ to obtain

$$f(l) = \frac{l^{v+\frac{1}{2}}}{\left(l^2 + a^2\right)^{\mu+1}} = \frac{l^{\frac{1}{2}}}{\left(l^2 + a^2\right)^{\frac{\gamma_2}{2}}} = \frac{l^{\frac{1}{2}}}{a^{\gamma_2}\left(1 + \left(\dfrac{l}{a}\right)^2\right)^{\frac{\gamma_2}{2}}}$$

and

$$\int_0^\infty \frac{J_0(lv) l\, dl}{\left(1 + \left(\dfrac{l}{a}\right)^2\right)^{\frac{\gamma_2}{2}}} = \frac{a^{\frac{\gamma_2}{2}+1} v^{\frac{\gamma_2}{2}-1} K_{-\frac{\gamma_2}{2}+1}(av)}{2^{\frac{\gamma_2}{2}-1} \Gamma\left(\dfrac{\gamma_2}{2}\right)} \, . \tag{3.5}$$

According to reference [27], Eq. (3.4) is valid for

$$-1 < v < 2\mu + \tfrac{3}{2} \Rightarrow -1 < 0 < \gamma_2 - \tfrac{1}{2}$$

This condition is satisfied for physically relevant $\gamma_2 > 2$, and the additional condition $a > 0$ will also hold when we set $a = 1/h_0$.

Now, in Eq. (3.5) pull out a factor of a^2 and use the equality $K_{-v}(z) = K_v(z)$ (e.g., see Eq. (9.6.6) of reference [28]) and set $a = 1/h_0$. Substitute the result into Eq. (3.3) to get

$$A(\underline{v}) = 2\pi w_2 \int_0^\infty \frac{J_0(lv) l\, dl}{\left(1 + (h_0 l)^2\right)^{\frac{\gamma_2}{2}}} = \frac{2\pi w_2 \left(\dfrac{v}{h_0}\right)^{\frac{\gamma_2}{2}-1} K_{\frac{\gamma_2}{2}-1}\left(\dfrac{v}{h_0}\right)}{h_0^2 2^{\frac{\gamma_2}{2}-1} \Gamma\left(\dfrac{\gamma_2}{2}\right)} \, . \tag{3.6}$$

Next, use Eq. (9.6.9) from reference [28]

$$K_v(z) \sim \frac{1}{2} \Gamma(v)\left(\tfrac{1}{2} z\right)^{-v} \quad \text{as } z \to 0; \ v > 0$$

to get

16

$$A(0) = \lim_{v \to 0} \left[2\pi w_2 \left(\frac{v}{h_0}\right)^{\frac{\gamma_2}{2}-1} \frac{\frac{1}{2}\Gamma\left(\frac{\gamma_2}{2}-1\right)\left(\frac{1}{2}\right)^{-\frac{\gamma_2}{2}+1}\left(\frac{v}{h_0}\right)^{-\frac{\gamma_2}{2}+1}}{h_0^2 \, 2^{\frac{\gamma_2}{2}-1}\Gamma\left(\frac{\gamma_2}{2}\right)} \right] = \frac{\pi w_2}{h_0^2}\frac{\Gamma\left(\frac{\gamma_2}{2}-1\right)}{\Gamma\left(\frac{\gamma_2}{2}\right)}.$$

Now, use the recursion relation

$$\Gamma\left(\frac{\gamma_2}{2}\right) = \left(\frac{\gamma_2}{2}-1\right)\Gamma\left(\frac{\gamma_2}{2}-1\right)$$

to get

$$A(0) = \frac{\pi w_2}{h_0^2}\frac{1}{\frac{\gamma_2}{2}-1}. \tag{3.7}$$

Substituting into Eq. (3.6), we get

$$A(v) = A(0)\frac{2\left(\frac{\gamma_2}{2}-1\right)}{2^{\frac{\gamma_2}{2}-1}\Gamma\left(\frac{\gamma_2}{2}\right)}\left(\frac{v}{h_0}\right)^{\frac{\gamma_2}{2}-1} K_{\frac{\gamma_2}{2}-1}\left(\frac{v}{h_0}\right), \tag{3.8}$$

and from the definition of $\rho(v) \equiv 2\left[A(0) - A(v)\right]$, we have

$$\rho(v) = 2A(0)\left[1 - \underbrace{\left(\frac{2\left(\frac{\gamma_2}{2}-1\right)}{2^{\frac{\gamma_2}{2}-1}\Gamma\left(\frac{\gamma_2}{2}\right)}\right)\left(\frac{v}{h_0}\right)^{\frac{\gamma_2}{2}-1} K_{\frac{\gamma_2}{2}-1}\left(\frac{v}{h_0}\right)}_{A(v)/A(0)}\right] \tag{3.9}$$

and since $K_v(z)$ goes to zero exponentially as $z \to \infty$,

$$\rho(\infty) = 2A(0) = \frac{2\pi w_2}{h_0^2}\frac{1}{\frac{\gamma_2}{2}-1}. \tag{3.10}$$

3.2 *Expanding to obtain a power law autocorrelation function* $A(v)$

Following Section IIIB of reference [6], we next replace the modified Bessel function $K_{\frac{\gamma_2}{2}-1}(v/h_0)$ with its first-order expansion to obtain a power law for $A(v)$. This is

reasonable because the function $K_{\frac{\gamma_2}{2}-1}\left(v/h_0\right)$ appears in the exponential in the integrand of Eq. (1.9), and so only small values of v/h_0 contribute to the final result. Furthermore, as discussed above Eq. (48) in reference [6], the first-order term in the expansion of $A(v)$ essentially corresponds to the power law tail of the surface roughness spectrum, which is assumed here in Section 3 to be all we know about the spectrum. Note that if the power-law tail is extended arbitrarily close to $k = 0$ (i.e., the large-scale limit), then there is no specular component to the interface, and the specular δ-function vanishes.

To expand $K_{\frac{\gamma_2}{2}-1}\left(v/h_0\right)$, first use Eq. (9.6.2) of reference [28] to recast it in terms of Bessel functions of the second kind (now with $v = \frac{1}{2}\gamma_2 - 1$):

$$K_v(z) = \frac{\pi}{2}\frac{I_{-v}(z)-I_v(z)}{\sin v\pi}, \tag{3.11}$$

and then expand for small z using Eq. (9.6.7) of that reference:

$$I_v(z) = \left(\tfrac{1}{2}z\right)^v \sum_{n=0}^{\infty}\frac{\left(\tfrac{1}{4}z^2\right)^n}{n!\Gamma(v+n+1)}.$$

This gives us

$$z^v I_{-v}(z) = \left(\frac{1}{2}\right)^{-v}\frac{1}{\Gamma(1-v)}+O\left(z^2\right) \quad ; \quad z^v I_v(z) = \frac{z^{2v}}{2^v}\frac{1}{\Gamma(1+v)}+O\left(z^{2(v+1)}\right).$$

Note that in our case, $2(v+1) = \gamma_2 > 2$, so the next order is $O\left(z^2\right)$. Now, substitute into Eq. (3.11) and use Eq. (6.1.17) of reference [28]:

$$\Gamma(v)\Gamma(1-v) = \frac{\pi}{\sin \pi v} \Rightarrow \Gamma(v)\sin \pi v = \frac{1}{\Gamma(1-v)}$$

to get[e]

$$z^v K_v(z) \approx \Gamma(v)2^{v-1} - \frac{\pi z^{2v}}{2\sin[v\pi]2^v\Gamma(v+1)}+O\left(z^2\right).$$

Substituting into Eq. (3.9)

$$\rho(\underline{v}) = 2A(0)\left[1 - \frac{2v}{\underbrace{2^v\,\Gamma(v+1)}_{v\Gamma(v)}}\left(\Gamma(v)2^{v-1} - \frac{\pi z^{2v}}{2\sin[v\pi]2^v\Gamma(v+1)}\right)\right]$$

$$= A(0)\frac{\pi v z^{2v}}{2^{2v-1}\Gamma^2(v+1)\sin[v\pi]}\quad,$$

and then recalling $v = \frac{1}{2}\gamma_2 - 1$, $z = v/h_0$ and the expression for $A(0)$ from Eq. (3.10), we get

---

[e] Note that Eq. (9.6.9) from reference [28] would only yield the first term, and so we needed to use this longer derivation starting with Eq. (9.6.2) of the reference.

$$\rho(\underline{v}) = \rho(v) = \frac{\pi^2 w_2}{h_0^2 2^{\gamma_2-3} \Gamma^2\left(\frac{\gamma_2}{2}\right) \sin\left[\left(\frac{\gamma_2}{2}-1\right)\pi\right]} \left(\frac{v}{h_0}\right)^{\gamma_2-2}. \tag{3.12}$$

Note that in this case the integrand goes to zero at infinity, and so when evaluating the stochastic cross-section there is no need to separate out the specular δ-function as in Eq. (1.8). We can substitute this expression for $\rho(\underline{v})$ directly into the expression for the cross-section (1.7). Performing the angular integration first, we have

$$\frac{\langle\sigma\rangle}{a} = \frac{|\beta|^2}{8\pi Q_z^2} \int_0^\infty v dv \; e^{-\frac{Q_z^2}{2}\rho(\underline{v})} J_0\left(|\underline{Q}|v\right) = \frac{|\beta|^2}{8\pi Q_z^2 |\underline{Q}|^2} \int_0^\infty y dy \; e^{-\frac{Q_z^2}{2}\rho(y/|\underline{Q}|)} J_0(y).$$

And then substituting (3.12), we have

$$\frac{\langle\sigma\rangle}{a} = \frac{|\beta|^2}{8\pi Q_z^2 |\underline{Q}|^2} \underbrace{\int_0^\infty y dy \; \exp\left[-\alpha y^{\gamma_2-2}\right] J_0(y)}_{I}, \tag{3.13}$$

where

$$\alpha = \frac{\pi^2 w_2 Q_z^2}{|\underline{Q}|^{\gamma_2-2} h_0^{\gamma_2} 2^{\gamma_2-2} \Gamma^2\left(\frac{\gamma_2}{2}\right) \sin\left[\left(\frac{\gamma_2}{2}-1\right)\pi\right]}. \tag{3.14}$$

It is important to keep in mind that $\alpha \to \infty$ as $\gamma_2 \to 4$ (or any even number), and this approach breaks down.

Also note that the form of Eq. (3.13) is very similar to Eq. (11) of reference [15]. However, the coefficient $|\beta|^2$ is not the same as the coefficient $|R|^2 \Delta^2$ found in that reference. The differences between the equations stems from the fact that the equation in the reference comes from the Kirchhoff approximation, while (3.13) comes from the small slope approximation.

3.3 Evaluating the integral in Eq. (3.13)

The challenge remains to evaluate Eq. (3.13). In this section, the integral

$$I = \frac{2\pi}{|\underline{Q}|^2} I = \int_0^\infty y dy \; J_0(y) \exp\left[-\alpha y^{\gamma_2-2}\right] \tag{3.15}$$

is evaluated by replacing it with a pair of power series expansions (recall that the integral I was originally defined in Eq. (1.9)). Subsection 3.3.1 develops an expansion roughly in powers of α that applies for $\alpha \le 0.15$ and Subsection 3.3.2 develops an expansion roughly in α^{-1} that applies for $\alpha > 0.15$. The dividing line between the ranges of applicability of the two series is somewhat arbitrary, but based on experience obtained for the special case considered in reference [6].

It should also be noted that an analytic solution to equation (3.15) exists for $\gamma_2 = 3$ (see Appendix B of reference [2]). This will no longer be the case when we consider roughness spectra whose power-law behavior is cutoff by a spectral peak (Sections 4 and 5 below).

3.3.1 The expansion good for $\alpha \leq 0.15$

This section provides an ad hoc derivation for an expansion in α that is based on expanding the exponential in Eq. (3.15). This approach will necessitate exchanging a series and an integral despite the fact that uniform convergence criteria are not met. The resultant series is asymptotic. A more rigorous derivation would follow reference [6], and employ a Watson-Sommerfeld transformation. This approach would also provide an error estimate. However, the approach outlined here provides a correct generalization of the results in reference [6] with relatively little effort, and the error estimates will be obtained using insights from reference [6] and by benchmarking against a new approach by Drumheller and Gragg [29] (for a more detailed description, see reference [30]).

To allow an easier match to formulas in reference [27], make the variable change $y \to x$ in Eq. (3.15). Expand the exponential

$$\exp\left[-\alpha x^{\gamma_2-2}\right] = \sum_{n=0}^{\infty} \frac{(-1)^n \alpha^n x^{\gamma_2 n - 2n}}{n!},$$

substitute into I and exchange summation and integration (see previous paragraphs for caveats) to obtain

$$I = \sum_{n=0}^{\infty} \frac{(-1)^n \alpha^n}{n!} \underbrace{\int_0^{\infty} dx\ \sqrt{x}\ x^{(\gamma_2-2)n+\frac{1}{2}} J_0(x)}_{I_n}.$$

Introduce an integrating factor e^{-ax} into I_n and let $a \to 0$:

$$I_n = \lim_{a \to 0}\left[\int_0^{\infty} dx\ e^{-ax} \sqrt{x}\ x^{(\gamma_2-2)n+\frac{1}{2}} J_0(x)\right].$$

Now, evaluate the integral using Eq. (6) in Section 8.6 (p. 29) of reference [27] with the following substitutions:

$$y = 1 \quad \mu = n(\gamma_2 - 2) + 2 \quad \nu = 0.$$

Also use the Lagrange polynomial equality $P_n^0(x) = P_n(x)$. The result is

$$I_n = \lim_{a \to 0}\left[\left(a^2 + 1\right)^{-\frac{1}{2}\left[n(\gamma_2-2)+2\right]} \Gamma\left(n(\gamma_2 - 2) + 2\right) P_{n(\gamma_2-2)+1}\left(\frac{a}{\left(a^2+1\right)^{\frac{1}{2}}}\right)\right] \qquad (3.16)$$

$$= \Gamma\left(n(\gamma_2 - 2) + 2\right) P_{n(\gamma_2-2)+1}(0) \quad.$$

Next, evaluate the Lagrange polynomial $P_\nu(0) = P_{n(\gamma_2-2)+1}(0)$. Begin with Eq. (8.1.4) of reference [28] (p. 332)

$$P_\nu^\mu(z) =$$

$$2^\mu \pi^{\frac{1}{2}} \left(z^2-1\right)^{-\frac{\mu}{2}} \left\{ \frac{F\left(-\frac{\nu}{2}-\frac{\mu}{2},\frac{1}{2}+\frac{\nu}{2}-\frac{\mu}{2},\frac{1}{2};z^2\right)}{\Gamma\left(\frac{1}{2}-\frac{\nu}{2}-\frac{\mu}{2}\right)\Gamma\left(1+\frac{\nu}{2}-\frac{\mu}{2}\right)} - 2z\frac{F\left(\frac{1}{2}-\frac{\nu}{2}-\frac{\mu}{2},1+\frac{\nu}{2}-\frac{\mu}{2},\frac{3}{2};z^2\right)}{\Gamma\left(\frac{1}{2}+\frac{\nu}{2}-\frac{\mu}{2}\right)\Gamma\left(-\frac{\nu}{2}-\frac{\mu}{2}\right)} \right\},$$

as well as Eq. (15.1.1) (p. 556)

$$F(a,b,c;z) = \frac{\Gamma(c)}{\Gamma(a)\Gamma(b)} \sum_{n=0}^{\infty} \frac{\Gamma(a+n)\Gamma(b+n)}{\Gamma(c+n)} \frac{z^n}{n!} \Rightarrow F(a,b,c;0) = 1$$

to obtain

$$P_\nu(x) = P_\nu^0(x) = \frac{\sqrt{\pi}}{\Gamma\left(\frac{1}{2}-\frac{\nu}{2}\right)\Gamma\left(1+\frac{\nu}{2}\right)}.$$

Next, use Eq. (6.1.17) of reference [28]: $\Gamma(z)\Gamma(1-z) = \pi\csc(\pi z)$ with $z = x + \frac{1}{2}$. Recalling that in Eq. (3.16), $\nu = n(\gamma_2-2)+1$, this leaves us with

$$P_{n(\gamma_2-2)+1}(0) = \frac{1}{\sqrt{\pi}} \frac{\Gamma\left(1+\frac{n}{2}(\gamma_2-2)\right)}{\Gamma\left(\frac{3}{2}+\frac{n}{2}(\gamma_2-2)\right)} \underbrace{\cos\left(\pi\left(\frac{n}{2}(\gamma_2-2)+\frac{1}{2}\right)\right)}_{-\sin\left[\pi\left(\frac{n}{2}(\gamma_2-2)\right)\right]}$$

and

$$I_n = -\frac{\Gamma\left(2\left[1+\frac{n}{2}(\gamma_2-2)\right]\right)\Gamma\left(1+\frac{n}{2}(\gamma_2-2)\right)}{\Gamma\left(\frac{3}{2}+\frac{n}{2}(\gamma_2-2)\right)\sqrt{\pi}} \sin\left[\pi\left(\frac{n}{2}(\gamma_2-2)\right)\right].$$

Now, use Eq. (6.1.18) from reference [28]:

$$\Gamma(2x) = \frac{1}{\sqrt{2\pi}} 2^{2x-\frac{1}{2}} \Gamma(x)\Gamma\left(x+\tfrac{1}{2}\right)$$

with $x = 1 + n(\gamma_2-2)/2$ to get

$$\Gamma\left(2\left[1+\frac{n}{2}(\gamma_2-2)\right]\right) = \frac{1}{\sqrt{\pi}} 2^{[n(\gamma_2-2)+1]} \Gamma\left(1+\frac{n}{2}(\gamma_2-2)\right)\Gamma\left(\frac{3}{2}+\frac{n}{2}(\gamma_2-2)\right).$$

Thus,

$$I_n = -\frac{2}{\pi}\left(2^{[n(\gamma_2-2)]}\left[\Gamma\left(1+\frac{n}{2}(\gamma_2-2)\right)\right]^2 \sin\left[\pi\left(\frac{n}{2}(\gamma_2-2)\right)\right]\right)$$

and

$$I = \int_0^\infty y\,dy\, J_0(y)\exp\left[-\alpha y^{\gamma_2-2}\right] = \sum_{n=0}^\infty \frac{(-1)^n \alpha^n}{n!} I_n$$

$$= -\frac{2}{\pi}\sum_{n=0}^\infty \frac{(-1)^n \alpha^n}{n!}\left(\left[\Gamma\left(1+\frac{n}{2}(\gamma_2-2)\right)\right]^2 \sin\left[\pi\left(\frac{n}{2}(\gamma_2-2)\right)\right]2^{[n(\gamma_2-2)]}\right),$$

and finally

$$\frac{\langle\sigma\rangle}{a} = \frac{-|\beta|^2}{4\pi^2 Q_z^2 |\underline{Q}|^2}\sum_{n=1}^{max}\frac{(-1)^n \alpha^n}{n!}\left(\left[\Gamma\left(1+\frac{n}{2}(\gamma_2-2)\right)\right]^2 \sin\left[\pi\left(\frac{n}{2}(\gamma_2-2)\right)\right]2^{[n(\gamma_2-2)]}\right),\quad(3.17)$$

with α given by Eq. (3.14). Note that the $n=0$ term in the summation would be zero, and so it has been dropped. Also note that since the expansion is asymptotic, we are now truncating the summation at some finite value. Based on experience from reference [6], it is generally safe to set $max \approx 10$.

3.3.2 The expansion good for $\alpha > 0.15$

To obtain an expansion for I that roughly goes as the reciprocal of α, take Eq. (3.15) and expand the Bessel function $J_0(y)$ in the series in y given by Eq. (9.1.12) of reference [28]:

$$J_0(y) = 1 - \frac{\left(\frac{1}{4}y^2\right)}{(1!)^2} + \frac{\left(\frac{1}{4}y^2\right)^2}{(2!)^2} - \cdots = \sum_{n=0}^\infty \frac{\left(-\frac{1}{4}y^2\right)^n}{(n!)^2}.$$

The convergence of this integral is uniform (e.g., see proofs of Borel's theorem).

We now have the equality

$$I = \sum_{n=0}^\infty \frac{\left(-\frac{1}{4}\right)^n}{(n!)^2}\int_0^\infty dy\, y^{2n+1}\exp\left[-\alpha y^{\gamma_2-2}\right].\tag{3.18}$$

Now, make the change of variable

$$z = \alpha y^{\gamma_2-2}$$

to obtain

$$\int_0^\infty dy\, y^{2n+1}\exp\left[-\alpha y^{\gamma_2-2}\right] = \frac{1}{\alpha^{\left[\frac{2n+2}{\gamma_2-2}\right]}}\frac{1}{\gamma_2-2}\int_0^\infty dz\, z^{\left[\frac{2n+4-\gamma_2}{\gamma_2-2}\right]}e^{-z}.$$

Now, use Eq. (6.1.1) from reference [28]

$$\Gamma(x) = \int_0^\infty dz\, z^{x-1}e^{-z}\quad;\quad \mathrm{Re}\,x > 0$$

with $x = (2n+2)/(\gamma_2-2)$ to evaluate the integral with respect to z. Substituting into Eq. (3.18), we get

$$I = \left[\frac{1}{\gamma_2 - 2}\right]\left[\frac{1}{\alpha^{2/(\gamma_2-2)}}\right]\sum_{n=0}^{\infty}\frac{(-1)^n}{(n!)^2}\left(\frac{1}{4\alpha^{2/(\gamma_2-2)}}\right)^n\Gamma\left(\frac{2(n+1)}{\gamma_2-2}\right),$$

and substituting back into (3.13) we have

$$\frac{\langle\sigma\rangle}{a} = \frac{|\beta|^2}{8\pi Q_z^2 |\underline{Q}|^2}\left[\frac{1}{\gamma_2 - 2}\right]\left[\frac{1}{\alpha^{2/(\gamma_2-2)}}\right]\sum_{n=0}^{\infty}\frac{(-1)^n}{(n!)^2}\left(\frac{1}{4\alpha^{2/(\gamma_2-2)}}\right)^n\Gamma\left(\frac{2(n+1)}{\gamma_2-2}\right), \quad (3.19)$$

with α given by Eq. (3.14). (The finite number of terms needed to accurately evaluate (3.19) are given in the next section below.)

3.4 Summary for the power-law spectrum $S(\underline{l}) = w_2 / (h_0 |\underline{l}|)^{\gamma_2}$

From Eqs. (3.17) and (3.19), we have

$$\frac{\langle\sigma\rangle}{a} = \begin{cases} \dfrac{-|\beta|^2}{4\pi^2 Q_z^2 |\underline{Q}|^2}\displaystyle\sum_{n=1}^{\max}\dfrac{(-1)^n \alpha^n}{n!}\left(\left[\Gamma\left(1+\frac{n}{2}(\gamma_2-2)\right)\right]^2 \sin\left[\pi\left(\frac{n}{2}(\gamma_2-2)\right)\right]2^{[n(\gamma_2-2)]}\right) \\ \hspace{6cm}\boxed{\alpha \le \alpha_{\text{transition}}} \\ \text{--} \\ \dfrac{|\beta|^2}{8\pi Q_z^2 |\underline{Q}|^2}\left[\dfrac{1}{\gamma_2 - 2}\right]\left[\dfrac{1}{\alpha^{2/(\gamma_2-2)}}\right]\displaystyle\sum_{n=0}^{N_{\max}}\dfrac{(-1)^n}{(n!)^2}\left(\dfrac{1}{4\alpha^{2/(\gamma_2-2)}}\right)^n\Gamma\left(\dfrac{2(n+1)}{\gamma_2-2}\right) \\ \hspace{6cm}\boxed{\alpha > \alpha_{\text{transition}}} \end{cases},$$

where

$$Q_z = \hat{z}\cdot(\vec{k}-\vec{q}), \quad \underline{Q} = (1-\hat{z}\hat{z})\cdot(\vec{k}-\vec{q}), \quad S(\underline{Q}) = \frac{w_2}{(h_0 |\underline{Q}|)^{\gamma_2}}. \quad (3.20)$$

The terms of Q_z and $|\underline{Q}|$ can be evaluated using Eq. (1.12). The prefactor β is discussed in Section 1.4.2 and Appendix A. The quantities $N_{\max}$ and $\alpha_{\text{transition}}$ depend on γ_2, and are determined empirically. The results are summarized in Table 1.

Table 1 – Sum-transition parameter values for Eq. (3.20)

γ_2	3.1	3.2	3.3	3.4	3.5	3.6	3.7	3.8	3.9
$\alpha_{\text{transition}}$	0.39	0.25	0.20	0.15	0.12	0.08	0.05	0.03	0.025
$N_{\max}$	6545	610	155	93	62	60	62	67	54

The branch good for $\alpha \le \alpha_{\text{transition}}$ is an asymptotic expansion, and the best choice for the number of terms is typically $\max = 10$. The branch good for $\alpha > \alpha_{\text{transition}}$ in principle

always converges, but as γ_2 dips below 3.1, the expansion may be so slowly converging that it requires an impractical level of precision and number of terms. $\Gamma(x)$ is the Gamma function defined, for example, in Section 6 of reference [28]. The scaling constant h_0 is typically chosen to be 1 m. The parameter α is given by Eq. (3.14). Recall that $\alpha \to \infty$ when $\gamma_2 = 4$, and this two-series approach breaks down.

As discussed in references [29, 30], the region of validity of this two-series approach turns out to be limited to $\gamma_2 > 3$. The rational function approach extends the region of validity down to $\gamma_2 = 2.4$. The parameter region $2.4 < \gamma_2 < 3$ is relevant to the study of rocky ocean bottoms.

4 Introducing a peaked spectrum formed by taking the difference between two power laws

This section evaluates the integral I defined in Eq. (1.9) for a power-law spectrum of the form

$$S(\underline{l}) = S_1(\underline{l}) - S_2(\underline{l}), \tag{4.1}$$

where

$$S_1(\underline{l}) = \frac{b_1}{\left(1 + (b_2 h_0 l)^2\right)^{\gamma_2/2}} \quad ; \quad S_2(\underline{l}) = \frac{b_1}{\left(1 + \left(\frac{b_2 h_0 l}{a_2}\right)^2\right)^{\gamma_2/2}}. \tag{4.2}$$

Here, b_1, b_2 and a_2 are chosen to fit some surface spectrum. The autocorrelation function is given by

$$A(\underline{v}) = A_1(\underline{v}) - A_2(\underline{v})$$

$$A_1(\underline{v}) = \int d^2\underline{l}\, S_1(\underline{l}) e^{-i\underline{l}\cdot\underline{v}} \quad ; \quad A_2(\underline{v}) = \int d^2\underline{l}\, S_2(\underline{l}) e^{-i\underline{l}\cdot\underline{v}}.$$

One example is considered in the discussion surrounding Eqs. (43) of reference [6], where these parameters are adjusted to approximate the Toba ocean surface spectrum for $\gamma_2 = 3.5$. This section generates a general procedure valid for arbitrary $\gamma_2 > 2$.

4.1 Evaluating the autocorrelation function and $\rho(\underline{v})$

Once again, we need to evaluate Eq. (1.8), and the first step is to calculate $\rho(\underline{v}) = 2\left(A(0) - 2A(\underline{v})\right)$ and $\rho(\infty) = 2A(0)$. Follow the calculation in Section 3.1 that leads from Eq. (3.2) to (3.6) with the substitutions $w_2 \to b_1$ and $h_0 \to b_2 h_0$ to obtain:

24

$$A_1(v) = \frac{2\pi b_1 \left(\dfrac{v}{b_2 h_0}\right)^{\frac{\gamma_2}{2}-1} K_{\frac{\gamma_2}{2}-1}\left(\dfrac{v}{b_2 h_0}\right)}{b_2^2 h_0^2 2^{\frac{\gamma_2}{2}-1} \Gamma\left(\dfrac{\gamma_2}{2}\right)}.$$ (4.3)

Similarly, the substitutions $w_2 \to b_1$ and $h_0 \to b_2 h_0 / a_2$ lead to:

$$A_2(v) = \frac{a_2^2 2\pi b_1 \left(\dfrac{a_2 v}{b_2 h_0}\right)^{\frac{\gamma_2}{2}-1} K_{\frac{\gamma_2}{2}-1}\left(\dfrac{a_2 v}{b_2 h_0}\right)}{b_2^2 h_0^2 2^{\frac{\gamma_2}{2}-1} \Gamma\left(\dfrac{\gamma_2}{2}\right)}.$$ (4.4)

Thus,

$$A(v) = A_1(v) - A_2(v)$$

$$= \frac{2\pi b_1 \left(\dfrac{v}{b_2 h_0}\right)^{\frac{\gamma_2}{2}-1}}{b_2^2 h_0^2 2^{\frac{\gamma_2}{2}-1} \Gamma\left(\dfrac{\gamma_2}{2}\right)} \left(K_{\frac{\gamma_2}{2}-1}\left(\dfrac{v}{b_2 h_0}\right) - a_2^{1+\frac{\gamma_2}{2}} K_{\frac{\gamma_2}{2}-1}\left(\dfrac{a_2 v}{b_2 h_0}\right)\right).$$ (4.5)

We also need $A(0)$. To get this quantity, follow the procedure used in Section 3.2 to take the $v \to 0$ limit of Eq. (3.6). Take Eq. (4.5) and use Eq. (9.6.9) from reference [28] to get the first term of the expansion for $v/(b_2 h_0)$, and then take the limit:

$A(0) =$

$$\frac{2\pi b_1}{b_2^2 h_0^2 2^{\frac{\gamma_2}{2}-1} \Gamma\left(\dfrac{\gamma_2}{2}\right)} \lim_{v \to 0}\left[\left(\dfrac{v}{b_2 h_0}\right)^{\frac{\gamma_2}{2}-1} \frac{1}{2}\Gamma\left(\dfrac{\gamma_2}{2}-1\right) 2^{\frac{\gamma_2}{2}-1}\left(\left(\dfrac{v}{b_2 h_0}\right)^{-\frac{\gamma_2}{2}+1} - a_2^{1+\frac{\gamma_2}{2}}\left(\dfrac{a_2 v}{b_2 h_0}\right)^{-\frac{\gamma_2}{2}+1}\right)\right]$$

$$= \frac{\pi b_1}{b_2^2 h_0^2} \frac{\Gamma\left(\dfrac{\gamma_2}{2}-1\right)}{\Gamma\left(\dfrac{\gamma_2}{2}\right)}(1 - a_2^2).$$

Finally, use the standard identity $\Gamma(\gamma_2/2) = ((\gamma_2/2)-1)\Gamma((\gamma_2/2)-1)$ to get

$$A(0) = \frac{\pi b_1}{b_2^2 h_0^2} \frac{1}{\dfrac{\gamma_2}{2}-1}(1 - a_2^2).$$ (4.6)

Substituting into the Eq. (4.5), we get

$$A(v) = A(0)\left[\frac{\dfrac{\gamma_2}{2}-1}{1-a_2^2}\right] \frac{1}{2^{\frac{\gamma_2}{2}-2} \Gamma\left(\dfrac{\gamma_2}{2}\right)} \left(\dfrac{v}{b_2 h_0}\right)^{\frac{\gamma_2}{2}-1}\left(K_{\frac{\gamma_2}{2}-1}\left(\dfrac{v}{b_2 h_0}\right) - a_2^{1+\frac{\gamma_2}{2}} K_{\frac{\gamma_2}{2}-1}\left(\dfrac{a_2 v}{b_2 h_0}\right)\right)$$ (4.7)

and

$$\rho(\underline{v}) = 2A(0)\left[1 - \frac{A(\underline{v})}{A(0)}\right]$$

$$= 2A(0)\left[1 - \left[\frac{\frac{\gamma_2}{2} - 1}{1 - a_2^2}\right] \frac{\left(\frac{v}{b_2 h_0}\right)^{\frac{\gamma_2}{2} - 1}}{2^{\frac{\gamma_2}{2} - 2} \Gamma\left(\frac{\gamma_2}{2}\right)} \left(K_{\frac{\gamma_2}{2} - 1}\left(\frac{v}{b_2 h_0}\right) - a_2^{1 + \frac{\gamma_2}{2}} K_{\frac{\gamma_2}{2} - 1}\left(\frac{a_2 v}{b_2 h_0}\right)\right)\right].$$
(4.8)

Finally, we also have

$$\rho(\infty) = 2A(0) = \frac{2\pi b_1}{b_2^2 h_0^2} \frac{1}{\frac{\gamma_2}{2} - 1}\left(1 - a_2^2\right).$$
(4.9)

4.2 Expressing the coefficients in terms of the power-law notation

The spectrum given by Eqs. (4.1) and (4.2) depends on five variables: a_2, b_1, b_2, h_0 and γ_2. Typically, the variables known are the coefficient of the power law tail w_2 (see Eq. (1.13)) as well as h_0, γ_2, and the root mean-squared surface height $\zeta = \sqrt{\langle h^2 \rangle} = \sqrt{A(0)}$. Additionally, for the sea surface in general and sometimes (but not in general) for specific locations on the ocean bottom, the wavenumber location of the spectral peak l_p is known as well. The spectrum given by Eqs. (4.1) and (4.2) is designed for this contingency. Then, only three equations are needed in order to express a_2, b_1 and b_2 in terms of w_2, h_0, γ_2, l_p and ζ. These three equations are adapted from the conditions listed in the caption to Fig. 3 in reference [6].

4.2.1 Requirement 1: Tail behavior as $l \to \infty$

As $l \to \infty$, the spectrum should approach the asymptotic form, Eq. (1.13):

$$\lim_{l \to \infty}\left(S(\underline{l})\right) = \frac{b_1}{(b_2 h_0 l)^{\gamma_2}}\left[1 - a_2^{\gamma_2}\right] = \frac{w_2}{\left(h_0 |\underline{l}|\right)^{\gamma_2}}$$

or

$$b_1 = \frac{w_2 b_2^{\gamma_2}}{\left[1 - a_2^{\gamma_2}\right]}.$$
(4.10)

26

4.2.2 The spectrum has a maximum at l_p

The spectral peak occurs when the derivative is zero:

$$\left.\frac{dS}{dl}\right|_{l=l_p} = 0 .$$

This occurs when

$$\left.\frac{dS}{dl}\right|_{l=l_p} \propto \frac{1}{\left(1+\left(b_2 h_0 l_p\right)^2\right)^{1+\gamma_2/2}} - \frac{1}{a_2^2\left(1+\left(\frac{b_2 h_0 l_p}{a_2}\right)^2\right)^{1+\gamma_2/2}} = 0 .$$

Or solving for b_2

$$b_2 = \frac{1}{h_0 l_p}\left[\frac{a_2^{\left[\frac{2}{1+\gamma_2/2}\right]}-1}{1-a_2^{\left[\frac{2}{1+\gamma_2/2}-2\right]}}\right]^{\frac{1}{2}} . \tag{4.11}$$

It should be noted that for the ocean surface, a standard choice is $l_p = g/u^2$, though this is a little higher than the value of the peak wavenumber for the Pierson-Moskowitz spectrum.

Note that Eq. (4.11) can be substituted into Eq. (4.10) so that both b_1 and b_2 can be expressed in terms of a_2. It now remains to find a criterion for determining a_2.

4.2.3 Use the root mean-square surface height to obtain a_2

A spectrum of the form (4.1)/(4.2) cannot typically provide a spectrum that is peaked as sharply as the one implied by the criteria outlined following Eqs. (43a)-(43c) in reference [6] or as possessed by the widely-used Pierson-Moskowitz spectrum. To obtain the best approximation, use a_2 close to but less than one. In reference [6], the choice $a_2 = 0.9$ was made for the ocean surface. (Section 5 will introduce a method for making the spectrum even more sharply peaked, and present a technique for evaluating the corresponding cross-section.)

4.3 Summary and numerical implementation of the difference spectrum

Choose a_2 close to but less than one, then use condition (4.11) to obtain b_2, and finally use condition (4.10) to obtain b_1. Then, use Eq. (4.6) to obtain $A(0)$ followed by Eq.

(4.9) to get $\rho(\infty)$ and Eq. (4.8) to get $\rho(\underline{v})$. Then, substitute the values for $\rho(\infty)$ and $\rho(\underline{v})$ in a numerical evaluation of (1.10) rewritten in the form

$$\frac{\langle\sigma\rangle}{a} = \frac{|\beta|^2}{8\pi Q_z^2}\int_0^\infty v\,dv \left(e^{-\frac{Q_z^2}{2}\rho(\underline{v})} - e^{-\frac{Q_z^2}{2}\rho(\infty)} \right) J_0\left(|\underline{Q}|v\right). \tag{4.12}$$

(Since the δ-function is zero for all non-specular geometries – i.e., $\forall\underline{Q}\neq 0$, it is left out of Eq. (4.12).)

This integral may be solved numerically by following the procedure developed in reference [6]. The integrand has a period of π, and so the integration is performed for the following intervals:

$$0 \rightarrow y_0$$
$$y_0 \rightarrow y_0 + \pi$$
$$y_0 + \pi \rightarrow y_0 + 2\pi$$
$$\vdots$$
$$y_0 + (n_{max}-1)\pi \rightarrow y_0 + n_{max}\pi.$$

Experience gained in reference [6] indicated that $n_{max} = 40$ and $y_0 = {}^{3\pi}\!/_8$ were good choices for the air-sea interface parameters used there. The sum of the contributions from these intervals can be viewed as an alternating series of monotonically decreasing terms. As discussed in reference [6] convergence of such a series can be accelerated by averaging adjacent terms:

$$\sum_{n=0}^{n_{max}} (-1)^n \underbrace{u_n}_{>0} \rightarrow \frac{u_0}{2} + \sum_{n=1}^{n_{max}} \frac{(-1)^{n-1} u_{n-1} + (-1)^n u_n}{2}.$$

More recent work on the numerical evaluation of the integral in Eq. (4.12) has modified this picture [31]. For many parameter regimes of interest, the behavior of this integral differs profoundly from that encountered in reference [6]. In particular, note that Eq. (4.8) for $\rho(\underline{v})$ suggests the change of variables to $x = v/(b_2 h_0)$. Then, taken as a function of x, the envelope, which can be approximated as[f]

$$\sqrt{\frac{2x}{\pi|\underline{Q}|b_2 h_0}} \left(e^{-\frac{Q_z^2}{2}\rho(v(x))} - e^{-\frac{Q_z^2}{2}\rho(\infty)} \right),$$

is primarily influenced by the parameters γ_2 and a_2. Furthermore, the argument of the Bessel function becomes $|\underline{Q}|b_2 h_0 x$.

---

[f] The square root prefactor comes from $x J_0\left(|\underline{Q}|b_2 h_0 x\right) \approx \sqrt{2x/\pi|\underline{Q}|b_2 h_0}\,\cos\left(|\underline{Q}|b_2 h_0 x - \pi/4\right)$, where the cosine has been absorbed elsewhere.

A typical curve comparing the envelope and the Bessel function is shown in Fig. 3. It is best to perform a straight sum (i.e., without averaging adjacent terms) out to $x = x_p$, and then sum pairs of alternating values for about 10 additional terms.
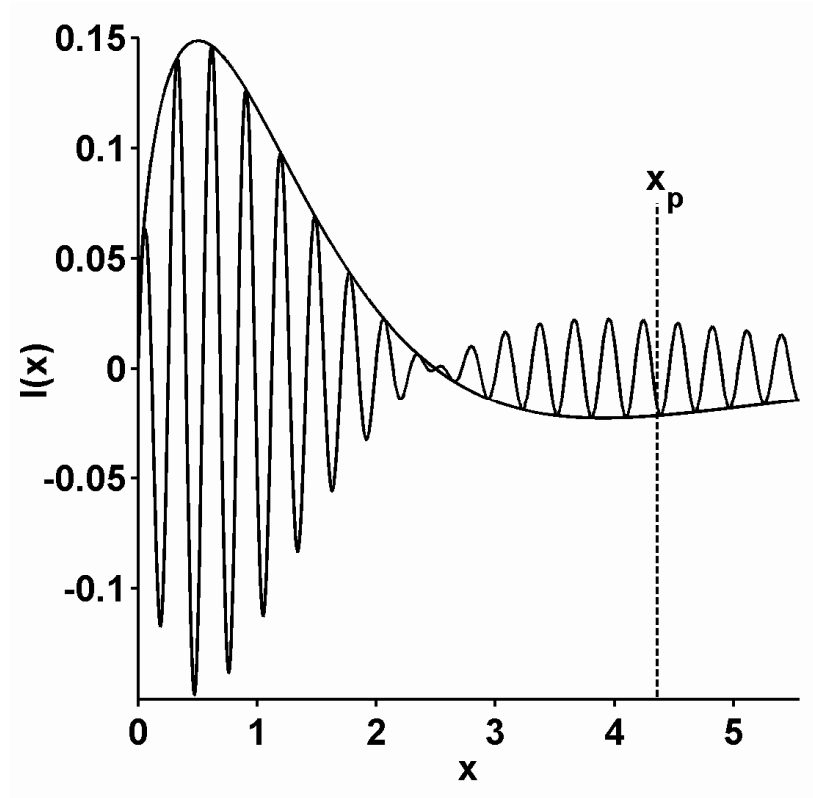
Fig. 3 - A typical curve comparing the envelope and the Bessel function in the integrand of Eq. (4.12). The plot is of the magnitude of these quantities vs. the parameter $x = v/(b_2 h_0)$. It is best to perform a straight sum out to a transition point $x = x_p$, and then sum pairs of alternating values for about 10 additional terms. As γ_2 varies from 2 to 4, the transition point x_p varies more or less linearly from 2.97 to 4.39. In this curve, $\theta_{in} = \theta_{out} = 20\,\mathrm{deg}$, $\varphi_{out} = 180\,\mathrm{deg}$, $u = 10\,\mathrm{m/s}$, $f = 400\,\mathrm{Hz}$, $k_p = g/u^2$, $w_2 = \left[\alpha_{TOBA}/(100\pi)\right]\sqrt{u^2/g}$ (with $\alpha_{TOBA} = 0.08$), $\gamma_2 = 4$ and $h_0 = 1$. The transition occurs at $x_p = 4.39$. These parameters reflect the examples examined in Section 6.

For a majority of parameter values, $|\underline{Q}|b_2 h_0$ is not small, and the number of terms to x_p is given by

$$n_p = \left(|\underline{Q}|b_2 h_0 x_p - 3\pi/4\right)\big/\pi + 1.$$

The total number of terms is $n_p + 10$.

In a few cases, $\left|\underline{Q}\right|b_2 h_0 \square\ 1$ and the envelope dominates the convergence–i.e., it becomes very small during the first oscillation of the Bessel function. In general, $\left|\underline{Q}\right|$ is small at low frequency, or when θ_{in} and θ_{out} are near $90°$, or when θ_{in} and θ_{out} are similar and ϕ_{out} is near $0°$. Likewise, b_2 is small for large k_p, which for the sea surface occurs at low wind speed U as, for example, $l_p \square\ g/U^{2}$ [g]. Then, one needs to integrate out to where the envelope is sufficiently small ($3\pi/4 + 10\pi$ beyond x_p is usually a good choice). A similar situation occurs if $\exp\left(-Q_z^2 \rho(\infty)/2\right)$ is very small. Then the envelope integration goes out to where $\exp\left(-Q_z^2 \rho(\underline{v}(\underline{x}))/2\right)$ is also very small.

For more details on the new numerics, see reference [21].

5 Sharpening the cutoff

As noted in Section 4.2.3 above, a spectrum of the form (4.1) (known as the difference spectrum) cannot be made as peaked as some standard spectra. Consider the ocean surface, w_2 and γ_2 are set by the relatively easily observed tail of the spectrum, l_p is widely acknowledged to be at least roughly in the vicinity of u^2/g, and the root mean square of the surface displacement is a measured quantity. These criteria are sufficient to impose a peak on the spectrum that must be sharper than is allowed by the difference spectrum. (As will be seen in Section 6, the difference spectrum in practice provides an adequately accurate description of the ocean surface spectrum.)

This section introduces two new spectra that have sharper peaks. Subsection 5.1 considers the spectrum generated when a lower cutoff is imposed on the spectrum considered above in Section 4. Subsection 5.2 considers a spectrum based on the Pierson-Moskowitz spectrum, but modified in such a way that the autocorrelation function can be expressed in closed form. The modified Pierson-Moskowitz spectrum will be explicitly compared to the true Pierson-Moskowitz spectrum and to the difference spectrum in Fig. 5 in Section 6. The impact of the modified Pierson-Moskowitz spectrum and the difference spectrum on the stochastic cross-section will also be discussed in Section 6 (along with the impact of using a pure power law spectrum and a step-function cutoff).

---

[g] In many cases, l_p goes as u^{-b}, where b is some fraction between 0.5 and 2. This result is fairly robust as the relation between l_p and u is modified in this way.

5.1 A spectrum generated by sharpening the low-frequency dropoff of the spectrum considered in Section 4

5.1.1 A step-function low-frequency cutoff

A new parameter Λ is introduced that sets a small wavenumber cutoff for the spectrum (see Fig. 1). The utility of this spectrum will be addressed in Section 6 below. Here we will derive the corresponding expression for $\rho(\underline{v})$ that must be substituted into Eq. (1.8) to evaluate the stochastic cross-section per unit area $\langle\sigma\rangle/a$.

The autocorrelation function is given by

$$A(\underline{v}) = \int d^2 l\, S(\underline{l})e^{-i\underline{l}\cdot\underline{v}} = \int_{|\underline{l}|>\Lambda} d^2 l\, S(\underline{l})e^{-i\underline{l}\cdot\underline{v}}.$$

Since we assume that the two-dimensional spectrum is angle-independent, we have

$$
\begin{aligned}
A(\underline{v}) &= \int_0^\infty dl\, 2\pi l S(l) J_0(lv) = \int_\Lambda^\infty dl\, 2\pi l S(l) J_0(lv) \\
&= \int_0^\infty dl\, 2\pi l S(l) J_0(lv) - \int_0^\Lambda dl\, 2\pi l S(l) J_0(lv)
\end{aligned}
\tag{5.1}
$$

Note that the cross-hatched area in Fig. 1 is effectively removed from the integral.

Formally, the spectrum is

$$
S(\underline{l}) = \begin{cases}
0 & |\underline{l}| < \Lambda \\[2ex]
\underbrace{\dfrac{b_1}{\left(1+(b_2 h_0 l)^2\right)^{\gamma_2/2}}}_{S_1(\underline{l})} - \underbrace{\dfrac{b_1}{\left(1+\left(\dfrac{b_2 h_0 l}{a_2}\right)^2\right)^{\gamma_2/2}}}_{S_2(\underline{l})} & |\underline{l}| > \Lambda
\end{cases},
\tag{5.2}
$$

and so, combining with Eq. (5.1), the autocorrelation function is

$$A(\underline{v}) = A_1(\underline{v}) - A_2(\underline{v}),\tag{5.3}$$

with

$$
\begin{aligned}
A_1(\underline{v}) &= \int_0^\infty dl\, 2\pi l S_1(l) J_0(lv) - \int_0^\Lambda dl\, 2\pi l S_1(l) J_0(lv) \\
A_2(\underline{v}) &= \int_0^\infty dl\, 2\pi l S_2(l) J_0(lv) - \int_0^\Lambda dl\, 2\pi l S_2(l) J_0(lv)
\end{aligned}
$$

The integrals from 0 to infinity just reproduce the values for $A_1(\underline{v})$ and $A_2(\underline{v})$ from Section 4 (from here on renamed $\left[A_1(\underline{v})\right]_{\Lambda=0}$ and $\left[A_2(\underline{v})\right]_{\Lambda=0}$). Thus, we have

$$A(\underline{v}) = \left[A(\underline{v})\right]_{\Lambda=0}$$

$$-\int_0^\Lambda dl\ 2\pi l \frac{b_1}{\left(1+\left(b_2 h_0 l\right)^2\right)^{\gamma_2/2}} J_0(lv) + \int_0^\Lambda dl\ 2\pi l \frac{b_1}{\left(1+\left(\dfrac{b_2 h_0 l}{a_2}\right)^2\right)^{\gamma_2/2}} J_0(lv), \quad (5.4)$$

where $\left[A(\underline{v})\right]_{\Lambda=0} = \left[A_1(\underline{v})\right]_{\Lambda=0} - \left[A_2(\underline{v})\right]_{\Lambda=0}$ is evaluated using Eqs. (4.3) and (4.4). The finite integrals will need to be evaluated numerically.

Finally, we need to evaluate $A(0)$. Recall that Eq. (4.6) provides a value for the autocorrelation function in the absence of a cutoff: $\left[A(0)\right]_{\Lambda=0}$. Introducing a non-zero cutoff Λ, we now have

$$A(0) = \left[A(0)\right]_{\Lambda=0} \overbrace{-2\pi \int_0^\Lambda ldl \frac{b_1}{\left(1+\left(b_2 h_0 l\right)^2\right)^{\frac{\gamma_2}{2}}}}^{I_1} + \overbrace{2\pi \int_0^\Lambda ldl \frac{b_1}{\left(1+\left(\dfrac{b_2 h_0 l}{a_2}\right)^2\right)^{\frac{\gamma_2}{2}}}}^{I_2}.$$

Making the change of variable $u = b_2^2 h_0^2 l^2$ to obtain

$$I_1 = \frac{b_1}{2 b_2^2 h_0^2 \left(1 - \dfrac{\gamma_2}{2}\right)} \left(\left(1 + b_2^2 h_0^2 \Lambda^2\right)^{(1-\gamma_2/2)} - 1\right)$$

and then substitute $b_2 \to b_2/a_2$ to get

$$I_2 = \frac{b_1 a_2^2}{2 b_2^2 h_0^2 \left(1 - \dfrac{\gamma_2}{2}\right)} \left(\left(1 + \left(\dfrac{b_2 h_0 \Lambda}{a_2}\right)^2\right)^{(1-\gamma_2/2)} - 1\right).$$

This leads to

$$A(0) = \left[A(0)\right]_{\Lambda=0} + \frac{\pi b_1}{b_2^2 h_0^2 \left(1 - \dfrac{\gamma_2}{2}\right)} \left(a_2^2 \left(1 + \left(\dfrac{b_2 h_0 \Lambda}{a_2}\right)^2\right)^{(1-\gamma_2/2)} - \left(1 + \left(b_2 h_0 \Lambda\right)^2\right)^{(1-\gamma_2/2)} + \underbrace{1 - a_2^2}_{\text{Cancels } \left[A(0)\right]_{\Lambda=0}}\right)$$

or

$$A(0) = \frac{\pi b_1}{b_2^2 h_0^2 \left(\dfrac{\gamma_2}{2} - 1\right)} \underbrace{\left(\left(1 + \left(b_2 h_0 \Lambda\right)^2\right)^{(1-\gamma_2/2)} - a_2^2 \left(1 + \left(\dfrac{b_2 h_0 \Lambda}{a_2}\right)^2\right)^{(1-\gamma_2/2)}\right)}_{\text{Properly reduces to } 1-a_2^2 \text{ for } \Lambda=0}. \quad (5.5)$$

Note that

$$\frac{\left[A(0)\right]_{\Lambda=0}}{A(0)} = \frac{1-a_2^2}{\left(1+\left(b_2 h_0 \Lambda\right)^2\right)^{(1-\gamma_2/2)} - a_2^2\left(1+\left(\frac{b_2 h_0 \Lambda}{a_2}\right)^2\right)^{(1-\gamma_2/2)}}. \quad (5.6)$$

Now, using the definition of $\rho(\underline{v})$ and Eq. (5.4):

$$\rho(\underline{v}) = 2A(0)\left[1-\frac{A(\underline{v})}{A(0)}\right]$$

$$= 2A(0)\left[1-\frac{\left[A(\underline{v})\right]_{\Lambda=0}}{A(0)}\right]$$

$$+4\pi\int_0^\Lambda dl\, l\,\frac{b_1}{\left(1+\left(b_2 h_0 l\right)^2\right)^{\gamma_2/2}} J_0(lv) - 4\pi\int_0^\Lambda dl\, l\,\frac{b_1}{\left(1+\left(\frac{b_2 h_0 l}{a_2}\right)^2\right)^{\gamma_2/2}} J_0(lv)$$

$$= 2A(0)\left[1-\frac{\left[A(\underline{v})\right]_{\Lambda=0}}{\left[A(0)\right]_{\Lambda=0}}\frac{\left[A(0)\right]_{\Lambda=0}}{A(0)}\right]$$

$$+4\pi\int_0^\Lambda dl\, l\,\frac{b_1}{\left(1+\left(b_2 h_0 l\right)^2\right)^{\gamma_2/2}} J_0(lv) - 4\pi\int_0^\Lambda dl\, l\,\frac{b_1}{\left(1+\left(\frac{b_2 h_0 l}{a_2}\right)^2\right)^{\gamma_2/2}} J_0(lv).$$

Using (4.7) to evaluate $\left[A(\underline{v})\right]_{\Lambda=0}\big/\left[A(0)\right]_{\Lambda=0}$ and Eq. (5.6) to evaluate $\left[A(0)\right]_{\Lambda=0}\big/A(0)$, we have

$$\rho(\underline{v}) = 2A(0)\left[1-\alpha\beta\right] + 4\pi b_1\int_0^\Lambda ldl\, J_0(lv)\left[\frac{1}{\left(1+\left(b_2 h_0 l\right)^2\right)^{\gamma_2/2}} - \frac{1}{\left(1+\left(\frac{b_2 h_0 l}{a_2}\right)^2\right)^{\gamma_2/2}}\right], \quad (5.7)$$

where

33

$$\alpha \equiv \frac{\dfrac{\gamma_2}{2}-1}{\underbrace{\left(1+\left(b_2 h_0 \Lambda\right)^2\right)^{(1-\gamma_2/2)}-a_2^2\left(1+\left(\dfrac{b_2 h_0 \Lambda}{a_2}\right)^2\right)^{(1-\gamma_2/2)}}_{\text{Properly reduces to } 1-a_2^2 \text{ for } \Lambda=0}} .$$

(5.8)

$$\beta \equiv \frac{\left(\dfrac{v}{b_2 h_0}\right)^{\frac{\gamma_2}{2}-1}}{2^{\frac{\gamma_2}{2}-2}\Gamma\left(\dfrac{\gamma_2}{2}\right)}\left(K_{\frac{\gamma_2}{2}-1}\left(\dfrac{v}{b_2 h_0}\right)-a_2^{1+\frac{\gamma_2}{2}}K_{\frac{\gamma_2}{2}-1}\left(\dfrac{a_2 v}{b_2 h_0}\right)\right)$$

The finite integral from 0 to Λ can be evaluated numerically using a standard method such as Gaussian quadratures.

Note that $\lim_{x\to\infty}\left[K_v(x)\right]$ approaches zero exponentially and $\lim_{x\to\infty}J_0(x)\to 0$, and use Eq. (5.5) to evaluate $A(0)$:

$$\rho(\infty)=2A(0)$$

$$=\frac{2\pi b_1}{b_2^2 h_0^2\left(\dfrac{\gamma_2}{2}-1\right)}\underbrace{\left(\left(1+\left(b_2 h_0 \Lambda\right)^2\right)^{(1-\gamma_2/2)}-a_2^2\left(1+\left(\dfrac{b_2 h_0 \Lambda}{a_2}\right)^2\right)^{(1-\gamma_2/2)}\right)}_{\text{Properly reduces to } 1-a_2^2 \text{ for } \Lambda=0}.$$

(5.9)

In summary, for the spectrum with a sharp cutoff, Eqs. (5.5), (5.7) and (5.8) give $\rho(v)$ and Eq. (5.9) gives $\rho(\infty)$. This is then substituted into Eq. (1.8) to obtain the stochastic cross-section per unit area.

5.1.2 An exponential low-frequency cutoff

Now, consider a spectrum cutoff at low wavenumbers by an exponential. In addition to the parameter Λ introduced in the last subsection, we need to add two more parameters:

- c, a measure of the concavity of the relevant section of the exponential curve. For $c>0$, the spectrum is concave from the right. For $c\gg 0$, the section of the spectrum between $l=b$ and $l=\Lambda$ is very concave from the right, while for $c\approx 0$, the section is nearly linear. For $c<0$, the spectrum is concave from the left (see the left bound of the black area in Fig. 1).
- b, the x-intercept point.

The cutoff parameters Λ, b are both positive and $b<\Lambda$. The parameters Λ, c and b appear in the spectrum as follows:

$$S(\underline{l}) = \begin{cases} 0 & l < b \\[2ex] S(\Lambda)\dfrac{e^{c(\Lambda-b)}-e^{c(\Lambda-l)}}{e^{c(\Lambda-b)}-1} & b < l < \Lambda \\[3ex] \underbrace{\dfrac{b_1}{\left(1+(b_2 h_0 l)^2\right)^{\gamma_2/2}}}_{S_1(\underline{l})} - \underbrace{\dfrac{b_1}{\left(1+\left(\dfrac{b_2 h_0 l}{a_2}\right)^2\right)^{\gamma_2/2}}}_{S_2(\underline{l})} & l \geq \Lambda \end{cases} \qquad (5.10)$$

Recall that $l \equiv |\underline{l}|$. This spectrum is illustrated in Fig. 1.

As before, the stochastic cross-section per unit area is calculated using the formula (1.10). This equation is integrated numerically. To evaluate formula (1.10), we need the quantities $\rho(v)$ and $\rho(\infty)$ corresponding to spectrum (5.10). Since $\rho(v) \equiv 2(A(0) - A(v))$, it follows that we must take the Fourier transform of spectrum (5.10) to find the autocorrelation function $A(v)$. We need to be able to evaluate this quantity for arbitrary v positive and finite, and we also need to determine its value as we take the limits $v \to 0$ and $v \to \infty$.

The autocorrelation function associated with this spectrum differs from the autocorrelation function generated in Subsection 5.1.1 in that the Fourier transform includes a contribution from the area under the exponential (i.e., the area in black). Thus Eq. (5.4) becomes

$$A(\underline{v}) = \left[A(\underline{v})\right]_{\Lambda=0}$$

$$-\int_0^\Lambda dl\ 2\pi l \frac{b_1}{\left(1+(b_2 h_0 l)^2\right)^{\gamma_2/2}} J_0(lv) + \int_0^\Lambda dl\ 2\pi l \frac{b_1}{\left(1+\left(\dfrac{b_2 h_0 l}{a_2}\right)^2\right)^{\gamma_2/2}} J_0(lv)$$

$$+ \frac{2\pi S(\Lambda)}{e^{c(\Lambda-b)}-1}\left(e^{c(\Lambda-b)}\int_b^\Lambda dl\ l J_0(lv) - e^{c\Lambda}\int_b^\Lambda dl\ l J_0(lv)e^{-cl}\right) \qquad (5.11)$$

$$= \left[A(\underline{v})\right]_{\text{step}} + \frac{2\pi S(\Lambda)}{e^{c(\Lambda-b)}-1}\left(e^{c(\Lambda-b)}\int_b^\Lambda dl\ l J_0(lv) - e^{c\Lambda}\int_b^\Lambda dl\ l J_0(lv)e^{-cl}\right).$$

Note that from Eq. (5.4), $\left[A(\underline{v})\right]_{\text{step}}$ is the autocorrelation function corresponding to the step-function cutoff discussed in Section 5.1.1 above.

Next, we need to evaluate $A(0)$. Recall that Eq. (5.5) provides a value for the autocorrelation function corresponding to the step-function cutoff: $\left[A(0)\right]_{\text{step}}$. Setting $v=0$ in Eq. (5.11) and noting that $J_0(0)=1$, we obtain $A(0)$ corresponding to the spectrum given in Eq. (5.10):

$$A(0)=\left[A(0)\right]_{\text{step}}+\frac{2\pi S(\Lambda)}{e^{c(\Lambda-b)}-1}\left(e^{c(\Lambda-b)}\int_b^\Lambda dl\, l-e^{c\Lambda}\int_b^\Lambda dl\, le^{-cl}\right). \qquad (5.12)$$

Evaluating the trivial integrals in Eq. (5.12) leads to

$$A(0)=\left[A(0)\right]_{\text{step}}+\frac{2\pi S(\Lambda)}{e^{c(\Lambda-b)}-1}\left(e^{c(\Lambda-b)}\left(\frac{\left(\Lambda^2-b^2\right)}{2}-\left(\frac{1}{c^2}+\frac{b}{c}\right)\right)+\left[\left(\frac{1}{c^2}+\frac{\Lambda}{c}\right)\right]\right). \qquad (5.13)$$

Now, using the definition of $\rho(v)$ as well as Eq. (5.11) for $A(v)$ and Eq. (5.13) for $A(0)$, we have

$$\begin{aligned}
\rho(v)&=2A(0)-2A(v)\\
&=2\left(\left[A(0)\right]_{\text{step}}+\frac{2\pi S(\Lambda)}{e^{c(\Lambda-b)}-1}\left(e^{c(\Lambda-b)}\left(\frac{\left(\Lambda^2-b^2\right)}{2}-\left(\frac{1}{c^2}+\frac{b}{c}\right)\right)+\left[\left(\frac{1}{c^2}+\frac{\Lambda}{c}\right)\right]\right)\right)\\
&\quad -2\left(\left[A(v)\right]_{\text{step}}+\frac{2\pi S(\Lambda)}{e^{c(\Lambda-b)}-1}\left(e^{c(\Lambda-b)}\int_b^\Lambda dl\, lJ_0(lv)-e^{c\Lambda}\int_b^\Lambda dl\, lJ_0(lv)e^{-cl}\right)\right) \qquad (5.14)\\
&=\rho_{\text{step}}(v)+\frac{4\pi S(\Lambda)}{e^{c(\Lambda-b)}-1}\left(e^{c(\Lambda-b)}\left(\frac{\left(\Lambda^2-b^2\right)}{2}-\left(\frac{1}{c^2}+\frac{b}{c}\right)\right)+\left[\left(\frac{1}{c^2}+\frac{\Lambda}{c}\right)\right]\right)\\
&\quad -\frac{4\pi S(\Lambda)}{e^{c(\Lambda-b)}-1}\left(e^{c(\Lambda-b)}\int_b^\Lambda dl\, lJ_0(lv)-e^{c\Lambda}\int_b^\Lambda dl\, lJ_0(lv)e^{-cl}\right).
\end{aligned}$$

Equation (5.7) gives us the value of ρ for the step function $\rho_{\text{step}}(v)$, which we substitute into Eq. (5.14) to obtain:

$$\rho(\underline{v}) = \left| 2A_{\text{step}}(0)[1-\alpha\beta] + 4\pi b_1 \int_0^\Lambda l\,dl\, J_0(lv) \left[\frac{1}{\left(1+(b_2 h_0 l)^2\right)^{\gamma_2/2}} - \frac{1}{\left(1+\left(\dfrac{b_2 h_0 l}{a_2}\right)^2\right)^{\gamma_2/2}} \right] \right|$$

$$+ \frac{4\pi S(\Lambda)}{e^{c(\Lambda-b)}-1}\left(e^{c(\Lambda-b)}\left(\frac{(\Lambda^2-b^2)}{2} - \left(\frac{1}{c^2}+\frac{b}{c}\right)\right) + \left[\left(\frac{1}{c^2}+\frac{\Lambda}{c}\right)\right]\right) \qquad (5.15)$$

$$- \frac{4\pi S(\Lambda)}{e^{c(\Lambda-b)}-1}\left(e^{c(\Lambda-b)}\int_b^\Lambda dl\, lJ_0(lv) - e^{c\Lambda}\int_b^\Lambda dl\, lJ_0(lv)e^{-cl} \right).$$

α and β are given by Eq. (5.8) and $A_{\text{step}}(0)$ is given by Eq. (5.5). These equations are repeated here for clarity:

$$\alpha \equiv \frac{\dfrac{\gamma_2}{2}-1}{\left(1+(b_2 h_0 \Lambda)^2\right)^{(1-\gamma_2/2)} - a_2^2\left(1+\left(\dfrac{b_2 h_0 \Lambda}{a_2}\right)^2\right)^{(1-\gamma_2/2)}}, \qquad (5.16)$$

$$\beta \equiv \frac{\left(\dfrac{v}{b_2 h_0}\right)^{\frac{\gamma_2}{2}-1}}{2^{\frac{\gamma_2}{2}-2}\Gamma\left(\dfrac{\gamma_2}{2}\right)}\left(K_{\frac{\gamma_2}{2}-1}\left(\frac{v}{b_2 h_0}\right) - a_2^{1+\frac{\gamma_2}{2}} K_{\frac{\gamma_2}{2}-1}\left(\frac{a_2 v}{b_2 h_0}\right)\right)$$

$$A_{\text{step}}(0) = \frac{\pi b_1}{b_2^2 h_0^2\left(\dfrac{\gamma_2}{2}-1\right)}\left(\left(1+(b_2 h_0 \Lambda)^2\right)^{(1-\gamma_2/2)} - a_2^2\left(1+\left(\dfrac{b_2 h_0 \Lambda}{a_2}\right)^2\right)^{(1-\gamma_2/2)}\right). \qquad (5.17)$$

(The boxed quantity in Eq. (5.15) corresponds to Eq. (5.7), the result $\rho_{\text{step}}(\underline{v})$ for the difference spectrum with a step cutoff.)

Finally, recall that in addition to $\rho(v)$, its limit as $v\to\infty$, $\rho(\infty)$, also appears in the expression for the scattering cross-section, Eq. (1.10). To obtain this quantity, once again note that $\lim_{x\to\infty} J_0(x)\to 0$, and so $A(\infty)=0$. Use Eq. (5.13) to evaluate $A(0)$:

$$\rho(\infty) = 2A(0)$$

$$= 2\left[A(0)\right]_{\text{step}} + \frac{4\pi S(\Lambda)}{e^{c(\Lambda-b)}-1}\left(e^{c(\Lambda-b)}\left(\frac{(\Lambda^2-b^2)}{2}-\left(\frac{1}{c^2}+\frac{b}{c}\right)\right)+\left[\left(\frac{1}{c^2}+\frac{\Lambda}{c}\right)\right]\right). \quad (5.18)$$

We can substitute for $A_{\text{step}}(0)$ using Eq. (5.17):

$$\rho(\infty) = \frac{2\pi b_1}{b_2^2 h_0^2\left(\dfrac{\gamma_2}{2}-1\right)}\left(\left(1+\left(b_2 h_0\Lambda\right)^2\right)^{(1-\gamma_2/2)}-a_2^2\left(1+\left(\frac{b_2 h_0\Lambda}{a_2}\right)^2\right)^{(1-\gamma_2/2)}\right)$$

$$+\frac{4\pi S(\Lambda)}{e^{c(\Lambda-b)}-1}\left(e^{c(\Lambda-b)}\left(\frac{(\Lambda^2-b^2)}{2}-\left(\frac{1}{c^2}+\frac{b}{c}\right)\right)+\left[\left(\frac{1}{c^2}+\frac{\Lambda}{c}\right)\right]\right) . \quad (5.19)$$

In summary, for the spectrum with an exponential cutoff, $\rho(v)$ is given by Eq. (5.15) supplemented with Eq. (5.17) to give $A_{\text{step}}(0)$ and Eq. (5.16) to give α and β. $\rho(\infty)$ is given by Eq. (5.19). These results are then substituted into Eq. (1.10), which is evaluated numerically to obtain the stochastic cross-section per unit area.

5.1.3 Discussion: the difference spectra with step and exponential cutoffs

The difference spectrum with a step function cutoff suffers from anomalies and can be overly sensitive to parameter values (e.g., see Fig. 7 and related discussion in Section 6.2). It should therefore be used very carefully and sparingly–in particular the cutoff parameter Λ should be kept well below the wavenumber of the spectral peak. (Recall that in our implementation, Λ is generally between the peak of the difference spectrum and zero.) The difference spectrum with an exponential cutoff is more stable, but to avoid problems similar to those encountered with the step cutoff, the exponential slope parameter c should be kept small enough that the exponent cutoff to the difference spectrum does not closely resemble the step-function cutoff and consequently suffer from its drawbacks. As discussed in Section 8, the exponential cutoff provides a peak-sharpening correction to the difference spectrum in cases where this effect needs to be studied for non-integer values of γ_2.

Recall that the exponential cutoff is designed to be inserted between the peak of the difference spectrum and zero. Under these circumstances, it should be noted that while the exponential cutoff provides a narrower peak, it does not increase the height of the peak (keeping the tail behavior fixed). This is the big limitation of all cutoff difference spectra. Some spectra for the air-sea interface, such as the Pierson-Moskowitz spectrum, are characterized by very large spectral values near the peak relative to the values along

the power-law tail. A numerically tractable spectrum that can in principle provide better models for this spectrum is examined next.

5.2 A <u>modified</u> *Pierson-Moskowitz spectrum*

Section 5.2.1 considers a <u>modified</u> Pierson-Moskowitz spectrum of the form

$$S(\underline{l}) = \frac{w_2 e^{-a/l}}{(h_0 l)^4}. \tag{5.20}$$

This differs from a true Pierson-Moskowitz spectrum in power of $1/l$ in the exponential. This quantity would be squared in a true Pierson-Moskowitz spectrum. This spectrum for the air-sea interface is defined in reference [32] and included here for completeness:

$$S(\underline{l}) = \frac{\alpha}{4\pi l^4} e^{\left[-\left(\beta g^2\right)/\left(u^4 l^2\right)\right]} \tag{5.21}$$

with $\alpha = 8.10 \times 10^{-3}$ and $\beta = 0.74$.

The modified spectrum is considered because this spectrum can be Fourier transformed to generate a closed-form expression for the autocorrelation function $A(\underline{v})$, which can in turn be substituted into $\rho(\underline{v}) = 2\left(A(0) - A(\underline{v})\right)$ in the integrand of integral (1.9). Note that the spectrum peak occurs at

$$l_p = \frac{a}{4}.$$

For the Pierson-Moskowitz spectrum, it turns out that $l_p \approx 0.6 g/u^2$, while in the discussion of the peaked spectrum made up of a difference of power laws, we noted that $l_p = g/u^2$ is a standard choice. (The difference spectrum is very flexible, and another choice for l_p could have been imposed on this spectrum as well.) In the examples considered in Section 6, the difference spectra will use the standard choice of $l_p = g/u^2$.

Section 5.2.2 considers a further modification to the Pierson-Moskowitz spectrum. It is characterized by a tail of $1/l^3$ rather than the standard $1/l^4$. This spectrum resembles a spectrum that has been used to model the ocean bottom [3, 33]. Furthermore, the result can in the future be used to benchmark other calculations along the lines of those discussed in Sections 5.1 and 6.

5.2.1 Standard $1/l^4$ power law tail

The autocorrelation function corresponding to spectrum (5.20) is given by the integral

$$A(\underline{v}) = \int d^2l\, S(\underline{l})e^{i\underline{l}\cdot\underline{v}} = \frac{w_2}{h_0^4}\int_0^\infty dl\, l\frac{e^{-a/l}}{l^4}\underbrace{\int_0^{2\pi}d\varphi}_{2\pi}\underbrace{\int_0^\pi d\theta e^{ilv\cos\theta}}_{J_0(lv)}$$

or

$$A(\underline{v}) = \frac{2\pi w_2}{h_0^4}\int_0^\infty dl\, \frac{e^{-a/l}}{l^3}J_0(lv) = \frac{2\pi w_2}{h_0^4}\frac{d^2}{da^2}\left[\int_0^\infty dl\, \frac{e^{-a/l}}{l}J_0(lv)\right].$$

The quantity in the brackets is a Hankel transform that can once again be evaluated using entry (15), Section 8.6 of reference [27]:

$$\int_0^\infty \frac{e^{-a/x}}{x^{3/2}}J_0(xy)x^{1/2}y^{1/2}dx = 2y^{1/2}J_0\left(\sqrt{2ay}\right)K_0\left(\sqrt{2ay}\right),$$

or, making the substitutions $x \to l$ and $y \to v$

$$\int_0^\infty \frac{e^{-a/l}}{l}J_0(lv)dl = 2J_0\left(\sqrt{2av}\right)K_0\left(\sqrt{2av}\right).$$

This leaves us with

$$A(\underline{v}) = \frac{4\pi w_2}{h_0^4}\frac{d^2}{da^2}\left[J_0\left(\sqrt{2av}\right)K_0\left(\sqrt{2av}\right)\right].$$

Evaluation of the second derivative is trivial. Maple[®] was used to take the derivatives and following further simplification, we have:

$$A(\underline{v}) = \frac{4\pi w_2}{h_0^4}\left[\begin{array}{l}\frac{\sqrt{2av}}{2a^2}\left(J_1\left(\sqrt{2av}\right)K_0\left(\sqrt{2av}\right)+J_0\left(\sqrt{2av}\right)K_1\left(\sqrt{2av}\right)\right)\\[2mm]+\frac{v}{a}J_1\left(\sqrt{2av}\right)K_1\left(\sqrt{2av}\right)\end{array}\right] \qquad (5.22)$$

for the spectrum given in Eq. (5.20).

We also have

$$A(0) = \frac{4\pi w_2}{h_0^4}\left[\begin{array}{l}\frac{1}{2a^2}\left(\begin{array}{l}\underbrace{\lim_{\sqrt{2av}\to 0}\left(J_1\left(\sqrt{2av}\right)\sqrt{2av}K_0\left(\sqrt{2av}\right)\right)}_{0}\\[2mm]+\underbrace{\lim_{\sqrt{2av}\to 0}\left(J_0\left(\sqrt{2av}\right)\sqrt{2av}K_1\left(\sqrt{2av}\right)\right)}_{1}\end{array}\right)\\[4mm]+\frac{1}{a}\underbrace{\lim_{\sqrt{2av}\to 0}\left(J_1\left(\sqrt{2av}\right)vK_1\left(\sqrt{2av}\right)\right)}_{0}\end{array}\right] = \frac{2\pi w_2}{a^2 h_0^4} \qquad (5.23)$$

and

40

$$A(\infty) = \frac{4\pi w_2}{h_0^4} \left[\frac{1}{2a^2} \left[\underbrace{\lim_{\sqrt{2av}\to\infty} \left(J_1\left(\sqrt{2av}\right)\sqrt{2av}K_0\left(\sqrt{2av}\right)\right)}_{0} + \underbrace{\lim_{\sqrt{2av}\to\infty} \left(J_0\left(\sqrt{2av}\right)\sqrt{2av}K_1\left(\sqrt{2av}\right)\right)}_{0} \right] + \frac{1}{a}\underbrace{\lim_{\sqrt{2av}\to\infty} \left(J_1\left(\sqrt{2av}\right)vK_1\left(\sqrt{2av}\right)\right)}_{0} \right] = 0. \qquad (5.24)$$

This gives us for the "$1/l^4$ modified Pierson-Moskowitz" spectrum defined by Eq. (5.20):

$$\rho(v) \equiv 2\left[A(0) - A(v)\right]$$

$$= \frac{4\pi w_2}{a^2 h_0^4}\left[1 - 2\left[\frac{\sqrt{2av}}{2}\left(J_1\left(\sqrt{2av}\right)K_0\left(\sqrt{2av}\right) + J_0\left(\sqrt{2av}\right)K_1\left(\sqrt{2av}\right)\right) + avJ_1\left(\sqrt{2av}\right)K_1\left(\sqrt{2av}\right)\right]\right] \qquad (5.25)$$

and

$$\rho(\infty) \equiv 2\left[A(0) - A(\infty)\right]$$
$$= \frac{4\pi w_2}{a^2 h_0^4}. \qquad (5.26)$$

The results of Eqs. (5.25) and (5.26) can now be substituted into Eq. (1.8), and the integral I defined by Eq. (1.9) can now once again be evaluated numerically.

Note that as $a \to 0$, $A(v) \to 0$ as $1/a^2$ (as does $\rho(v)$). Given that a pure power law like (1.13) cut off by a step function has a similar singularity as $a \to 0$:

$$A(v) = \int d^2\underline{l}\, S(\underline{l})e^{i\underline{L}\cdot\underline{v}} = 2\pi\int_0^\infty dl\, lS(l)J_0(lv) = \frac{2\pi w_2}{h_0^4}\lim_{a\to 0}\int_a^\infty dl\,\frac{J_0(lv)}{l^3} \square \lim_{a\to 0}\frac{1}{a^2},$$

this is exactly the behavior we would expect. Note that Eqs. (3.7) and (3.8) correspond to a different kind of low-wavenumber cutoff that does not lend itself to a direct comparison.

5.2.2 A $1/l^3$ power-law tail

Now, we consider the spectrum

$$S(\underline{l}) = \frac{w_2 e^{-a/l}}{(h_0 l)^3}. \qquad (5.27)$$

Note that the "$1/l^3$ modified Pierson-Moskowitz" spectrum defined by Eq. (5.27) can be used to describe some rough ocean bottoms or as a one-dimensional version of the $1/l^4$ case.

Spectrum (5.27) implies the autocorrelation function

$$A(\underline{v}) = \frac{2\pi w_2}{h_0^3} \int_0^\infty dl \ \frac{e^{-a/l}}{l^2} J_0(lv)$$

$$= \frac{2\pi w_2}{h_0^3} (-1) \frac{d}{da} \left[\int_0^\infty dl \ \frac{e^{-a/l}}{l} J_0(lv) \right] \qquad .$$

$$= \frac{4\pi w_2}{h_0^3} (-1) \frac{d}{da} \left[J_0\left(\sqrt{2av}\right) K_0\left(\sqrt{2av}\right) \right]$$

(5.28)

Now,

$$(-1) \frac{d}{da} \left[J_0\left(\sqrt{2av}\right) K_0\left(\sqrt{2av}\right) \right]$$

$$= \frac{\sqrt{2av}}{2a} \left[\left(J_1\left(\sqrt{2av}\right) K_0\left(\sqrt{2av}\right) + J_0\left(\sqrt{2av}\right) K_1\left(\sqrt{2av}\right) \right) \right]$$

and

$$A(\underline{v})$$

$$= \frac{2\pi w_2}{ah_0^3} \sqrt{2av} \left[\left(J_1\left(\sqrt{2av}\right) K_0\left(\sqrt{2av}\right) + J_0\left(\sqrt{2av}\right) K_1\left(\sqrt{2av}\right) \right) \right] .$$

(5.29)

It follows that

$$A(0)$$

$$= \frac{2\pi w_2}{ah_0^3} \left(\underbrace{\lim_{\sqrt{2av} \to 0} \left(J_1\left(\sqrt{2av}\right) \sqrt{2av} K_0\left(\sqrt{2av}\right) \right)}_{0} + \underbrace{\lim_{\sqrt{2av} \to 0} \left(J_0\left(\sqrt{2av}\right) \sqrt{2av} K_1\left(\sqrt{2av}\right) \right)}_{1} \right)$$

$$= \frac{2\pi w_2}{ah_0^3}$$

and

$$A(\infty)$$

$$= \frac{2\pi w_2}{ah_0^3} \left(\underbrace{\lim_{\sqrt{2av} \to \infty} \left(J_1\left(\sqrt{2av}\right) \sqrt{2av} K_0\left(\sqrt{2av}\right) \right)}_{0} + \underbrace{\lim_{\sqrt{2av} \to \infty} \left(J_0\left(\sqrt{2av}\right) \sqrt{2av} K_1\left(\sqrt{2av}\right) \right)}_{0} \right)$$

$$= 0.$$

This gives us for the "$1/l^3$ modified Pierson-Moskowitz" spectrum defined by Eq. (5.27):

$$\rho(\underline{v}) \equiv 2\left[A(0) - A(\underline{v}) \right]$$

$$= \frac{4\pi w_2}{ah_0^3} \left[1 - \sqrt{2av} \left[\left(J_1\left(\sqrt{2av}\right) K_0\left(\sqrt{2av}\right) + J_0\left(\sqrt{2av}\right) K_1\left(\sqrt{2av}\right) \right) \right] \right]$$

(5.30)

and

$$\rho(\infty) \equiv 2\left[A(0) - \cancel{A(\infty)}\right] = \frac{4\pi w_2}{ah_0^3}. \tag{5.31}$$

The results of Eqs. (5.30) and (5.31) can now be substituted into Eq. (1.8), and the integral I defined by Eq. (1.9) can now once again be evaluated numerically.

5.2.3 Issues related to the numerical implementation of the <u>modified</u> Pierson-Moskowitz spectrum

The numerical implementation of the <u>modified</u> Pierson-Moskowitz spectrum resembles that for the difference spectrum described at the end of Section 4.3. The key difference results from the fact that the parameter $\rho(\underline{v})$ defined by equations (5.25) and (5.30) involves Bessel functions of the first kind $J_0\left(\sqrt{2av}\right)$ and $J_1\left(\sqrt{2av}\right)$. This modifies the scenario presented by Fig. 3 since now the envelope itself oscillates. Thus, the case of $|\underline{Q}|b_2h_0$ needs to be approached with increased care. One must be sure to integrate out far enough that *both* oscillations have died down.

6 A look at the various spectra

This section includes several figures illustrating the utility and acoustic implications of the various spectra.

6.1 Comparing just the spectra

First, we include a set of figures comparing the spectra themselves. Examples of parameter sets to be used in the comparison follow. All expressions assume MKS units throughout.

The difference spectrum (i.e., the spectrum made up of the difference between two power laws) is given by Eqs. (4.1) and (4.2). In this section, the parameters in these equations will be assigned values appropriate for the air-sea interface:

$$b_2 = \frac{u^2}{g}\frac{1}{h_0}\sqrt{\frac{a_2^{\left[\frac{2}{\gamma_2/2+1}\right]}-1}{1-a_2^{\left[\frac{2}{\gamma_2/2+1}-2\right]}}}$$

$$w_2 = \frac{\alpha_{TOBA}}{100\pi}h_o^{\gamma_2}\sqrt{\frac{u^2}{g}} \qquad (6.1)$$

$$b_1 = \frac{w_2 b_2^{\gamma_2}}{1-a_2^{\gamma_2}}$$

$$h_0 = 1 \text{ m}$$

The expression for b_1 and b_2 come from Eqs. (4.10) and (4.11) respectively with $l_p = g/u^2$, while the expression for w_2 comes from item (i) in the caption of Fig. 3 in reference [6].

The relevant numerical parameters are:

$$\alpha_{\text{Toba}} = 0.08 \text{ m}^{3.5-\gamma_2},$$
$$a_2 = 0.9,$$

γ_2 is taken to vary from 2.0 to 4.0,
g is the gravitational constant 9.80612 m/s^2.

As discussed in Subsection 4.2.3, the value a_2 is set close to but less than 1. (Note that we could also absorbe a factor of $h_0^{\gamma_2}$ into α_{Toba} and have units m$^{3.5}$.)

Fig. 4 illustrates difference spectra for the listed values of γ_2 (the power of the tail) and wind speed. The higher wind speeds (corresponding to spectral peak locations $l_p \square 1$) considered in Fig. 4c and d each have a "cross-over point" at wavenumber $l=1$, where the order of the largest to the smallest spectrum reverses. This happens because $l=1$ is on the tail of the spectrum, so that the spectrum $S(l)\big|_{l=1} \approx w_2 / (h_0 l)^{\gamma_2}\big|_{l=1} \approx w_2$ is independent of γ_2 at this point only. As the wind speed decreases, the spectral peak location increases and the situation changes. For a wind speed of 5 m/s (i.e., $l_p \approx 0.4$), then the situation in Fig. 4b applies and there is no single cross-over point. For even lower wind speeds such that $l_p > 0.4$, the curves do not come together at all (Fig. 4a).
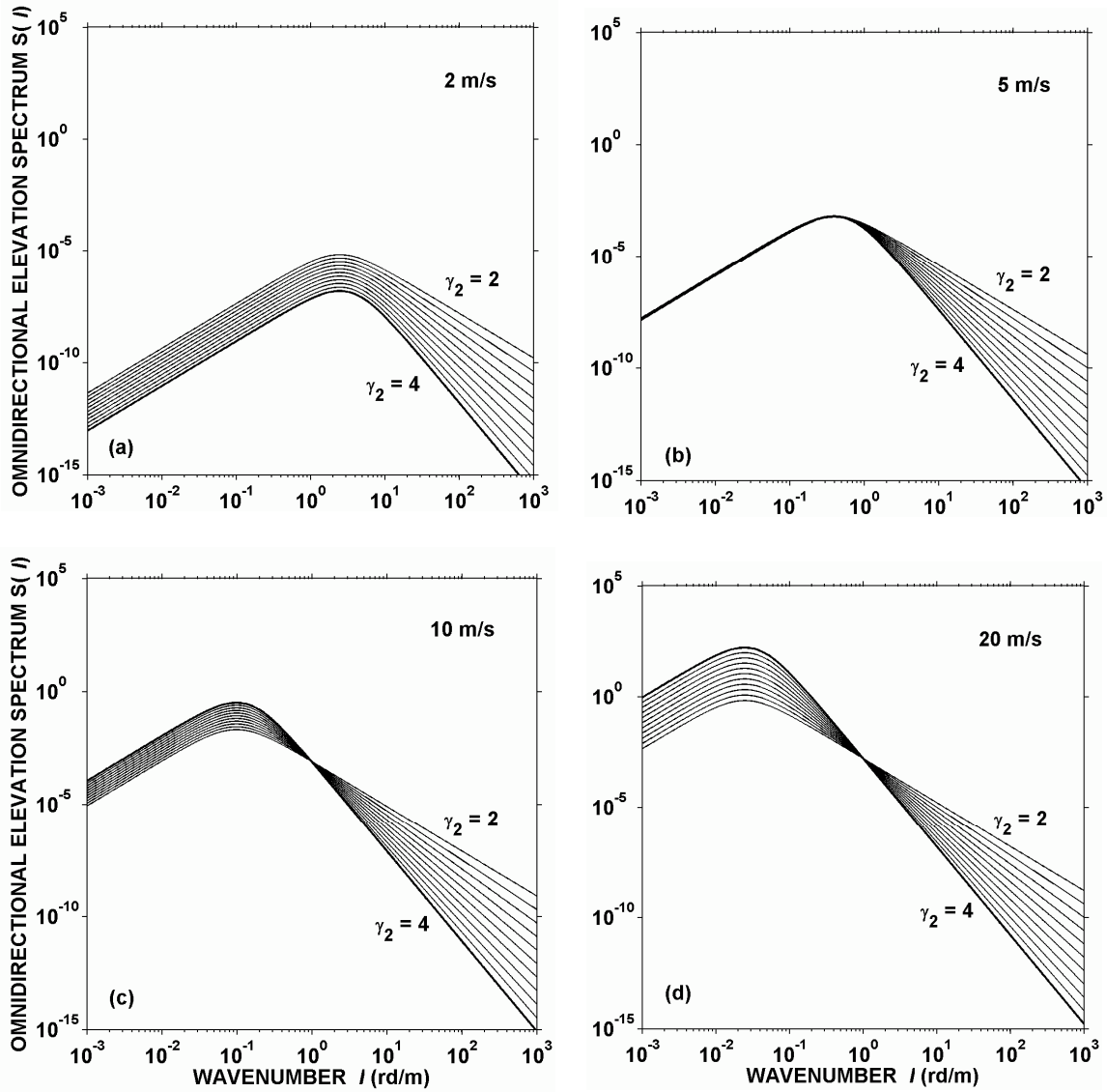
Fig. 4 – Difference spectra (defined by Eqs. (4.1) and (4.2)) with parameters appropriate for the air-sea interface. The tail of the difference spectrum goes as $w_2 / (h_0 l)^{\gamma_2}$. γ_2 steps from 2.0 to 4.0 in increments of 0.2. The wind speed varies from 2 m/s to 20 m/s.

Now the difference spectrum will be compared to the modified Pierson-Moskowitz spectrum (5.20). The new parameter in the exponent of the modified Pierson-Moskowitz spectrum is given by

$$a = 4l_p = 4\left(g/u^2\right) \qquad (6.2)$$

Note that g/u^2 is the standard peak wavenumber, and this choice insures that the peak wavenumbers l_p of the difference spectrum (4.1)/(4.2) and the modified Pierson-Moskowitz spectrum (5.20) coincide. The coefficient w_2 remains as above.

The difference spectrum (4.1)/(4.2), the standard Pierson-Moskowitz spectrum (5.21) and the modified Pierson-Moskowitz spectrum (5.20) are illustrated in Fig. 5. Note that compared to the difference spectrum, the modified Pierson-Moskowitz spectrum more closely reproduces the sharp peaks that are accepted as characteristic of the air-sea interface. We have a family of modified Pierson-Moskowitz spectra that closely match the difference spectra for all wavenumbers l above the sharp cutoffs. In this case, the modified Pierson-Moskowitz spectra have peak heights that are a little lower than those found on the difference spectra. Furthermore, note that the modified Pierson-Moskowitz spectra closely match the appropriate difference spectra along the tail, where the dominant contribution to the scattering cross-section occurs.

It is possible to use an empirical $[w_2]_{\text{Modified Pierson-Moskowitz}}$ to modestly improve agreement with the difference spectrum, but there is no compelling physical reason to do so[h]. More interestingly, it is possible to select values for a that produce a match in peak height between the modified Pierson-Moskowitz spectrum on the one hand and the true Pierson-Moskowitz spectrum on the other, while maintaining the tail behavior of the difference spectrum. Specifically, $a = 0.436\left(u/15\right)^{1/4} 4l_p = 0.436\left(u/15\right)^{1/4} 4\left(g/u^2\right)$ with the standard w_2 achieves this goal, but the modified Pierson-Moskowitz spectral peak is shifted to lower wavenumber (particularly at low wind speeds). It turns out that such modified Pierson-Moskowitz spectra yield cross-sections for one-dimensional benchmark problems of the sort examined in references [3, 33] that are in poor agreement with the results generated by both the difference spectrum and the standard Pierson-Moskowitz spectrum. The latter two agree very well, as does the modified Pierson-Moskowitz spectrum with the parameter a given by (6.2). It follows that for scattering scenarios such as those considered here, where the Bragg wavenumber falls along the tail of the spectrum, the peak location is more important than the peak magnitude in determining the behavior of the stochastic cross-section.

---

[h] Specifically, use equation (6.2) combined with the empirical choice $w_2 = \left(1.67 - 0.0017u^2\right)\left[1.44 - 0.29\arctan\left(5\left(u-3\right)\right)\right]\left[w_2\right]_{\text{difference spectrum}}$ to obtain closer overall agreement between the cross-sections generated by the difference and modified Pierson-Moskowitz spectra. This empirical formula is for $l_p = g/u^2$.
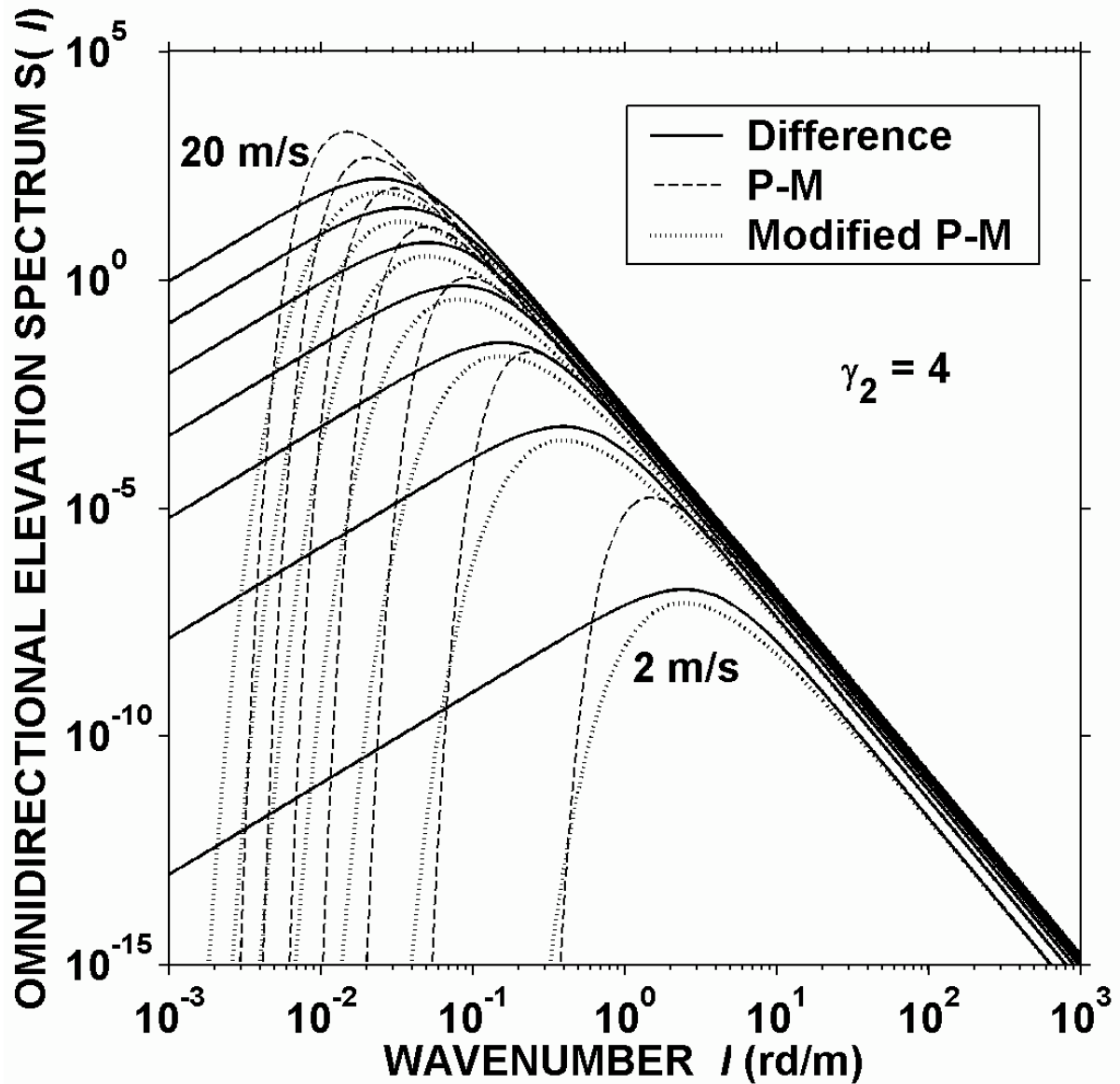
Fig. 5 – Comparison of the difference spectra (4.1) [solid curves], Pierson-Moskowitz spectra (5.21) [dashed curves], and <u>modified</u> Pierson-Moskowitz spectra (5.20)/(6.2) [dotted curves]. The tails are characterized by $\gamma_2 = 4$ power laws, and the wind speed goes from 2 m/s to 20 m/s in increments of 3 m/s. Note that at low windspeed, the difference and <u>modified</u> Pierson-Moskowitz spectra have tails that are below those for the corresponding Pierson-Moskowitz spectra. This is an artifact of choice of l_p and the definition of w_2 in Eq. (6.1).

6.2 Scattering cross-sections: Examples

Fig. 6 provides examples comparing the cross-sections associated with the difference spectra and the modified Pierson-Moskowitz spectra. The pure power-law spectrum given by Eq. (1.13) is considered as well. The stochastic cross-section for the monostatic (i.e., backscattered) case is graphed as a function of the grazing angle, the frequency, and the wind speed. We also consider a bistatic problem with the incoming grazing angle fixed at 20 degrees, and vary the outgoing angle. For the pure power law, the tail power γ_2 is chosen to be 3.95, close to the modified Pierson-Moskowitz value of $\gamma_2 = 4$, but not exactly equal to 4. (Recall that the pure power law is calculated using algorithms developed in Section 3 that do not work at exactly $\gamma_2 = 4$ (see the statement after Eq. (3.14)), while the modified Pierson-Moskowitz spectrum must employ an integer power law.) The difference spectrum also has a tail power of $\gamma_2 = 4$.

Fig. 6a fixes the frequency at 400 Hz and the wind speed at 10 m/s, and graphs the monostatic cross-section as a function of the grazing angle. Fig. 6b considers bistatic scattering. The incoming grazing angle is fixed at 20 degrees, the frequency at 400 Hz, and the wind speed at 10 m/s. The null at 160 degrees is expected. This is the angle for specular reflection, and here coherent reflected radiation dominates. Fig. 6c fixes the grazing angle at 20 deg and the wind speed at 10 m/s. It graphs the monostatic cross-section as a function of the frequency. Fig. 6d fixes the frequency at 400 Hz and the grazing angle at 20 degrees and graphs the backscattered cross-section as a function of the wind speed.

The differences between the results occur where we expect them to be: near specular for Fig. 6a and Fig. 6b, and at low frequencies for Fig. 6c. The differences in Fig. 6d at low wind speeds derive from this particular choice of l_p (at such wind speeds, the spectral peaks are at relatively high wavenumbers–e.g., for $u = 1$ m/s, $l_p \square 10$ m^{-1}). Also note that whereas a pure power law becomes frequency independent as γ_2 approaches 4, this is not true in general for a peaked spectrum.

Fig. 7 examines the stochastic scattering cross-section for the difference spectrum cut off with a step function (see Eq. (5.2)). Fig. 7a graphs the bistatic scattering cross-section as a function of outgoing angle for a frequency of 400 Hz, a wind speed of 10 m/s and an incoming grazing angle of 20 deg.   Fig. 7b magnifies the behavior of this graph in the near-specular direction to highlight the unphysical ringing associated with the sharp cutoff. This effect is particularly pronounced for a cutoff Λ wavenumber near the peak wavenumber l_p. Fig. 7c graphs backscattering strength versus frequency for a wind speed of 10 m/s and an incoming/outgoing grazing angle of 20 deg. Note once again the the highest cutoff Λ produces pronounced ringing at the low frequencies. Fig. 7d graphs backscattering strength versus wind speed for a frequency of 400 Hz and an incoming/outgoing grazing angle of 20 deg. In Fig. 7c and Fig. 7d, note the unphysical dropoff in backscattering strength for high frequencies and wind speeds, when the cutoff is near the spectral peak.
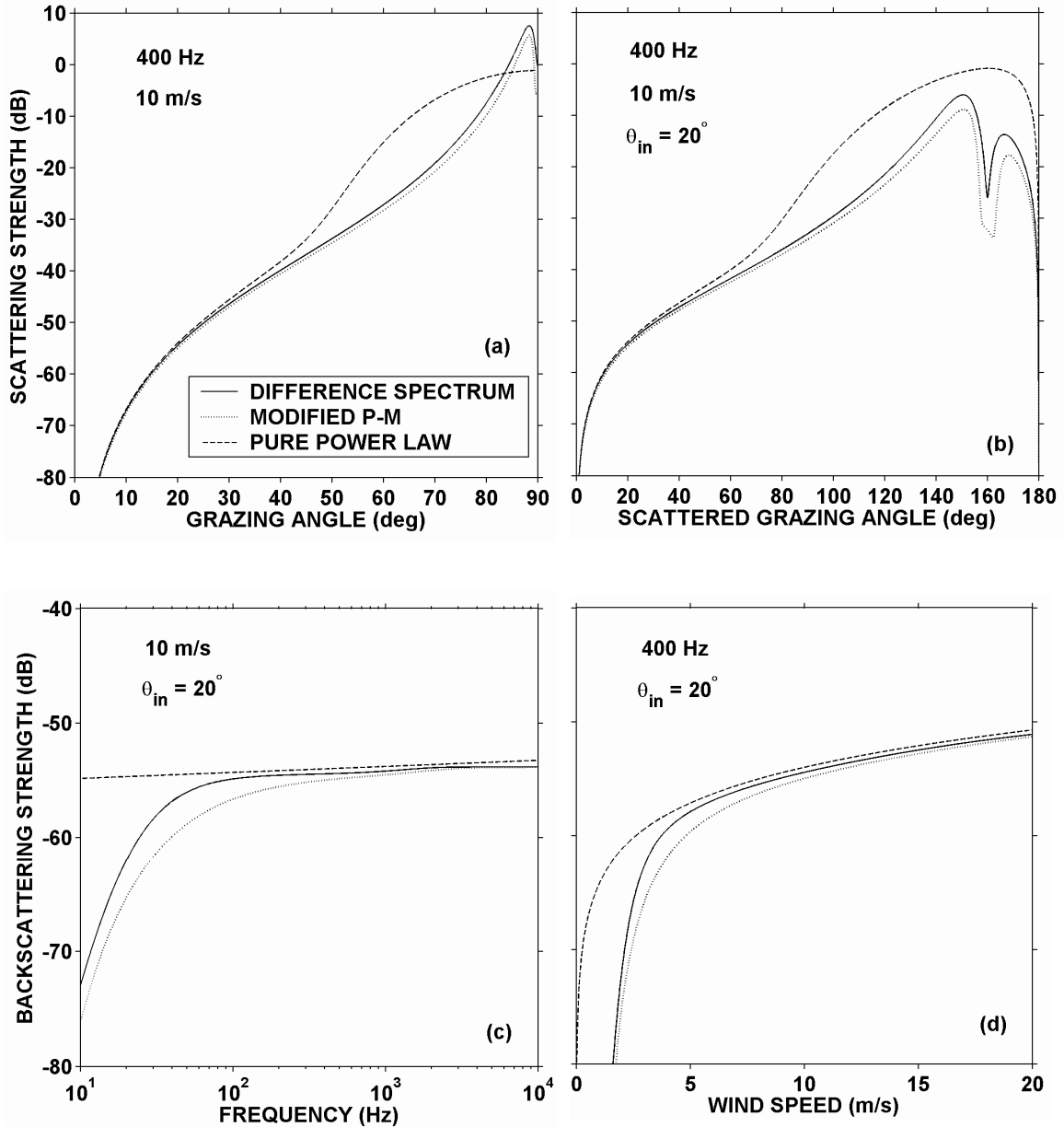
Fig. 6 - Various curves comparing in-plane scattering strength for three spectra: the pure power law given by Eq. (1.13) with $\gamma_2 = 3.95$, the difference spectrum given by Eqs. (4.1)/(4.2) with $\gamma_2 = 4$, and the <u>modified</u> Pierson-Moskowitz (P-M) spectrum given by Eq. (5.20)/(6.2) with the tail fixed at $\gamma_2 = 4$. Fig. 6a illustrates the stochastic backscattered cross-section as a function of the (incoming) grazing angle. Fig. 6b provides the stochastic bistatic cross-section as a function of the outgoing angle. The incoming angle is set to be 20 degrees, the frequency is fixed at 400 Hz, and the wind speed at 10 m/s. Fig. 6c provides the stochastic backscattered cross-section as a function of the frequency. The grazing angle is fixed at 20 degrees and the wind speed at 10 m/s. Fig. 6d graphs the stochastic backscattered cross-section as a function of the wind speed. The frequency is fixed at 400 Hz and the grazing angle at 20 degrees. (In all plots, the outgoing azimuthal angle $\varphi_{\text{out}} = 180 \deg$.)

49
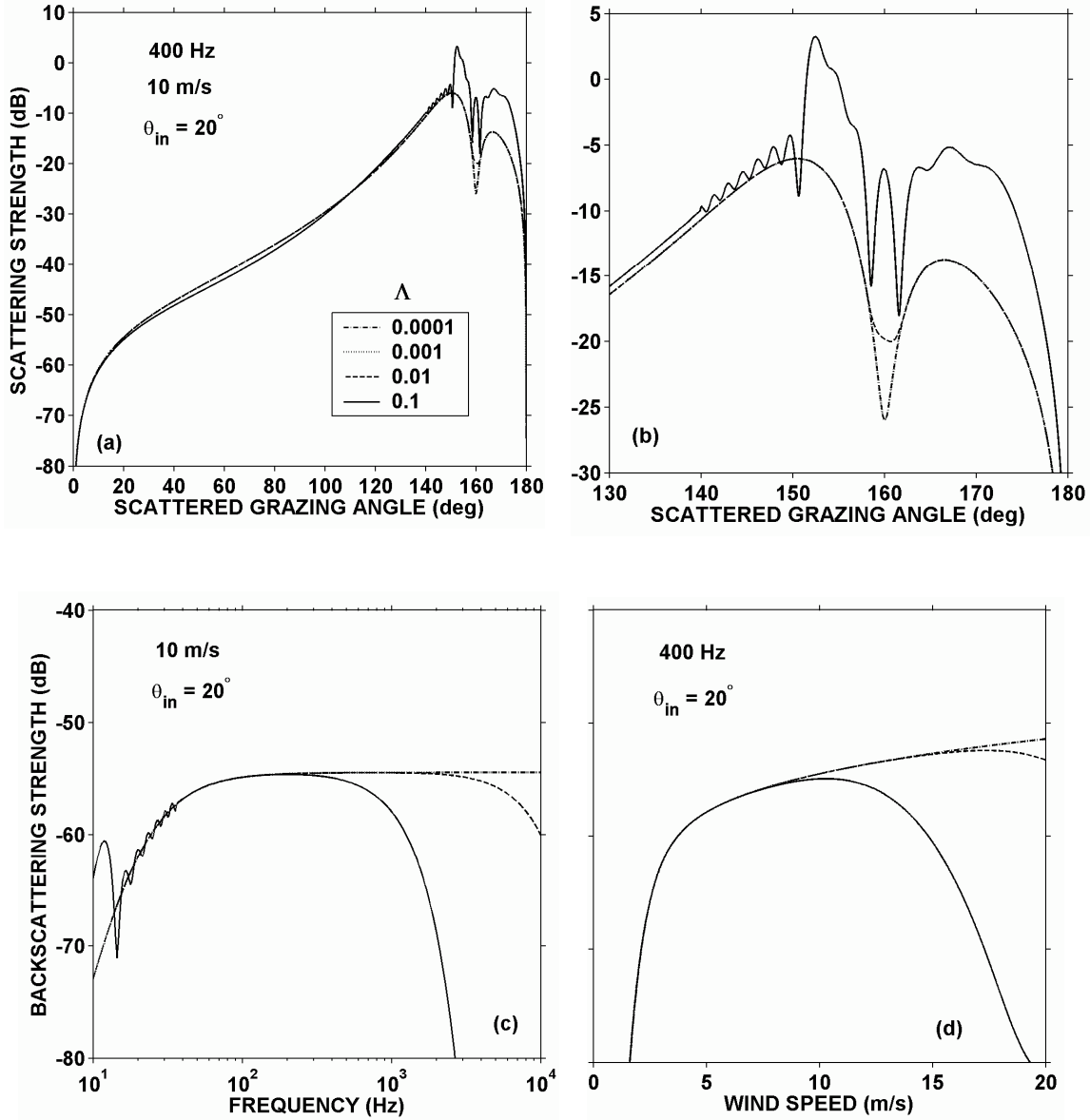
Fig. 7 – Scattering strengths for the difference spectrum with a step cutoff (Eq. (5.2)). The tail goes as $\gamma_2 = 4$ and the step cutoff is at wavenumber Λ given by the legends. The remaining parameters are defined by Eq. (6.1). The legend in Fig. 7a applies to Fig. 7b and Fig. 7c as well. Fig. 7b is a blowup of Fig. 7a in the vicinity of the specular direction. Since $l_p = g/u^2$ and $u = 10$ m/s, we have $l_p = 0.098$ m^{-1}, and the parameter values for Λ therefore go from the peak wavenumber l_p down to $0.001 l_p$. The lowest value of Λ closely approximates the pure difference spectrum. Note the unphysical effects associated with a step cutoff Λ near the peak wavenumber l_p: ringing occurs for near-specular scattering and at low frequencies, and there is an unphysical dropoff in the backscatter at high wind speeds and frequencies.

50

The anomalous behavior exhibited by the cutoff difference spectrum (for a cutoff wavenumber Λ near the peak wavenumber l_p) is associated with a discontinuity. It is important to recall that the difference spectrum is being cutoff with the step function so that the peak can be narrowed. For this to be significant, it will be necessary that Λ is indeed near the peak. Thus, this implies a significant limitation of the usefulness of the step-cutoff difference spectrum. The "softer" cutoffs associated with the exponential-cutoff difference spectrum (Eq. (5.10)) and the modified Pierson-Moskowitz spectrum ameliorate these problems. However, some care should be used in choosing the parameter giving the slope of the exponential cutoff: c (see Eq. (5.10)). An exponential cutoff with a very large c will approximate the step cutoff and consequently lead to many of the same problems.

6.3 Discussion

The modified Pierson-Moskowitz spectrum with the condition on a (6.2) leads to results for the cross-section that are similar to those calculated for the corresponding difference spectrum. The primary utility of the modified Pierson-Moskowitz is to provide an example of a spectrum that is similar to the difference spectrum, but has a sharper peak. This can be used to verify that the effect of peak sharpness is modest in such calculations. However, this conclusion will not be true in general. The reason that the nature of the peak had relatively little influence on the stochastic cross-section for the air-sea interface was because these parameters generated a dependence mostly on the tail and the region immediately to the high-wavenumber side of the peak. That may no longer hold true in other examples such as a rippled ocean bottom.

7 Non-isotropic spectra

Detailed modern ocean-surface spectra such as the Elfouhaily *et al.* spectrum [22] and the Donelan-Pierson spectrum [24] contain a dependence on the angle relative to the wind direction[i]. Furthermore, some swell-related effects and some ocean bottoms can generate spectra that depend on the azimuthal angle. Therefore, non-isotropic spectra must sometimes be used. (For an example of the measurement of non-isotropic spectra

---

[i] As noted by McDaniel [12], an additional factor needs to be inserted on the right-hand side of her Eq. (3.9)–i.e., Eq. 41 of [22]–to obtain spectra consistent with those shown in the figures of [22]. McDaniel [12] also provides an important caveat concerning air-sea interface scattering. She notes that for light wind speeds and radar in the C- and Ku- bands (wavelengths roughly comparable to those associated with underwater acoustic frequencies above 20 kHz–i.e., higher than those being considered here), the small slope approximation using the *directional* spectrum proposed by reference [22] gives poor agreement for out-of-plane (i.e., azimuthal) V-V scattering from the air-sea interface. At these wavelengths, capillary waves significantly affect the shape of the air-sea interface spectrum, while for acoustic frequencies typical of most long-range underwater remote sensing applications, the surface spectrum is in a pure gravity region or in a mixed region that still follows the power law typical for gravity waves (see the second paragraph of Section 1.3 for more on this). Finally, also note that reference [22] defines the isotropic spectrum in such a way that it must be rescaled by a factor of $1/2\pi l$ to match the conventions used here.

for the air-sea interface and their use in conjuction with the small slope approximation, see reference [10].)

Obtaining the cross-section per unit area for a non-isotropic spectrum involves two nested numerical integrations. First, the autocorrelation function $A(\underline{v})$ is obtained using Eq. (3.2)[j]:

$$A(\underline{v}) = \int d^2\underline{l}\ S(\underline{l})e^{i\underline{L}\cdot\underline{v}}.$$ (7.1)

Note that, as indicated in Eq. (3.2), *for an omnidirectional (i.e., isotropic) spectrum*, this reduces to

$$A(\underline{v}) = 2\pi\int_0^\infty dl\ lS(l)J_0(lv).$$ (7.2)

Spectra such those developed by Donelan-Pierson and Elfouhaily *et al.* have angular dependencies, and it is desirable to find a way to reduce the associated expression for the autocorrelation function to a one-dimensional form similar to Eq. (3.2)/(7.2).

As will be shown in Section 7.2 below, a spectrum with an angular dependence like that of the Elfouhaily *et al.* spectrum (i.e., proportional to $\cos(2\varphi)^k$) lends itself to a similar closed-form integration. Subsection 7.2.1 considers the general case, while Subsection 7.2.2 obtains a closed-form solution for the autocorrelation function for a special case. This special case concerns a specific spectrum that combines the difference spectrum considered in Section 4 with a specific angular dependence consistent with the basic form proposed by Elfouhaily *et al.* [22].

Once the autocorrelation functions $A(0)$ and $A(\underline{v})$ are evaluated, then we have $\rho(\underline{v}) = 2(A(0) - A(\underline{v}))$. This is once again substituted into the fundamental Eq. (1.8) for the cross section per unit area (reproduced here):

$$\frac{\langle\sigma\rangle}{a} = \frac{|\beta|^2}{16\pi^2Q_z^2}\left[(2\pi)^2 e^{-\frac{Q_z^2}{2}\rho(\infty)}\delta(\underline{Q}) + \int d^2\underline{v}\left(e^{-\frac{Q_z^2}{2}\rho(\underline{v})} - e^{-\frac{Q_z^2}{2}\rho(\infty)}\right)e^{i\underline{Q}\cdot\underline{v}}\right].$$ (7.3)

Recall that for an *omnidirectional spectrum* this would reduce to Eq. (1.10):

---

[j] It is important to note that Eq. (3.2) implicitly assumes that $S(\underline{l})$ is symmetric with respect to reflection across the origin (i.e., $S(\underline{l}) = S(-\underline{l})$, or in terms of the azimuthal angle φ, $S(l, \varphi+\pi) = S(l, \varphi)$). This is inherent in the frozen-surface approximation, and it is a necessary condition so that $A(\underline{v})$ and $S(\underline{l})$ can both be real. To put it another way, a frozen (time-independent) surface must be made of standing waves, which have equal backward and forward traveling components. Time-dependent theories require formulations that are sensitive to differences under the transformation $\underline{l} \to -\underline{l}$, but this paper is concerned exclusively with the time-independent problem.

[k] φ is the azimuthal angle–i.e., the angular coordinate in the x-y plane.

$$\frac{\langle\sigma\rangle}{a} = \frac{|\beta|^2}{16\pi^2 Q_z^2}\left[(2\pi)^2 e^{-\frac{Q_z^2}{2}\rho(\infty)}\delta(\underline{Q}) + 2\pi\int dv\, v\left(e^{-\frac{Q_z^2}{2}\rho(v)} - e^{-\frac{Q_z^2}{2}\rho(\infty)}\right)J_0(Qv)\right]. \quad (7.4)$$

Section 7.3 explicitly considers a spectrum with the angular dependence proposed by Elfouhaily *et al.*, and outlines how in such cases, Eq. (1.8)/(7.3) can be reduced to a more tractable form. Assuming the coefficient of the angular dependence is small, we obtain a result like that encountered in Eq. (1.10)/(7.4) plus an additional term involving a similar one-dimensional integral.

This result is quite general. The significance of the specific spectrum considered in Subsection 7.2.2 is that it produces a closed form expression for $\rho(\underline{v})$, thus avoiding the need for nested numerical integrations.

Section 7.4 will summarize the results for non-isotropic spectra.

7.1 A modification of the basic notation

Before we proceed, it is necessary to modify the notation established in Subsection 1.4.3. Now, the positive x-axis points in some preferred direction set by the rough surface itself and azimuthal angles must be given relative to this direction. The projection of the incoming wave vector $\vec{k}$ onto the x-y plane must now be associated with an arbitrary direction:

$$\vec{k} = k\left(\cos\theta_{in}\left(\cos\varphi_{in}\hat{x} + \sin\varphi_{in}\hat{y}\right) - \sin\theta_{in}\hat{z}\right), \quad (7.5)$$

while $\vec{q}$ is as before. Note that in addition to outgoing azimuthal angle φ_{out}, we now need to specify an incoming azimuthal angle φ_{in} relative the preferred direction set, for example, by swell on the ocean surface or ripples on bottom. This is summarized in Fig. 8.

7.2 The autocorrelation function for an angular dependence proportional to $\cos(2\varphi)$

Subsection 7.2.1 derives the contribution to the autocorrelation function associated with an angular dependence of the sort proposed by Elfouhaily *et al.* [22] in that paper's Eqs. (49) and (67). In other words, the spectrum is of the basic form

$$S(\underline{l}) = 2\pi S_{\text{isotropic}}(l)\cdot\Phi(l,\varphi_l), \quad (7.6)$$

with

$$\Phi(l,\varphi_l) \equiv \frac{1}{2\pi}\left[1 + \Delta(l)\cos(2\varphi_l)\right]. \tag{7.7}$$

and

$$\underline{l} = l\left(\cos\varphi_l\hat{x} + \sin\varphi_l\hat{y}\right).$$

The function $\Delta(l)$ is a new parameter introduced in this equation.
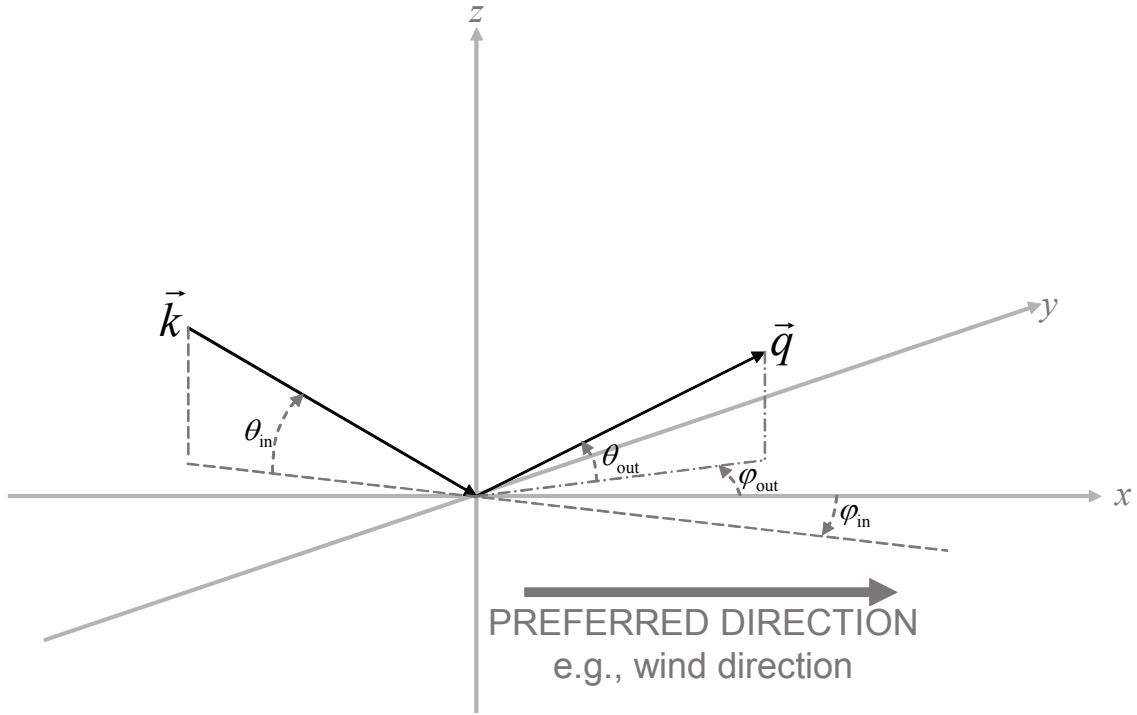
Fig. 8 – The modified geometry for an angle-dependent spectrum. This differs from Fig. 2 in that there is an intrinsic preferred direction distinct from the direction defined by the incoming wave vector $\vec{k}$. Most typically for the air-sea interface, the preferred direction is the direction toward which the local wind is blowing. However, it could in principle be another direction–for example, swell is associated with far-away storms and does not depend primarily on the local wind direction.

The now angle-dependent functions $\rho(\underline{v})$ (and $\rho(\infty)$) needed to evaluate the stochastic cross-section (Eq. (7.3)) follows immediately from the autocorrelation function.

Subsection 7.2.2 follows with a derivation of the closed-form solution corresponding to the scenario where $S_{\text{isotropic}}(l)$ (i.e., the isotropic component of the spectrum) is the difference spectrum (introduced in Section 4) and $\Delta(l)$ is a constant.

7.2.1 Autocorrelation function: The general case

For the polar coordinates given by Fig. 8, we have for the spectral wavenumber $\underline{l}$ and the vector $\underline{v}$ connecting a pair of points on the x-y plane,

$$\underline{l} = l\left(\cos\varphi_l \hat{x} + \sin\varphi_l \hat{y}\right) \quad ; \quad \underline{v} = v\left(\cos\varphi_v \hat{x} + \sin\varphi_v \hat{y}\right).$$

From Eqs. (7.1) and (7.6), we have

$$A(\underline{v}) = \int d^2\underline{l}\, S(\underline{l})e^{i\underline{l}\cdot\underline{v}} = 2\pi\int_0^\infty l\,dl\, S_{\text{isotropic}}(l)\int_{-\pi}^{\pi} d\varphi\, \Phi(l,\varphi_l)e^{i\underline{l}\cdot\underline{v}}. \tag{7.8}$$

To evaluate the angular integration, we need

$$\underline{l} = l\left(\cos\varphi_l \hat{x} + \sin\varphi_l \hat{y}\right) \quad ; \quad \underline{v} = v\left(\cos\varphi_v \hat{x} + \sin\varphi_v \hat{y}\right),$$

and so

$$\underline{l}\cdot\underline{v} = lv\left[\cos\varphi_l \cos\varphi_v + \sin\varphi_l \sin\varphi_v\right] = lv\cos\left(\varphi_l - \varphi_v\right).$$

So, we have

$$A(\underline{v}) = 2\pi\int_0^\infty l\,dl\, S_{\text{isotropic}}(l)\int_{-\pi}^{\pi} d\varphi\, \Phi(l,\varphi_l)e^{ilv\cos(\varphi_l-\varphi_v)}$$

$$\downarrow \tilde{\varphi} = \varphi_l - \varphi_v$$

$$= 2\pi\int_0^\infty l\,dl\, S_{\text{isotropic}}(l)\int_{-\pi-\varphi_v}^{\pi-\varphi_v} d\tilde{\varphi}\, \Phi(l,\tilde{\varphi}+\varphi_v)e^{ilv\cos\tilde{\varphi}}$$

Note that the integrand of the angular integration $\Phi(l,\tilde{\varphi}+\varphi_v)e^{ilv\cos\tilde{\varphi}}$ is 2π-periodic and drop the tilde to obtain

$$A(\underline{v}) = 2\pi\int_0^\infty l\,dl\, S_{\text{isotropic}}(l)\, S_{\text{angular}}(l,\varphi_v,v) \tag{7.9}$$

with

$$S_{\text{angular}}(l,\varphi_v,v) \equiv \int_{-\pi}^{\pi} d\varphi\, \Phi(l,\varphi+\varphi_v)e^{ilv\cos\varphi}$$

$$= \frac{1}{2\pi}\int_{-\pi}^{\pi} d\varphi\,\left[1+\Delta(l)\cos\left[2(\varphi+\varphi_v)\right]\right]e^{ilv\cos\varphi}$$

Use the sum formula: $\cos\left[2(\varphi+\varphi_v)\right] = \cos(2\varphi)\cos(2\varphi_v) - \sin(2\varphi)\sin(2\varphi_v)$ to get

$$S_{\text{angular}}(l,\varphi_v,v) = \frac{1}{2\pi}\int_{-\pi}^{\pi} d\varphi\, e^{ilv\cos\varphi} + \frac{\Delta(l)}{2\pi}\cos(2\varphi_v)\underbrace{\int_{-\pi}^{\pi} d\varphi\,\cos(2\varphi)e^{ilv\cos\varphi}}_{\text{integrand is even}}$$

$$-\frac{\Delta(l)}{2\pi}\sin(2\varphi_v)\underbrace{\int_{-\pi}^{\pi} d\varphi\,\sin(2\varphi)e^{ilv\cos\varphi}}_{\text{integrand is odd}}$$

Next, use Eq. (9.1.21) of reference [28] to obtain for integer n

$$i^n J_n(z) = \frac{1}{2\pi} \int_{-\pi}^{\pi} d\varphi \, \cos(n\varphi) e^{iz\cos\varphi}.$$

With $n = 0$, $n = 2$ and $z = lv$ this gives us

$$S_{\text{angular}}(l, \varphi_v, v) = J_0(lv) - \Delta(l)\cos(2\varphi_v)J_2(lv), \tag{7.10}$$

and substituting into Eq. (7.9)

$$A(\underline{v}) = \underbrace{2\pi \int_0^\infty l \, dl \, S_{\text{isotropic}}(l) J_0(lv)}_{A_{\text{isotropic}}(v)} + \cos(2\varphi_v) \cdot \underbrace{(-2\pi) \int_0^\infty l \, dl \, S_{\text{isotropic}}(l) \Delta(l) J_2(lv)}_{A_2(v)} \tag{7.11}$$

$$= A_{\text{isotropic}}(v) + \cos(2\varphi_v) A_2(v)$$

Note that the isotropic part of the autocorrelation function $A_{\text{isotropic}}(v)$ matches the old result given by Eq. (7.2). $A_2(v)$ is a new quantity associated with angular dependence. Since $J_2(0) = 0$, it follows that $A_2(0) = 0$.

Now,

$$\rho(\underline{v}) \equiv 2(A(0) - A(\underline{v})) = \rho_{\text{isotropic}}(v) + \cos(2\varphi_v)\rho_2(v) \tag{7.12}$$

with

$$\rho_{\text{isotropic}}(v) \equiv 2(A_{\text{isotropic}}(0) - A_{\text{isotropic}}(v)) = 4\pi \int_0^\infty l \, dl \, S_{\text{isotropic}}(l)(1 - J_0(lv))$$

$$\rho_2(v) \equiv 2(A_2(0) - A_2(v)) = -2A_2(v) = 4\pi \int_0^\infty l \, dl \, S_{\text{isotropic}}(l)\Delta(l)J_2(lv) \tag{7.13}$$

The equalities on the far right-hand side of Eq. (7.13) follow from (7.11). Note that $\rho_{\text{isotropic}}(v)$ is identical to the function $\rho(\underline{v})$ corresponding to a pure isotropic spectrum given by $S_{\text{isotropic}}(l)$.

For any realistic spectrum, two points infinitely far apart are uncorrelated and $A_{\text{isotropic}}(\infty) = A_2(\infty) = 0$. Thus, $\rho_2(\infty) = 0$, and

$$\rho(\infty) = \rho_{\text{isotropic}}(\infty) = 2A_{\text{isotropic}}(0). \tag{7.14}$$

Equations (7.13) and (7.14) constitute the core results of this subsection. The next subsection considers these results for the difference spectrum considered in Section 4.

7.2.2 Autocorrelation function: The difference spectrum

This subsection evaluates $\rho(\underline{v}) = \rho_{\text{isotropic}}(v) + \cos(2\varphi_v)\rho_2(v)$ corresponding to the difference spectrum (4.1)/(4.2):

$$S_{\text{isotropic}}(l) = \frac{b_1}{\left(1+\left(b_2 h_0 l\right)^2\right)^{\gamma_2/2}} - \frac{b_1}{\left(1+\left(\dfrac{b_2 h_0 l}{a_2}\right)^2\right)^{\gamma_2/2}}. \tag{7.15}$$

Furthermore, the parameter $\Delta(l)$ is assumed to be a constant Δ, giving us

$$\Phi(l,\varphi_l) \equiv \frac{1}{2\pi}\left[1 + \Delta\cos(2\varphi_l)\right]. \tag{7.16}$$

Equation (4.8) supplemented by Eq. (4.6) evaluates the first line of Eq. (7.13) to give

$$\rho_{\text{isotropic}}(v)$$

$$= 2A_{\text{isotropic}}(0)\left[1 - \left[\frac{\dfrac{\gamma_2}{2}-1}{1-a_2^2}\right]\frac{\left(\dfrac{v}{b_2 h_0}\right)^{\frac{\gamma_2}{2}-1}}{2^{\frac{\gamma_2}{2}-2}\Gamma\left(\dfrac{\gamma_2}{2}\right)}\left(K_{\frac{\gamma_2}{2}-1}\left(\frac{v}{b_2 h_0}\right) - a_2^{1+\frac{\gamma_2}{2}}K_{\frac{\gamma_2}{2}-1}\left(\frac{a_2 v}{b_2 h_0}\right)\right)\right], \tag{7.17}$$

with

$$A_{\text{isotropic}}(0) = \frac{\pi b_1}{b_2^2 h_0^2}\frac{1}{\dfrac{\gamma_2}{2}-1}\left(1-a_2^2\right). \tag{7.18}$$

Equation (4.9) in Section 4.1 evaluates Eq. (7.14) for the difference spectrum:

$$\rho(\infty) = \rho_{\text{isotropic}}(\infty) = 2A_{\text{isotropic}}(0). \tag{7.19}$$

The second line of Eq. (7.13) is all that is left. It becomes

$$\rho_2(v) = 4\pi\Delta b_1\left(\xi\left(v,\gamma_2,1/[b_2 h_0]\right) - \xi\left(v,\gamma_2,a_2/[b_2 h_0]\right)\right), \tag{7.20}$$

with

$$\xi(v,\gamma_2,\alpha) \equiv \int_0^\infty l\, dl\, \frac{J_2(lv)}{\left(1+\left(\dfrac{l}{\alpha}\right)^2\right)^{\gamma_2/2}}. \tag{7.21}$$

This is new. We will need to evaluate an integral of the form

$$\int_0^\infty \frac{J_2(lv)l\, dl}{\left(1+\left(\dfrac{l}{\alpha}\right)^2\right)^{\gamma_2/2}}$$

with $\alpha = 1/b_2 h_0$ and $\alpha = a_2/b_2 h_0$. To do so, use Eq. (21) from Section 8.5 of reference [27]:

57

$$\int_0^\infty f(x) J_\nu(xy) \sqrt{xy}\, dx$$

$$= \frac{y^{\nu+\frac{1}{2}} \Gamma\left(\frac{\lambda}{2}+\frac{\nu}{2}\right) \Gamma\left(\mu-\frac{\lambda}{2}-\frac{\nu}{2}+1\right)}{2^{\nu+1} \alpha^{2\mu-\lambda-\nu+2} \Gamma(\mu+1) \Gamma(\nu+1)} \cdot {}_1F_2\left(\tfrac{\lambda}{2}+\tfrac{\nu}{2};\tfrac{\lambda}{2}+\tfrac{\nu}{2}-\mu,\nu+1;y^2\alpha^2/4\right) \quad ,$$

$$+ \frac{y^{2\mu-\lambda+\frac{5}{2}} \Gamma\left(\frac{\lambda}{2}+\frac{\nu}{2}-\mu-1\right)}{2^{2\mu-\lambda+3} \Gamma\left(\frac{\nu}{2}-\frac{\lambda}{2}+\mu+2\right)} \cdot {}_1F_2\left(\mu+1;\mu+2+\tfrac{\lambda}{2}-\tfrac{\nu}{2},\mu+2-\tfrac{\lambda}{2}-\tfrac{\nu}{2};y^2\alpha^2/4\right)$$

with

$$f(x) \equiv x^{\lambda-\frac{3}{2}}\left(x^2+\alpha^2\right)^{-\mu-1}.$$

In this equation, set $\lambda=2$, $\nu=2$, $\mu=\gamma_2/2-1$, and make the substitutions $x\to l$, $y\to v$ to obtain

$$f(l) = \frac{l^{\lambda-\frac{3}{2}}}{\left(l^2+a^2\right)^{\mu+1}} = \frac{l^{\frac{1}{2}}}{\left(l^2+a^2\right)^{\frac{\gamma_2}{2}}} = \frac{l^{\frac{1}{2}}}{a^{\gamma_2}\left(1+\left(\dfrac{l}{a}\right)^2\right)^{\frac{\gamma_2}{2}}}$$

and

$$\int_0^\infty \frac{J_2(lv)\, l\, dl}{\left(1+\left(\dfrac{l}{\alpha}\right)^2\right)^{\frac{\gamma_2}{2}}} = \frac{v^2\alpha^4}{16}\frac{\Gamma\left(\gamma_2/2-2\right)}{\Gamma\left(\gamma_2/2\right)} \cdot {}_1F_2\left(2;3-\gamma_2/2,3;v^2\alpha^2/4\right)$$

$$+ \frac{v^{\gamma_2-2}\alpha^{\gamma_2}\Gamma\left(2-\gamma_2/2\right)}{2^{\gamma_2-1}\Gamma\left(\gamma_2/2+1\right)} \cdot {}_1F_2\left(\gamma_2/2;\gamma_2/2+1,\gamma_2/2-1;v^2\alpha^2/4\right)$$

.(7.22)

Note that the required condition $-\operatorname{Re}\nu < \operatorname{Re}\lambda < 2\mu+\tfrac{1}{2} \Rightarrow -2 < 2 < \gamma_2+\tfrac{3}{2}$ holds for physically relevant $\gamma_2 > 2$, and the additional condition $\alpha > 0$ will also hold when we set $\alpha = 1/b_2 h_0$ and $\alpha = a_2/b_2 h_0$.

We can obtain an alternate form for Eq. (7.22) by making the substitution

$$\frac{\Gamma\left(\gamma_2/2-2\right)}{\Gamma\left(\gamma_2/2\right)} = \frac{1}{\left(\dfrac{\gamma_2}{2}-1\right)\left(\dfrac{\gamma_2}{2}-2\right)}.$$

Inserting equality (7.22) (with the above substitution) into Eq. (7.21) gives us

$$\xi(v,\gamma_2,\alpha) = \frac{v^2\alpha^4}{16}\frac{1}{\left(\dfrac{\gamma_2}{2}-1\right)\left(\dfrac{\gamma_2}{2}-2\right)} \cdot {}_1F_2\left(2;3-\gamma_2/2,3;v^2\alpha^2/4\right)$$

$$+ \frac{v^{\gamma_2-2}\alpha^{\gamma_2}\Gamma\left(2-\gamma_2/2\right)}{2^{\gamma_2-1}\Gamma\left(\gamma_2/2+1\right)} \cdot {}_1F_2\left(\gamma_2/2;\gamma_2/2+1,\gamma_2/2-1;v^2\alpha^2/4\right)$$

, (7.23)

which is in turn substituted into (7.20) to obtain $\rho_2(v)$. This result is combined with (7.17) for $\rho_{\text{isotropic}}(v)$ to obtain $\rho(\underline{v}) = \rho_{\text{isotropic}}(v) + \cos(2\varphi_v)\rho_2(v)$ for the difference spectrum (7.15). Recall that $\rho(\infty)$ is given by Eq. (7.19) (with (7.18)). Thus, we have all the statistical quantities that go into the stochastic scattering cross-section corresponding to the difference spectrum (7.15).

7.3 The cross-section for an angular dependence proportional to $\cos(2\varphi)$

Begin with integral Eq. (1.7):

$$\frac{\langle \sigma \rangle}{a} = \frac{|\beta|^2}{16\pi^2 Q_z^2} \int d^2\underline{v}\, e^{-\frac{Q_z^2}{2}\rho(\underline{v})} e^{i\underline{Q}\cdot\underline{v}}. \tag{7.24}$$

Consideration of the specular term proportional to

$$\int d^2\underline{v}\, e^{-\frac{Q_z^2}{2}\rho(\infty)} e^{i\underline{Q}\cdot\underline{v}} \tag{7.25}$$

is deferred to the end of this section because it adds nothing new to the problem[l].

For the angular dependence proposed by Elfouhaily *et al.* [22], Eq. (7.24) will require evaluation of a one-dimensional integral to obtain the autocorrelation function[m], and another one-dimensional integral to obtain the stochastic cross-section. In principle, the cross-section also involves an additional one-dimensional integral in the angular direction, which can be solved and/or tabulated[n]. However, here we will choose to expand to first order in the angular dependent term, and this allows us to evaluate the angular integration in closed form, winding up with an expression very similar to Eq. (1.10)/(7.4).

Thus, consider the integral

$$I_1(\vec{Q}) = \int d^2\underline{v}\, e^{-\frac{Q_z^2}{2}\rho(\underline{v})} e^{i\underline{Q}\cdot\underline{v}}$$

$$= \int_0^\infty v\, dv\, e^{-\frac{Q_z^2}{2}\rho_{\text{isotropic}}(v)} \underbrace{\int_{-\pi}^{\pi} d\varphi\, e^{-\frac{Q_z^2}{2}\rho_2(v)\cos(2\varphi_v)} e^{i\underline{Q}\cdot\underline{v}}}_{I_2}.$$

---

[l] Note that from Eq. (7.14), $\rho(\infty)$ is the same as $\rho_{\text{isotropic}}(\infty)$, and so adding the term proportional to integral (7.25) provides a standard specular δ-function that has no angular dependence, and subtracting it guarantees that the isotropic part of the integrand in Eq. (7.24) properly goes to zero. Recall that since $\rho_2(\infty) \to 0$, the angle-dependent part automatically goes to zero.

[m] This can be evaluated in closed form in certain cases. For example, recall that Subsection 7.2.2 considers the case where the isotropic part of the spectrum $S_{\text{isotropic}}(l)$ is the difference spectrum, and obtains a closed-form expression for the autocorrelation function.

[n] The integral is some function similar to a Bessel function or a confluent hypergeometric function, but it is not common enough to have been officially defined and comprehensively studied as these have.

Now, with $p(v) \equiv -\left(Q_z^2/2\right)\rho_2(v)$, and

$$\underline{Q} = |\underline{Q}|\left(\cos\varphi_Q \hat{x} + \sin\varphi_Q \hat{y}\right) \quad ; \quad \underline{v} = v\left(\cos\varphi_v \hat{x} + \sin\varphi_v \hat{y}\right),$$

we have

$$I_2\left(p,|\underline{Q}|,\varphi_Q\right) = \int_{-\pi}^{\pi} d\varphi_v \ e^{p(v)\cos(2\varphi_v)} e^{i|\underline{Q}|v\cos(\varphi_v - \varphi_Q)}. \tag{7.26}$$

This integral is a well-behaved function, which could be tabulated numerically. Alternately, it could be studied systematically, and algorithms developed to solve it given values of p, $|\underline{Q}|$ and φ_Q. However, here we consider an alternative. We expand the exponential to first order: $e^{p(v)\cos(2\varphi_v)} = 1 + p(v)\cos(2\varphi_v)$. Now

$$I_2\left(p,|\underline{Q}|,\varphi_Q\right) = \int_{-\pi}^{\pi} d\varphi_v \ e^{i\underline{Q}\cdot\underline{v}} + p(v)\int_{-\pi}^{\pi} d\varphi_v \ \cos(2\varphi_v)e^{i|\underline{Q}|v\cos(\varphi_v - \varphi_Q)}.$$

The second integral becomes

$$\int_{-\pi}^{\pi} d\varphi_v \ \cos(2\varphi_v)e^{i|\underline{Q}|v\cos(\varphi_v - \varphi_Q)} \overset{\tilde{\varphi} = \varphi_v - \varphi_Q}{=} \int_{-\pi-\varphi_Q}^{\pi-\varphi_Q} d\tilde{\varphi} \ \cos\left(2\left(\tilde{\varphi}+\varphi_Q\right)\right)e^{i|\underline{Q}|v\cos\tilde{\varphi}}$$

$$\underset{\substack{\text{integrand is} \\ 2\pi \text{ periodic}}}{=} \int_{-\pi}^{\pi} d\tilde{\varphi} \ \cos\left(2\left(\tilde{\varphi}+\varphi_Q\right)\right)e^{i|\underline{Q}|v\cos\tilde{\varphi}}$$

$$= \int_{-\pi}^{\pi} d\tilde{\varphi} \ \cos\left(2\left(\tilde{\varphi}+\varphi_Q\right)\right)\cos(z\cos\tilde{\varphi}) + i\int_{-\pi}^{\pi} d\varphi_v \ \cos\left(2\left(\tilde{\varphi}+\varphi_Q\right)\right)\sin(z\cos\tilde{\varphi}).$$

$$= \cos(2\varphi_Q)\int_{-\pi}^{\pi} d\tilde{\varphi} \ \underbrace{\cos(2\tilde{\varphi})\cos(z\cos\tilde{\varphi})}_{\text{even}} - \sin(2\varphi_Q)\int_{-\pi}^{\pi} d\varphi_v \ \underbrace{\cancel{\sin(2\tilde{\varphi})\cos(z\cos\tilde{\varphi})}}_{\text{odd}}$$

$$+ i\cos(2\varphi_Q)\int_{-\pi}^{\pi} d\tilde{\varphi} \ \underbrace{\cos(2\tilde{\varphi})\sin(z\cos\tilde{\varphi})}_{\text{even}} - i\sin(2\varphi_Q)\int_{-\pi}^{\pi} d\varphi_v \ \underbrace{\cancel{\sin(2\tilde{\varphi})\sin(z\cos\tilde{\varphi})}}_{\text{odd}}$$

$$= 2\cos(2\varphi_Q)\int_{0}^{\pi} d\tilde{\varphi} \ \cos(2\tilde{\varphi})\cos(z\cos\tilde{\varphi}) + 2i\cos(2\varphi_Q)\int_{0}^{\pi} d\tilde{\varphi} \ \cos(2\tilde{\varphi})\sin(z\cos\tilde{\varphi})$$

Use Eqs. (3.715-18) and (3.715-13) of reference [28] both with $n=2$ to get

$$\int_{0}^{\pi} d\tilde{\varphi}\cos(2\tilde{\varphi})\cos(z\cos\tilde{\varphi}) = \pi\cos\left(\frac{2\pi}{2}\right)J_2(z) = -\pi J_2(z)$$

$$\int_{0}^{\pi} d\tilde{\varphi} \ \cos(2\tilde{\varphi})\sin(z\cos\tilde{\varphi}) = \pi\sin\left(\frac{2\pi}{2}\right)J_2(z) = 0$$

and recalling $z \equiv |\underline{Q}|v$

$$\int_{-\pi}^{\pi} d\varphi_v \ \cos(2\varphi_v)e^{i|\underline{Q}|v\cos(\varphi_v - \varphi_Q)} = -2\pi\cos(2\varphi_Q)J_2\left(|\underline{Q}|v\right).$$

Thus,

$$I_2\left(p,\left|\underline{Q}\right|,\varphi_Q\right)=\int_{-\pi}^{\pi}d\varphi_v\ e^{i\underline{Q}\cdot\underline{v}}-2\pi p(v)\cos\left(2\varphi_Q\right)J_2\left(\left|\underline{Q}\right|v\right)$$

and

$$I_1\left(\vec{Q}\right)=\int_0^{\infty}v\,dv\ e^{-\frac{Q_z^2}{2}\rho_{\text{isotropic}}(v)}\int_{-\pi}^{\pi}d\varphi_v\ e^{i\underline{Q}\cdot\underline{v}}-2\pi\cos\left(2\varphi_Q\right)\int_0^{\infty}v\,dv\ e^{-\frac{Q_z^2}{2}\rho_{\text{isotropic}}(v)}p(v)J_2\left(\left|\underline{Q}\right|v\right)$$

$$=\underbrace{\int d^2\underline{v}\ e^{-\frac{Q_z^2}{2}\rho_{\text{isotropic}}(v)}e^{i\underline{Q}\cdot\underline{v}}}_{\text{old isotropic result}}+\cancel{2}\pi\frac{Q_z^2}{\cancel{2}}\cos\left(2\varphi_Q\right)\int_0^{\infty}v\,dv\ e^{-\frac{Q_z^2}{2}\rho_{\text{isotropic}}(v)}\rho_2(v)J_2\left(\left|\underline{Q}\right|v\right)\ .$$

Substituting into Eq. (7.24) gives

$$\frac{\langle\sigma\rangle}{a}$$

$$=\frac{|\beta|^2}{16\pi^2Q_z^2}\left[\underbrace{\int d^2\underline{v}\ e^{-\frac{Q_z^2}{2}\rho_{\text{isotropic}}(v)}e^{i\underline{Q}\cdot\underline{v}}}_{\text{old isotropic result}}+\pi Q_z^2\cos\left(2\varphi_Q\right)\int_0^{\infty}v\,dv\ e^{-\frac{Q_z^2}{2}\rho_{\text{isotropic}}(v)}\rho_2(v)J_2\left(\left|\underline{Q}\right|v\right)\right]\ .\qquad(7.27)$$

Adding and subtracting the specular term (7.25), and recalling that from Eq. (7.14), $\rho(\infty)$ is the same as $\rho_{\text{isotropic}}(\infty)$, we have

$$\frac{\langle\sigma\rangle}{a}=$$

$$\frac{|\beta|^2}{16\pi^2Q_z^2}\left[\underbrace{(2\pi)^2\,e^{-\frac{Q_z^2}{2}\rho_{\text{isotropic}}(\infty)}\delta\left(\underline{Q}\right)+\int d^2\underline{v}\left(e^{-\frac{Q_z^2}{2}\rho_{\text{isotropic}}(v)}-e^{-\frac{Q_z^2}{2}\rho_{\text{isotropic}}(\infty)}\right)e^{i\underline{Q}\cdot\underline{v}}}_{\text{old isotropic result}}\\+\pi Q_z^2\cos\left(2\varphi_Q\right)\int_0^{\infty}v\,dv\ e^{-\frac{Q_z^2}{2}\rho_{\text{isotropic}}(v)}\rho_2(v)J_2\left(\left|\underline{Q}\right|v\right)\right]\ .\qquad(7.28)$$

Note that this consists of the result for an isotropic spectrum given by Eq. (1.10)/(7.4) and an additional term involving φ_Q, the azimuthal angle between the preferred (e.g., wind) direction and the projection of $\vec{Q}$ onto the x-y plane:

$$\vec{Q}=Q\left(\cos\theta_Q\left(\cos\varphi_Q\hat{x}+\sin\varphi_Q\hat{y}\right)-\sin\theta_Q\hat{z}\right)$$

$$\underline{Q}=\left(1-\hat{z}\hat{z}\right)\cdot\vec{Q}=\underbrace{Q\cos\theta_Q}_{|\underline{Q}|}\left(\cos\varphi_Q\hat{x}+\sin\varphi_Q\hat{y}\right)=\left|\underline{Q}\right|\left(\cos\varphi_Q\hat{x}+\sin\varphi_Q\hat{y}\right)\cdot$$

The relationship between φ_{in}, φ_{out} and φ_Q is in general complicated, but for backscattering it is $\varphi_{\text{in}}=\varphi_Q$ and $\varphi_{\text{out}}=\varphi_{\text{in}}+180\deg$.

Also note that result (7.28) does not make any assumptions about $S_{\text{isotropic}}(l)$ or $\Delta(l)$. The significance of the special case discussed in Subsection 7.2.2 is that this instance provides closed-form results for $\rho_{\text{isotropic}}(v)$ and $\rho_2(v)$.

7.4 Summary for non-isotropic spectra

Section 0 considers non-isotropic spectra–i.e., those that depend on both the azimuthal angle and the magnitude of the wavenumber. The basic form of the spectrum is the product of an isotropic spectrum and a term introducing the angular dependence:

$$S(\underline{l}) = 2\pi S_{\text{isotropic}}(l) \Phi(l, \varphi_l).$$

(The notation is loosely based on reference [22].) In the most general case, two nested two-dimensional integrals are required: one to obtain the autocorrelation function $A(\underline{v})$ from the spectrum $S(\underline{l})$ and a second to obtain the stochastic cross-section. The stochastic cross-section involves an integral that contains the function $\rho(\underline{v}) \equiv 2\left[A(0) - A(\underline{v})\right]$ in the integrand.

However, if we assume a specific azimuthal dependence for the surface spectrum–that suggested by reference [22]–then the problem simplifies. Then, the first angular integration can be solved in closed form (Eq. (7.10)), which in turn leads to the two-part expression (7.13) for the isotropic component and the coefficient of the angle-dependent component of the function $\rho(\underline{v})$. The second angular integration leads to a function that can be tabulated (Eq. (7.26)). Furthermore, when we expand the integrand in the second angular integration (i.e., the integrand in Eq. (7.26)) to first order in the angular dependence, this integration can be evaluated to give us the cross-section in terms of a sum of one-dimensional integrals (Eq. (7.28)). In fact, Eq. (7.28) involves isotropic terms that precisely mirror Eq. (1.10)/(7.4) and a new correction term associated with the angular dependence. The new correction term involves a one-dimensional infinite integral that is quite similar to the one-dimensional integral appearing in Eq. (1.10)/(7.4).

In Sections 3 to 6, we examined various purely isotropic spectra that were chosen to produce a closed form for the quantity $\rho(\underline{v})$ (or in the terminology used here in Section 7, $\rho_{\text{isotropic}}(v)$). Above in Section 7.2.2, one of these, the difference spectrum (first introduced in Section 4) is used to construct an angle-dependent spectrum $S(\underline{l}) = 2\pi S_{\text{isotropic}}(l) \Phi(l, \varphi_l)$ with $S_{\text{isotropic}}(l)$ given by Eq. (7.15) and $\Phi(l, \varphi_l)$ by Eq. (7.16):

$$S(\underline{l}) = \left[\frac{b_1}{\left(1 + (b_2 h_0 l)^2\right)^{\gamma_2/2}} - \frac{b_1}{\left(1 + \left(\frac{b_2 h_0 l}{a_2}\right)^2\right)^{\gamma_2/2}} \right] \left[1 + \Delta \cos(2\varphi_l)\right]. \qquad (7.29)$$

Note that angle-averaging this spectrum reproduces the old isotropic difference spectrum.

The isotropic part of the cross-section given in Eq. (7.28) can then be solved (as before) by numerical integration with $\rho_{\text{isotropic}}(v)$ given by Eq. (7.17)/(7.18) and $\rho_{\text{isotropic}}(\infty)$ given by Eq. (7.19)/(7.18). The new angle-dependent term can be solved by numerical integration with $\rho_2(v)$ given by Eq. (7.20)/(7.23).

This result can be used to benchmark more general numerical calculations that by necessity involve nested integrations. Additionally, noting that most physically realistic spectra have power-law tails, the pure power-law result (summarized in Section 3.4) can also be used to benchmark the numerical evaluation of (7.3) in the region where Bragg scattering falls well within the region of the power-law tail of the spectrum. Furthermore, crude guidance about the behavior of the cross-section can be obtained when isotropic results from Sections 3 to 6 are applied to one-dimensional slices of non-isotropic spectra.

8   Summary and discussion

This paper develops spectra that allow tractable evaluation of the integral in the stochastic cross-section per unit area $\langle \sigma \rangle / a$ given by Eq. (1.8), the lowest-order small slope approximation.

As a first step, perturbation theory is generated by expanding the integral to first order in the roughness spectrum (Section 2). The resultant value for the stochastic cross-section per unit area $\langle \sigma \rangle / a$ is given by Eq. (2.2), where the integral is simply proportional to the surface roughness spectrum.

To evaluate the small slope expression that involves the full integral, three isotropic rough surface scenarios are considered, and methods for evaluating the integral are developed for each. As discussed in Section 1.2, the spectra reflect one of two tradeoffs:

- A tradeoff between the tractability of the numerical evaluation of the cross-section on the one hand versus the ability of the various spectra to accurately reflect as many characteristics of observed physical roughness spectra as possible.
- A tradeoff between competing physical approximations.

 The three isotropic scenarios considered are as follows.

- The first scenario (Section 3) concerns an ensemble of rough surfaces, where only the power-law behavior of the tail is known. In this case, the integral reduces to a pair of summations that apply in different parameter regimes. This result is expressed by Eq. (3.20) and the associated commentary outlining the technique for evaluating $\langle \sigma \rangle / a$.

63

- The second scenario is discussed in Section 4. It addresses peaked spectra formed by taking the difference between two power laws. This is known as the difference spectrum. In this case, the integral reduces to a one-dimensional integral from zero to infinity with a slowly decaying oscillating integrand. This integral can be evaluated using Gaussian quadratures over finite intervals each covering one period as the integrand oscillates, and the oscillating terms can be resummed to accelerate convergence. The summary section Section 4.3 outlines the numerical procedure for evaluating $\langle\sigma\rangle/a$ for such a peaked spectrum.

- The third scenario considers spectra that have sharper peaks than can be constructed by simply taking the difference between two power-law spectra.

  - The first case is discussed in Section 5.1. Here the spectrum constructed by taking the difference between two power-law spectra is artificially cut off at a low wavenumber in one of two ways: using a step function cutoff (Subsection 5.1.1) or an exponential cutoff (Subsection 5.1.2) grafted onto the spectrum cutoff by a step-function. The integral evaluation described for the second scenario just above (the spectrum formed by taking the difference between two power laws) is now supplemented by additional finite integrations that can be evaluated using standard technique such as Gaussian quadratures. The actual procedures for evaluating the $\langle\sigma\rangle/a$ for these kinds of peaked spectra with an additional hard low-wavenumber cutoff are summarized in the last two sentences of Section 5.1.1 and the last three sentences of Subsection 5.1.2.

  - The second case is discussed in Section 5.2, a spectrum is cut off by multiplication to the exponential of the reciprocal of the wavenumber. The spectrum discussed in Subsection 5.2.1 closely resembles the Pierson-Moskowitz spectrum, while the version described in Subsection 5.2.2 has a different power law tail ($1/l^3$ rather than $1/l^4$). As with the difference spectrum, the associated autocorrelation functions can be evaluated in closed form and we are once again left with a closed-form oscillating integrand. The approach previously used to evaluate the cross-section per unit area $\langle\sigma\rangle/a$ for the difference spectrum can be used again in this case. This procedure is outlined in the last sentences of Subsections 5.2.1 and of 5.2.2.

The step-function and exponentially cutoff difference spectra provide the user community with extra tools for analyzing the roles of very sharp peaks (as perhaps found along a rippled ocean bottom), but their importance is generally secondary to that of the three spectra considered in more detail in Section 6: the pure power law, the difference spectrum and the modified Pierson-Moskowitz spectrum.

The power law spectrum without any peak is primarily useful in cases where

- little is known about the nature of the spectral peak, while the nature of the tail is known,
- and the Bragg scale is well into the power-law region of the spectrum, and the influence of the peak on the scattering cross-section is relatively modest.

This scenario applies, for example, to the ocean bottom in many parts of the world. It should be noted that the peak can be measured and recorded for specific locations. In this case the difference spectrum and possibly its "peakier" variations will prove particularly useful, since there are a wide variety of γ_2's involved. Application of even modest cutoffs can sometimes significantly alter the scattering (see, for example, Fig. 6).

Section 6 examined the various spectra in the context of acoustic scattering (up to about 10 kHz) from the air-sea interface. These examples relied on numerical implementation of the theory by Joe Fialkowski (NRL). They indicate that the extra-sharp cutoff introduced by the <u>modified</u> Pierson-Moskowitz spectrum has a relatively modest effect on the cross-section generated by the difference spectrum. They also indicate that the pure power-law spectrum can introduce some error, particularly at the high grazing angles, near the specular reflection, and at low frequencies and wind speeds. The difference spectrum provides the best balance between the tradeoffs. The hard cutoff at $\Lambda < l_p$ on the other hand stands out as a poor choice.

Section 0 considers the issues associated with evaluation of the stochastic cross-section corresponding to angle-dependent two-dimensional spectra. The angular dependence proposed by Elfouhaily *et al.* [22] is examined in detail. The resultant cross-section Eq. (7.28) takes the form of the isotropic result plus a correction associated with azimuthal dependence. The basic approach used to calculate the cross-section associated with the isotropic spectrum can be applied to evaluate the new term associated with the azimuthal dependence. This is done explicity for the spectrum consisting of the product of the difference spectrum and the angular dependence proposed by Elfouhaily *et al.* The result is Eq. (7.20)/(7.23), which provides the quantity needed so that the new integral that appears in Eq. (7.28) reduces to the now standard numerical calculation of a one-dimensional infinite integral with an oscillating integrand.

9 Conclusions

This work presents the formalism associated with numerical solutions of the incoherent cross-section per unit area for quasi-planar stochastically rough surfaces. The lowest-order small slope approximation is widely used to model the scattering cross-section per unit area from such interfaces. This approximation consists of a prefactor, which contains information about the scattering geometry, the media involved and the boundary

conditions, and an integral that contains information about the scattering geometry and the surface roughness spectrum. The former involves a closed-form algebraic expression, but evaluation of the integral is nontrivial. Some simplification of this integral occurs when the surface is assumed to be isotropic, but for this integral to be truly tractable, the isotropic surface spectrum must be chosen with care. The choice primarily involves a tradeoff between tractability and the completeness of the physical description.

Generally, the most useful expressions for the stochastic scattering cross-section come from perturbation theory (where the integral disappears altogether) and the small slope result associated with the difference spectrum (where the integral is numerically tractable). The former is extremely tractable: it is trivial to calculate for any spectrum. However, it must be used with care. As noted in Section 6 above and in references [6] and [2], the associated cross-section for scattering from the air-sea interface and the ocean bottom may in some cases differ significantly from the correct value.

The small slope result associated with the (isotropic) difference spectrum is also very flexible: it works for any power $\gamma_2 > 2$. The peak location can be selected at will, and the spectrum shape can be adjusted from narrow to wide. Physical spectra found in underwater acoustics applications typically obey $2 < \gamma_2 < 4$[o]. Even though the <u>modified</u> Pierson-Moskowitz spectrum (characterized by a very sharp, tall peak) provided the most faithful rendering of the known characteristics of the air-sea interface spectrum, it was found that the difference spectrum provides perfectly adequate values for the scattering cross-section. It can be concluded that for roughly similar frequencies and spectra (as may occur in acoustic scattering from the ocean bottom), the difference spectrum provides the optimal tradeoff between tractability and broad applicability. Hence, it is a good default spectrum to use for underwater acoustics applications in the low- to mid-frequency range.

A step function or exponential cutoff can be grafted onto the basic difference spectra. In a typical case, this cutoff will be placed between the peak of the difference spectrum and zero wavenumber. Such spectra can provide a platform for examining the effects of peak narrowness, but the cutoff procedure does not by itself affect the height of the peak. This limits the utility of these cutoff difference spectra, since it is generally acknowledged that some physical spectra (e.g., the Pierson-Moskowitz spectrum for the air-sea interface) are characterized by spectral values near the peak that are very large relative to the values along the power-law tail. It should be further noted that the step function cutoff generates a very strong dependence on the choice of parameters, and that therefore this spectrum should be used very carefully if at all.

---

[o] Spectra with power-laws $\gamma_2 < 2$ yield autocorrelation functions that are extremely sensitive to some high-wavenumber cutoff imposed either by the field (the renormalization problem) or by the characteristics of the physical interface itself. If they are employed in perturbative scattering theories (including the small slope), extreme care must be exercised to ensure that key expansion parameters are small. Spectra with power-laws $\gamma_2 > 4$ are perfectly well-behaved at high wavenumbers and should produce decent expansion parameters, but they are quite sensitive to low wavenumbers. There are no examples of such spectra in this paper.

The <u>modified</u> Pierson-Moskowitz is a very useful tool for examining the effects of peaks that are both narrower *and taller* than is allowed by the difference spectrum (such as on the air-sea interface and possibly a rippled ocean bottom). While the peak location can be chosen at will, the <u>modified</u> Pierson-Moskowitz spectrum only provides a closed form auto-correlation function (and consequently a tractable cross-section) when the tail goes as an *integral power* ($\gamma_2 = 3$ or 4). The width of the peak follows once the location of the peak is chosen. For the difference spectrum the height of the spectrum is fixed by the behavior of the tail, the choice of the peak wavenumber, and the shape of the spectrum. For the <u>modified</u> Pierson-Moskowitz, the shape is fixed so that the first two considerations alone fix the height of the peak. For the <u>modified</u> Pierson-Moskowitz spectrum, the height of the peak can vary widely depending on the value of the peak wavenumber. This rigid adherence to a limited set of peak shapes and to integer power tails limits the utility of the <u>modified</u> Pierson-Moskowitz spectrum. It can certainly be productively used as a benchmark (here used to verify the adequacy of the difference spectrum), and and perhaps for modeling the air-sea interface with a tail that goes as the integer 4^p. Some rippled ocean bottoms may go as the third power, and the <u>modified</u> Pierson-Moskowitz spectrum may also be used to model the scattering from such bottoms.

The angular dependence proposed by Elfouhaily *et al.* [22] generates a new term that must be added to the isotropic cross-section. This new term is very similar to the isotropic result. The methods were used to calculate the cross-section associated with an isotropic spectrum can be therefore be adapted to evaluate the new term associated with the azimuthal dependence.

The basic forms of all these results apply to both acoustic and electromagnetic fields (the latter subject to the caveat noted in footnote i on page 30).

Acknowledgements

---

[p] It has long been an unsettled question whether the tail characterizing the air-sea interface decays as l^{-4} or whether it decreases as some fractional power.

Appendix A   The prefactors corresponding to Dirichlet and fluid-elastic interfaces

This appendix discusses the evaluation of the prefactor β found in the small slope and perturbation theory results for scattering from a rough Dirichlet or fluid-elastic solid interface.   Although it is associated with the rough surface small slope scattering approximation, β in general depends on the quantities associated with a plane wave scattering from a planar fluid-solid interface.

A.1 Fluid-solid boundary conditions

The rough fluid-elastic interface will be considered first.   The label I will be connected with the fluid side and II will be associated with the elastic solid.   The incident and scattered fields are evaluated in the fluid.   The physical quantities input into β are the angles θ_{in}, θ_{out} and φ_{out} defined in Fig. 2 in Section 1.4.3, the densities of the media ρ_I and ρ_{II}, the sound speed in the fluid c_0, the Lamé parameters for the solid λ_{II} and μ_{II}, and the frequency of the field ω.   From these parameters, we get the primary(p)- and secondary(s)-wave sound speed and wavenumbers in the solid:

$$c_p = \sqrt{\frac{\lambda_{II} + 2\mu_{II}}{\rho_{II}}} \quad c_s = \sqrt{\frac{\mu_{II}}{\rho_{II}}}$$
$$k_p = \frac{\omega}{c_p} \qquad k_s = \frac{\omega}{c_s} \quad,$$

as well as the incident wavenumber $k_0 = \omega/c_0$.

The incident wavevector can be written in terms of horizontal and vertical components $\vec{k}_i = \underline{k} + k_{iz}\hat{z}$ (recall that vectors in the horizontal plane (x-y) are underlined), where $\underline{k} = k_0 \cos\theta_{in}\hat{x}$ and $k_{0z} = -k_0 \sin\theta_{in}$.   The sign in front of $\sin\theta_{in}$ reflects the conventions in Fig. 2.   The transmitted wave for the flat-interface problem is characterized by the p - and s - wavevectors given by:

$$\vec{k}_p = \underline{k} + k_{pz}\hat{z} \quad k_{pz} = -\sqrt{k_p^2 - |\underline{k}|^2}$$
$$\vec{k}_s = \underline{k} + k_{sz}\hat{z} \quad k_{sz} = -\sqrt{k_s^2 - |\underline{k}|^2} \quad \cdot \tag{A1}$$
$$|\underline{k}|^2 = k_0^2 \cos^2\theta_{in}$$

The prefactor β also depends on the conjugate problem. This problem involves the incoming wavevector $\vec{k}' = -\vec{q} = -k_0\hat{r}$ (where $\hat{r}$ is the direction of the observer):

$$\vec{q} = -\underline{k}' + k_0 \sin\theta_{\text{out}}\hat{z} \qquad \vec{k}'_i = \underline{k}' - k_0 \sin\theta_{\text{out}}\hat{z}$$

$$\vec{k}'_p = \underline{k}' + k'_{pz}\hat{z} \qquad k'_{pz} = -\sqrt{k'^2_p - |\underline{k}'|^2}$$

$$\vec{k}'_s = \underline{k}' + k'_{sz}\hat{z} \qquad k'_{sz} = -\sqrt{k'^2_s - |\underline{k}'|^2} \qquad \text{(A2)}$$

$$\underline{k}' = -k_0 \cos\theta_{\text{out}}\left(\cos\varphi_{\text{out}}\hat{x} + \sin\varphi_{\text{out}}\hat{y}\right) \quad |\underline{k}'|^2 = k_0^2 \cos^2\theta_{\text{out}}$$

The prefactor β is deduced from Eq. (3.23) of reference [13] with $\hat{n} \to \hat{z}$:

$$\beta\left(\theta_{\text{in}},\theta_{\text{out}},\varphi_{\text{out}};\rho_I,\rho_{II};k_0,k_p,k_s\right) =$$

$$4\left(1 - \frac{\rho_{II}}{\rho_I}\right)\frac{k_{iz}q_{iz}}{(a_1+1)(a_2+1)} + 4\left(1 - \frac{\rho_{II}}{\rho_I}\right)\underline{k}\cdot\underline{q}\frac{\xi_1\xi_2}{(a_1+1)(a_2+1)}$$

$$+ 8\frac{\rho_{II}}{\rho_I k_s^2}\left(\underline{k}\cdot\underline{q}\right)^2\frac{\xi_1\xi_2}{(a_1+1)(a_2+1)} - 4\underline{k}\cdot\underline{q}\frac{(a_1-\xi_1)(a_2-\xi_2)}{(a_1+1)(a_2+1)} \qquad \text{(A3)}$$

$$+ 4k_0^2\frac{a_1 a_2}{(a_1+1)(a_2+1)} + 2k_s^2\frac{\rho_I}{\rho_{II}}\frac{(a_1-b_1)(a_2-b_2)}{(a_1+1)(a_2+1)}$$

$$- 4k_p^2\frac{b_1 b_2}{(a_1+1)(a_2+1)}$$

The label "1" refers to quantities derived from the flat-interface solution generated by the incoming plane wave $\vec{k}$, and the label "2" refers to those same quantities evaluated for an incoming wavevector for the conjugate problem $\vec{k}' = -\vec{q}$.

We are now ready to read off the quantities a_1, a_2, b_1, b_2, ξ_1 and ξ_2. We have

$$a\left(\theta;\rho_I,\rho_{II};k_0,k_p,k_s\right) = \frac{\rho_{II}}{\rho_I}\frac{k_{iz}}{k_{pz}}\left[1 - \frac{4|\underline{k}|^2 k_{sz}\left(k_{sz}-k_{pz}\right)}{k_s^4}\right]$$

$$= \frac{\rho_{II}}{\rho_I}\frac{k_0\sin\theta}{\sqrt{k_p^2 - k_0^2\cos^2\theta}}\left[1 - \frac{4k_0^2\cos^2\theta\sqrt{k_s^2 - k_0^2\cos^2\theta}\left(\sqrt{k_s^2 - k_0^2\cos^2\theta} - \sqrt{k_p^2 - k_0^2\cos^2\theta}\right)}{k_s^4}\right]$$

and

$$a_1 = a\left(\theta_{\text{in}};\rho_I,\rho_{II};k_0,k_p,k_s\right) \quad a_2 = a\left(\theta_{\text{out}};\rho_I,\rho_{II};k_0,k_p,k_s\right). \qquad \text{(A4)}$$

Similarly,

$$b\left(\theta;\rho_I,\rho_{II};k_0,k_p,k_s\right) = \frac{\rho_{II}}{\rho_I}\frac{k_{iz}}{k_{pz}}\left[1 - \frac{2|\underline{k}|^2}{k_s^2}\right] = \frac{\rho_{II}}{\rho_I}\frac{k_0\sin\theta}{\sqrt{k_p^2 - k_0^2\cos^2\theta}}\left[1 - \frac{2k_0^2\cos^2\theta}{k_s^2}\right]$$

and

$$b_1 = b\left(\theta_{\text{in}}; \rho_I, \rho_{II}; k_0, k_p, k_s\right) \quad b_2 = b\left(\theta_{\text{out}}; \rho_I, \rho_{II}; k_0, k_p, k_s\right). \tag{A5}$$

We also have

$$\xi\left(\theta; k_0, k_p, k_s\right) = \frac{k_{iz}}{k_{pz} k_s^2}\left[\left(k_{sz} - k_{pz}\right)^2 - k_p^2\right]$$

$$= \frac{k_0 \sin\theta}{k_s^2 \sqrt{k_p^2 - k_0^2 \cos^2\theta}}\left[\left(\sqrt{k_s^2 - k_0^2 \cos^2\theta} - \sqrt{k_p^2 - k_0^2 \cos^2\theta}\right)^2 - k_p^2\right]$$

and

$$\xi_1 = \xi\left(\theta_{\text{in}}; k_0, k_p, k_s\right) \quad \xi_2 = \xi\left(\theta_{\text{out}}; k_0, k_p, k_s\right). \tag{A6}$$

We can also read off

$$k_{0z} = -k_0 \sin\theta_{\text{in}} \quad ; \quad q_{0z} = -k_0' = k_0 \sin\theta_{\text{out}}, \tag{A7}$$

and finally use

$$\underline{k} = k_0 \cos\theta_{\text{in}}\hat{x} \quad ; \quad -\underline{q} = \underline{k}' = -k_0 \cos\theta_{\text{out}}\left(\cos\varphi_{\text{out}}\hat{x} + \sin\varphi_{\text{out}}\hat{y}\right)$$

to obtain

$$\underline{k} \cdot \underline{q} = \vec{k} \cdot \left(1 - \hat{z}\hat{z}\right) \cdot \vec{q} = k_0^2 \cos\theta_{\text{in}} \cos\theta_{\text{out}} \cos\varphi_{\text{out}}. \tag{A8}$$

Note that for pure (i.e., monostatic) backscatter, we have $\theta_{\text{in}} = \theta_{\text{out}}, \varphi_{\text{out}} = 180°$.

Substituting (A4) to (A8) into (A3) produces the prefactor β for a fluid-elastic interface.

A.2 The Dirichlet boundary conditions

The precise form of the prefactor β for an acoustic field incident on Dirichlet, Neumann and two-fluid boundary conditions, and for an electromagnetic field incident on a perfect conductor can be read off from the results given in Appendix C.1 of reference [6]. In particular, the result corresponding to the Dirichlet boundary conditions is

$$\beta = 4k_{iz}q_{iz} = 4k_0 \sin\theta_{\text{in}} \sin\theta_{\text{out}}. \tag{A9}$$

References

[1] S. O. Rice, "Reflections of electromagnetic waves from slightly rough surfaces," *Comm. Pure Appl. Math.* **4**, 351-378 (1951).

[2] R. F. Gragg, D. Wurmser and R. C. Gauss, "Small-slope scattering from rough elastic ocean floors: General theory and computational algorithm," *J. Acoust. Soc. Am.* **110**, 2878-2901 (2001).

[3] E. Thorsos, "A practical model for rough surface scattering: The small slope approximation," *Proceedings of the Institute of Acoustics' International Conference on Stochastic Volume and Surface Scattering: Recent Developments in Underwater Acoustics*, 15-17 Dec. 1999, Cambridge, UK, Volume **21** (Institute of Acoustics, St. Albans, UK, 1999).

[4] A. G. Voronovich, "Theory of sound scattering by a free corrugated surface," *Sov. Phys. Acoust.* **30**, 444-448 (1984).

[5] A. G. Voronovich, "A unified description of wave scattering at boundaries with large and small scale roughness," in *Progress in Underwater Acoustics*, edited by H. M. Merklinger (Plenum, New York, 1986), pp. 24-34.

[6] R. Dashen, F. S. Henyey and D. Wurmser, "Calculations of acoustical scattering from the ocean surface," *J. Acoust. Soc. Am.* **88**, 310-323 (1990).

[7] R. Dashen and D. Wurmser, "Approximate Representations of the Scattering Amplitude," *J. Math. Phys.* **32**, 986-996 (1991).

[8] S. L. Broschat and E. I. Thorsos, "An investigation of the small slope approximation for scattering from rough surfaces. Part I. Theory,"*J. Acoust. Soc. Am.* **97**, 2082-2093 (1995).

[9] S. L. Broschat and E. I. Thorsos, "An investigation of the small slope approximation for scattering from rough surfaces. Part II. Numerical studies,"*J. Acoust. Soc. Am.* **101**, 2615-2625 (1997).

[10] P. H. Dahl, "On bistatic sea surface scattering: Field measurements and modeling," *J. Acoust. Soc. Am.* **105**, 2155-2169 (1999).

[11] S. T. McDaniel, "Acoustic and radar scattering from directional seas," *Waves Random Media* **9**, 537-549 (1999).

[12] S. T. McDaniel, "Small-slope predictions of microwave backscatter from the sea surface," *Waves Random Media* **11**, 343-360 (2001).

[13] T. Yang and S. L. Broschat, "Acoustic scattering from a fluid-elastic-solid interface using the small slope approximation," *J. Acoust. Soc. Am.* **96**, 1796-1803 (1994).

[14] D. Wurmser, "A manifestly reciprocal theory for scattering in the presence of elastic media," *J. Math. Phys.* **37**, 4434-4479 (1996).

[15] K. L. Williams and D. R. Jackson, "Bistatic bottom scattering: Model, experiments, and model/data comparison," *J. Acoust. Soc. Am.* **103**, 169-181 (1998).

[16] D. R. Jackson, "High-frequency bistatic scattering model for elastic seafloors," APL-UW TM 2-00, Applied Physics Laboratory, Seattle, WA, 2000.

[17] R. C. Gauss, R. F. Gragg, R. W. Nero, D. Wurmser and J. M. Fialkowski, "Broadband models for predicting bistatic bottom, surface, and volume scattering strengths," NRL/FR/7100—02-10,042, Naval Research Laboratory, Washington, DC, September 30, 2002.

[18] R. C. Gauss, J. M. Fialkowski, and D. Wurmser, "Assessing the Variability of Near-Boundary Surface and Volume Reverberation Using Physics-Based Scattering Models," in *Impact of Littoral Environmental Variability on Acoustic Predictions and Sonar Performance*, ed. N.G. Pace and F.B. Jensen, 16-20 Sept. 2002, Lerici, Italy (Kluwer Academic, Dordrecht, 2002), pp. 345-352.

[19] D. Wurmser, R.F. Gragg and R.C. Gauss, "Calculations of acoustic scattering from an elastic ocean bottom.," *J. Acoust. Soc. Am.* **104**, Part 2, 1809 (Abstract-1998).

[20] R. J. Soukup and R. F. Gragg, , "Backscatter from a limestone elastic seafloor at 2–3.5 kHz: Measurements and modeling," *J. Acoust. Soc. Am.* **113**, 2501-2514 (2003).

[21] D. Wurmser, J. M. Fialkowski and R. C. Gauss, "Computationally tractable stochastic cross-sections based on the small slope approximation," submitted to *Waves in Random Media*, 2005.

[22] T. Elfouhaily, B. Chapron, K. Katsaros and D. Vandemark, "A unified directional spectrum for long and short wind-driven waves," *J. Geophys. Res.* **102**, 15,781-15,796 (1997).

[23] S. T. McDaniel, "Sea surface reverberation: A review," *J. Acoust. Soc. Am.* **94**, 1905-1922 (1993).

[24] M. Donelan and W. Pierson, "Radar scattering and equilibrium ranges in wind-generated waves with application to scatterometry," *J. Geophys. Res.* **92**, 4971-5029 (1987).

[25] A. Ivakin, personal communication, Applied Physics Laboratory–University of Washington, Seattle, WA, 2004.

[26] A. G. Voronovich, "Small-slope approximation in wave scattering by rough surfaces," *Sov. Phys. JETP* **62**, 65-70 (1985).

[27] H. Bateman, *Tables of Integral Transforms*, Volume II (McGraw-Hill, New York, 1954).

[28] A. Abramovitz, and I. A. Stegun, *Handbook of Mathematical Functions*, (Dover, New York, 1964).

[29] D. M. Drumheller and R. F. Gragg, "Evaluation of a fundamental integral in rough surface scattering," *J. Acoust. Soc. Am.* **110**, 2270-2275 (2001).

[30] D. M. Drumheller and R. F. Gragg, "Numerical evaluation of an integral found in the theory of scattering from random rough surfaces," NRL/MR/7100—00-8436, Naval Research Laboratory, Washington, DC, March 17, 2000.

[31] J. M. Fialkowski, personal communication, Naval Research Laboratory, Washington, D.C., 2004.

[32] W. J. Pierson, Jr., and L. Moskowitz, "A proposed spectral form for fully developed wind seas based on the similarity theory of S. A. Kitaigorodskii," *J. Geophys. Res.* **69**, 5181-5190 (1964).

[33] E. Thorsos, "Acoustic scattering from a 'Pierson-Moskowitz' sea surface," *J. Acoust. Soc. Am.* **88**, 335-349 (1990).